Evolution of Late Season Meltwater in Alpine and Arctic Glaciers: Sampling Strategies and Geochemical Observations

by

Mark J. Robbins

A dissertation submitted in partial fulfillment
of the requirements for the degree of
Doctor of Philosophy
(Earth and Environmental Sciences)
in the University of Michigan
2020

Doctoral Committee:

Professor Ingrid Hendy, Chair
Associate Professor Jeremy N. Bassis
Professor Joel D. Blum
Professor Julia Cole
Associate Professor Rose Cory

Mark J. Robbins

mjrobb@umich.edu

ORCID iD: 0000-0002-8118-6825

Acknowledgements

There are many people who have helped me over the years to reach this point and I would like to thank you all for your time, thoughts, feedback, laughter, and shared experiences. I can truthfully say I doubt I would have been successful without all your help – thank you.

The original GIGL lab group helped me as I began my Ph.D. career: Carli Arendt, Sarah Aarons, Yi-Wei Liu, Kyle Meyer, Molly Blakowski, and Anna Clinger were all instrumental in talking out ideas and troubleshooting problems as they arose. I would especially like to thank Emily Stevenson, my field partner for three months in the Canadian Rocky Mountains and two months in southern Greenland. Even with an unfortunate encounter involving a can of bear spray, I cannot imagine long term field work with anyone else.

To my instructors and cohort from the 2016 – 2017 year I spent at the McCall Outdoor Science School in McCall, Idaho: I learned so much about community, effective teaching, and communicating science from that year-long experience. I know I am a better instructor now, and I am quite confident I would not have succeeded in graduate school without my year in Idaho.

I would especially like to thank my advisor, Ingrid Hendy. She agreed to take me on as a student when I was already 2.5 years into my Ph.D., attempting to interpret data from projects she'd had no input in designing on topics she has not studied. Over the past years she's worked diligently to help me make sense of my results and write so that others can understand my conclusions. Similarly, I thank my committee members: Jeremy Bassis, Joel Blum, Julie Cole, and Rose Cory for their knowledge and expertise over the years.

I would also like to thank Jon and Ellen Martin from the University of Florida for taking me along on their 2018 field campaign to south Greenland. Work we conducted there comprises a chapter of my dissertation, and data collected allowed a better understanding of results in another chapter. Many people return home from fieldwork, think "I wish I had thought to do that!" and thanks to the Martins, I had the opportunity to address some of those concerns.

Friends and colleagues at the University of Michigan, while there are far too many of you for a comprehensive list here, you made this process far more enjoyable that it could have been otherwise: Erin Lynch, Xiaofei Pu, Will Bender, Alyssa Abbey, James Jolles, Sam Haugland, Sarah Walker, Brian Konecke, Tristan Childress, Alex Tye, Aaron Kurz, Kyle Meyer, Joe El Adli. To Jeroen Ritsema and Jamie Gleason, I appreciated working with you at Camp Davis and beyond. Lydia, you've made this last year better than I thought it could be.

Paris and Harper, my two dogs throughout my graduate career. I know plenty of people make it through graduate school without a pet, but I'm not sure I could have done it – or could have done it as well mentally – with these two dogs over the years. Paris was my companion for 10 years beginning in undergrad and will be forever missed. Harper is growing into an excellent companion and I look forward to the next life chapter with her.

Finally, I'd like to thank my family. To my mom, dad, and sister Steff, thank you for your time, patience, and love throughout this process. As you know, it's been neither smooth nor easy, but you were there to help as you could, from gifting me pounds of coffee over the holidays to watching my dog for months when I went into the field for three months. Thank you.

Table of Contents

List of Tables

List of Figures

Abstract

The presence, configuration, and efficiency of subglacial hydrologic systems has important implications for both glacial dynamics and the chemistry of meltwaters. These networks may exist in configurations that range from poorly connected and unable to accommodate large volumes of water to fast flowing and highly competent in different regions of the glacial bed, simultaneously or in different seasons. Direct study of the configuration and development of these networks is difficult as they are obscured by ice, yet network configuration is important in glaciological research as it controls the spatial distribution and residence time of subglacial water. Subglacial network efficiency, or the ability of the network to quickly evacuate water, controls under-ice water-rock interaction time affecting chemical weathering reactions and thus solute type and concentration expressed in proglacial meltwaters. Previous research into the configuration of subglacial hydrologic networks is limited in both temporal and spatial resolution, as field research generally occurs during summer months and is limited to more easily accessible glaciers. This dissertation investigates seasonal changes in subglacial hydrologic networks as evidenced by changing meltwater chemistry in late-summer at both a Canadian alpine glacier and an outlet glacier from the Greenland Ice Sheet. I undertook multi-month field campaigns at each location, during which I collected samples and made *in situ* measurements to correlate changes in chemical constituents carried within melt to changes in seasonality, improving understanding of this understudied time in seasonal glacial development.

This dissertation uses laboratory experiments with sediment samples collected at glacial termini to evaluate the use of radon-222 (^{222}Rn) activity concentrations, an intermediary in the

uranium-238 (^{238}U) decay chain, as a proxy for subglacial water residence time. These measurements are compared to in field ^{222}Rn activity concentration measurements at sediment collection locations. Results show ^{222}Rn activity concentration serves as a subglacial water residence time proxy but also reflects mineralogical sources of its parent isotope, radium-226 (^{226}Ra). Field measurements of ^{222}Rn activity concentrations as a proxy will be more robust and reliable if supported with laboratory leachate experiments with site-specific sediment samples, addressing likely lithological and sediment-size controls on ^{226}Ra concentrations.

I undertook a three-month field study of the alpine Athabasca Glacier in the Canadian Rockies in August through October, 2014. Both *in situ* and elemental chemistry of pro-glacial meltwaters are investigated relative to water discharge fluxes, air temperatures, and precipitation events to see how the subglacial network responds to climatic and glacial variables during the late summer-early fall. Different chemical weathering rates in response to changes in weather reveal shifts in network configuration, indicating the subglacial environment is dynamic and very responsive to climate conditions. Methods used at the Athabasca Glacier were then applied to Kiattuut Sermiat, an outlet glacier from the Greenland Ice Sheet to investigate possible differences in hydrology between alpine and outlet glaciers. Although environmental conditions are dissimilar between locations, the Kiattuut Sermiat results suggest the possible existence of an interannual subglacial drainage system capable of evacuating waters sourced from significantly further up into the Greenland Ice Sheet concurrent with a well-organized subglacial network configuration. This dissertation presents new measurements of glacial chemistry from an understudied period in seasonal glacial evolution, with interpretations unique to each glacier investigated.

Chapter I. Introduction

Glacial Systems

Earth's glaciers and ice sheets are an important resource, containing 70% of Earth's freshwater (Shiklomanov, 1993). Present and future climate change pose direct threats to their existence, with rising global temperatures leading to increased melt and negative annual mass balances. Many glaciers that existed only decades ago have melted, and many more are predicted to disappear through the 21st century (WGMS, 2017). Glaciers and ice sheets contain enough water to raise sea level by ~66 m (Vaughan et al., 2013); a large enough volume of water to submerge many of the world's largest cities. While the Greenland (GrIS) and Antarctic ice sheets would require millennia to fully melt, rates of mass loss are increasing in both locations with melt rate records being surpassed every few years (Bevis et al., 2019; Nghiem et al., 2012). Changes in melt rates have implications for downstream ecosystems through fluctuating water levels, sediment concentrations, nutrient availability, and general water chemistry (e.g. pH, alkalinity) (Brown et al., 2007; Hannah et al., 2007; Jacobsen et al., 2012; Milner et al., 2017). This dissertation investigates changes in the chemistry of outflow water from both a GrIS outlet glacier and an alpine glacier in order to learn more about evolution of meltwater routing and storage beneath glaciers as average air temperatures decline as the seasons transition from summer to autumn.

Ice masses broadly exist in two categories: those which are 'draped' over topography – ice sheets and ice caps, and those which are constrained by topography – glaciers. Ice sheets and ice caps flow outward from topographically high central accumulation areas by the weight of their own mass, eventually terminating as outlet glaciers where the majority of ice mass is lost. Ice flow

in alpine glaciers is not sourced from a larger ice mass and thus these glaciers are more vulnerable to mass loss and retreat due to their small mass. Through ice flow, mass is transferred from regions where rates of accumulation rates, through densification and metamorphosis of snow precipitation to glacial ice, exceed ablation rates to regions where ablation (melting or mass loss) is greater than accumulation. Ice sheets and ice caps have convex profiles with a central accumulation area; ice mass is lost at their boundaries due to melting and iceberg calving. Alpine glaciers accumulate mass at higher elevations characterized by colder temperatures and greater snowfall, losing mass at lower elevations with less snowfall and warmer air temperatures. Regardless of size, ice masses grow when accumulation exceeds ablation and shrink when the reverse is true.

Glaciers flow via two primary processes: internal deformation and basal sliding. Ice, while solid, behaves viscously and is capable of flowing. Internal deformation, termed 'creep,' is a strain response within individual ice crystals resulting from the mass of ice overburden; deformation occurs through atomic dislocations within the crystal lattice as a response to stress (Hooke, 2005). Conversely, basal slip occurs when the glacier moves along the basal substrate, by sliding along bedrock, deformation of subglacial sediments, or some combination of both processes (Cuffey and Paterson, 2010). Rates of basal sliding vary as a function of bed roughness, proportion of bed frozen to the bedrock below, and volume of water present (Davison et al., 2019; Iken and Bindschadler, 1986; Mair et al., 2003; Meierbachtol et al., 2013). Subglacial melt can lubricate the bed, enhancing sliding by decreasing ice-bed contact area and reducing friction (Iken and Bindschadler, 1986). The distribution of meltwater under the ice, whether contained within a few channels or spread over a wide area of the bed, thus has the potential to greatly affect glacial velocity and therefore ablation rates.

Subglacial Hydrology

Subglacial drainage networks must accommodate, transport, and eventually evacuate meltwater produced by the ice mass. While surficial melting due to insolation and above freezing air temperatures generates the largest volume of meltwater, ice is also melted at both the glacier base from geothermal heat flux and within the ice mass from friction. Glacial hydrologic systems are complex and include many components on, within, and under the ice (Figure I-1). Water

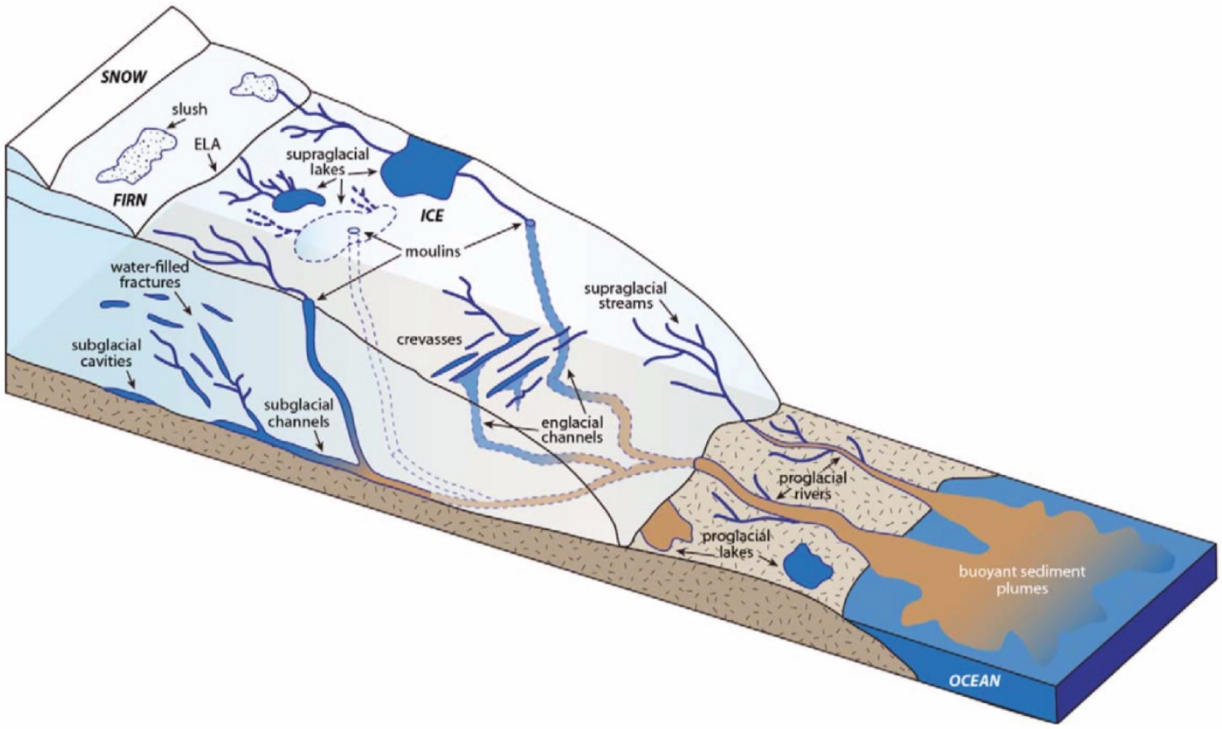

Figure I-1: Schematic diagram illustrating water routes through land terminating ice. Supraglacial melt exists in supraglacial lakes, flows off the ice terminus in supraglacial streams, and enters the ice body through moulins and crevasses. Englacial water fills fractures and flows through channels, eventually reaching the subglacial system where it acquires sediment. Subglacial water emanates from the glacial terminus in proglacial rivers. Figure adapted from Chu (2014).

created through melting of surface ice (supraglacial melt) may be temporarily stored in supraglacial lakes, flow off the ice surface in supraglacial streams, or enter the body of ice through crevasses or moulins (open conduits) on the ice surface. Englacial channels route water to the glacial bed, where it then enters the subglacial drainage network.

Meltwater flows through the subglacial hydrologic network before eventually leaving the glacial system at the glacier terminus. Glaciers may be either land- or marine-terminating. Sediment-laden meltwaters emerge in proglacial rivers from land-terminating alpine or outlet glaciers, whereas meltwater enters the ocean directly in marine-terminating tidewater glaciers or ice shelves. Chemical signatures of glacial melt from marine-terminating glaciers are immediately mixed immediately with the seawater they enter, complicating chemical interpretation of glacial melt. Thus, the chemistry of land-terminating glacial meltwater was selected for this dissertation research.

Subglacial drainage networks change in size and connectivity depending on volume of melt they must accommodate. Flowing subglacial meltwater melts ice walls through friction and latent heat, enlarging channels to fit the volume of water present (Röthlisberger, 1972). Subglacial channels may be incised into basal ice (Röthlisberger, or R-, channels) (Röthlisberger, 1972) or into the bedrock below the glacier (Nye, or N-, channels) (Nye, 1976). Because R-channel ice wall melt rates increase with increasing water flux, larger subglacial channels will have lower pressures than smaller subglacial channels, connecting conduits into an arborescent, or dendritic, configuration (Röthlisberger, 1972). Röthlisberger's (1972) calculations assumed steady-state conditions with creep closure exactly matched by channel growth; this condition is unlikely in natural glacial systems due to variable diurnal melting. Variable surface melt rates result in variable meltwater input volumes to the subglacial drainage system, with larger input volumes during the day and smaller volumes at night when air temperatures cool. Change in meltwater flux results in changing subglacial water pressure, with high pressures correlated with high input and vice-versa (Hubbard et al., 1995). A study at Haut Glacier d'Arolla, an alpine glacier in Switzerland, found daytime meltwater volumes above the subglacial drainage network's capacity flow out of the existing network of subglacial drainage channels into the surrounding subglacial bed, then when

water input volumes fell, pressure within channels also fell, pulling water back into the network from the now-higher pressure surroundings (Hubbard et al., 1995), producing a constantly changing and dynamic environment.

Glacial meltwater volumes display high seasonality in addition to diurnal variability. As such, subglacial drainage networks also exhibit changes in configuration on a seasonal basis. These configurations are understood in terms of two end members: 1.) a channelized, well connected, arborescent network (hereafter referred to as "fast configuration") (Figure I-2A) and 2.) a nonarborescent, less efficient network distributed over a larger area of the glacial bed (hereafter referred to as "slow configuration") (Figure I-2B) (Fountain and Walder, 1998).

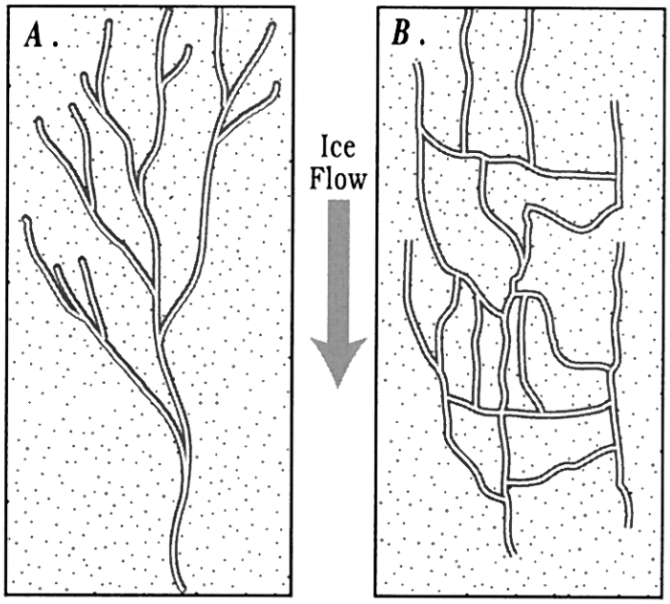

Figure I-2: A.) Idealized channelized, arborescent subglacial drainage network. B.) Idealized distributed, slow flowing subglacial drainage network. From Fountain and Walder, 1998.

Channelized subglacial hydrologic networks, comprised of R-channels and prevalent in summer concurrent with higher melt rates, cover a small area of the subglacial bed, yet can accommodate and efficiently evacuate large volumes of meltwater (Figure I-2A) (Fountain and Walder, 1998). Efficient subglacial drainage networks are shown to grow up-ice throughout the

melt season (e.g. Bartholomew et al., 2010; Chandler et al., 2013). When melting rates decrease as air temperatures cool at summer's end, existing subglacial channels are no longer filled leaving voids. Low pressure within voids allows ice inflow, closing channels and forcing a change in subglacial drainage network configuration (Figure I-2B). Distributed subglacial hydrologic networks, common in winter, are widely distributed over a large area of the subglacial bed, with water existing within thin films, subglacial cavities, and sediment layers (Fountain and Walder, 1998). Because these different components are not well connected resulting in slow movement of water through the system, subglacial water pressures are high (Downs et al., 2018; Gordon et al., 1998; Hooke et al., 1990). Slow flow rates also result in longer water residence times than in summertime fast-flow configurations. Longer residence times, and greater distribution over the subglacial bed, allow for longer water-rock interaction times and subsequently more chemical weathering reactions are possible than in a channelized system (e.g. Tranter et al., 1997).

Change from a connected to a distributed system is not instantaneous as it requires ice deformation. Rates of closure depend on ice thickness; the weight of ice overburden is the product of *g* (gravitational acceleration), ice density, and thickness. Weertman (1972) calculated channel radius as a function of time: $R(t) = R_0 \exp(-t/\tau)$, where R_0 is the radius at the end of the melt season and τ is proportional to ρ_i^{-n}, where $n \approx 3$ and ρ_i is ice density. Practically, for ice greater than 150 m thick, a surviving channel after winter would, even for a primary 'trunk' channel, have an R_0 at the start of the melt season no larger than a few millimeters (Fountain, 1996). Growth, however, from a principally distributed (winter) configuration to a more efficient channelized configuration occurs much more quickly: above-freezing temperatures generate significant volumes of surface melt, which then enters the subglacial hydrologic system. As this system – existing in a wintertime distributed configuration – is not yet competent enough to accommodate large fluxes, water flows out of the existing drainage network and into larger areas of the glacial

bed (Schoof, 2010; Zwally et al., 2002). Subglacial water pressure is high in this scenario, reducing the effective pressure of the glacier and enhancing sliding. This process has been documented at both alpine and outlet glaciers in the literature through vertical uplift of the surface of Unteraargletscher (Switzerland) at the beginning of melt seasons (Iken et al., 2017), increased springtime surface velocity measured at Haut glacier d'Arolla (Switzerland) in 1998 and 1999 (Mair et al., 2003), radar-measured increased surface velocity of a subset of 55 marine-terminating GrIS outlet glaciers from 2009 – 2013 (Moon et al., 2014), and in numerically modeled results for an idealized ice sheet margin (Hewitt, 2013).

Change from a distributed to channelized subglacial drainage network is also evident through meltwater chemistry. Longer residence time in subglacial distributed networks results in increased elemental concentrations and electrical conductivity because waters are in contact with greater mineral surface area for longer durations, allowing more chemical weathering to occur. In contrast, shorter residence time in faster flowing summertime configurations have greater dilution of weathering products, generating low elemental concentrations and electrical conductivity measurements (e.g. Bartholomaus et al., 2011; Hawkings et al., 2016; Stone and Clarke, 1996). The timing of this seasonal transition is notable both through glacial hydrochemistry and surface velocity, and as such as been the subject of much glaciological research. However, the reverse process, the return of the subglacial network to a distributed configuration, is poorly documented. As such I will investigate the chemical signatures in meltwater produced when this transition is assumed to occur to identify changes in the subglacial hydrology at the end of the summer melt season.

Approach

A primary difference between summertime, channelized, well-connected, fast-flowing subglacial drainage configuration (hereafter referred to as 'fast configuration') and a wintertime, distributed, poorly-connected, slow-flowing configuration (hereafter referred to as 'slow configuration') is water residence time. Meltwater flows quickly through fast configurations with short residence times, and slowly through slow configurations resulting in longer residence times. Previously, researchers have injected tracers into the subglacial drainage system, then monitored breakthrough at the ice terminus to measure residence time in an attempt to resolve connectivity of the subglacial system (e.g. Chandler et al., 2013; Hasnain et al., 2001; Nienow et al., 1998), but this method is dependent on possible locations for tracer injection. Tracers can be added to meltwater flowing into moulins, but as moulins an input source for surface melt to the en- and subglacial systems, these tracers may be added to a drainage configuration that is already partially channelized. Drilling boreholes allows access to non-channelized areas of the bed, but is more labor intensive and expensive. I employed an alternative method by utilizing the activity concentrations of ^{222}Rn in outflow meltwaters as a natural proxy for residence time. ^{222}Rn, an intermediary in the ^{238}U decay chain, is produced through natural radioactive decay. Furthermore, as Rn is a noble gas so it will not react with other chemical species in the subglacial environment, and will dissolve into water. Thus, higher ^{222}Rn activity concentrations imply water was stored in the subglacial environment for longer than waters collected from the same location with lower ^{222}Rn activity concentrations.

Other hydrochemical parameters (e.g. stable water isotopes, elemental concentrations, and *in situ* aqueous chemistry) were also measured and analyzed from field samples to provide evidence of changing subglacial hydrologic configurations as the summer transitioned to autumn. Elemental weathering products were used to investigate different occurrence and proportion of different

subglacial weathering reactions (e.g. carbonate dissolution vs silicate hydrolysis). Seasonal trends in water isotope values allowed qualitative assessment of water source, as well as identifying precipitation input to the subglacial system. Data collected for this work was then compared to published data from the same glaciers to better understand the annual chemical cycles of the two glaciers investigated, Kiattuut Sermiat, a GrIS outlet glacier, and the alpine Athabasca Glacier in the Canadian Rocky Mountains.

Outline of this Dissertation

Chapter II examines the methods used in this dissertation and explores potential complications that impact interpretation. ^{222}Rn activity concentration use as a proxy for subglacial meltwater residence time is evaluated by comparing laboratory experiment results to in-field measurements. Laboratory experiments leached size-sorted sediments collected in proglacial environments with 18.2 MΩ water for until ^{222}Rn was in secular equilibrium with its parent, then measured activity concentrations to compare to field measurements from the sediment source locations. Results show while ^{222}Rn concentrations may reveal subglacial residence time, there is a mineralogical component related to its concentrations that should be measured from source sediments for quantitative analysis.

Chapter III is in review in *Hydrological Processes*. This chapter presents geochemical results from a late melt season field sampling campaign at the Athabasca Glacier, an alpine glacier in the Canadian Rocky Mountains, August through October 2014. Changes in elemental concentrations, discharge fluxes, stable water isotopes, and ^{222}Rn concentrations show a change in rates of carbonate to silicate mineral weathering as air temperatures cool, revealing an immediate response in the configuration of the subglacial hydrologic network to seasonal changes.

Chapter IV scales up methods used in Chapter III to Kiattuut Sermiat, an outlet glacier from the GrIS, during a late summer field campaign in August and September, 2015. Comparison of results to geochemical results from the same glacier in previous years reveal annual cyclicity to measured parameters, providing a baseline with which to evaluate future hydrochemical changes.

References

Bartholomaus, T.C., Anderson, R.S., Anderson, S.P., 2011. Growth and collapse of the distributed subglacial hydrologic system of Kennicott Glacier, Alaska, USA, and its effects on basal motion. J. of Glaciol. 57, 985–1002. doi:10.3189/002214311798843269

Bartholomew, I., Nienow, P., Mair, D., Hubbard, A., King, M.A., Sole, A., 2010. Seasonal evolution of subglacial drainage and acceleration in a Greenland outlet glacier. Nat. Geosci. 3, 408–411. doi:10.1038/ngeo863

Bevis, M., Harig, C., Khan, S.A., Brown, A., Simons, F.J., Willis, M., Fettweis, X., van den Broeke, M.R., Madsen, F., Kendrick, E., Caccamise, D.J., van Dam, T., Knudsen, P., Nylen, T., 2019. Accelerating changes in ice mass within Greenland, and the ice sheet's sensitivity to atmospheric forcing. Proc. Nat. Acad. Sci. 116, 1934–1939. doi:10.1073/pnas.1806562116

Brown, L.E., Hannah, D.M., Milner, A.M., 2007. Vulnerability of alpine stream biodiversity to shrinking glaciers and snowpacks. Global Change Biol. 13, 958–966. doi:10.1111/j.1365-2486.2007.01341.x

Chandler, D.M., Wadham, J.L., Lis, G.P., Cowton, T., Sole, A., Bartholomew, I., Telling, J., Nienow, P., Bagshaw, E.B., Mair, D., Vinen, S., Hubbard, A., 2013. Evolution of the subglacial drainage system beneath the Greenland Ice Sheet revealed by tracers. Nature Geoscience 6, 195–198. doi:10.1038/ngeo1737

Chu, V.W., 2014. Greenland ice sheet hydrology: A review. Prog. in Phys. Geog. 38, 19–54. doi:10.1177/0309133313507075

Cuffey, K.M., Paterson, W., 2010. The Physics of Glaciers, fourth ed. Butterworth-Heinemann, Oxford.

Davison, B.J., Sole, A.J., Livingstone, S.J., Cowton, T.R., Nienow, P.W., 2019. The influence of hydrology on the dynamics of land-terminating sectors of the Greenland Ice Sheet. Front. Earth Sci. 7, 580–24. doi:10.3389/feart.2019.00010

Downs, J.Z., Johnson, J.V., Harper, J.T., Meierbachtol, T., Werder, M.A., 2018. Dynamic hydraulic conductivity reconciles mismatch between modeled and observed winter subglacial water pressure. J. Geophys. Res. Earth Surf. 123, 818–836. doi:10.1002/2017JF004522

Fountain, A.G., 1996. Effect of snow and firn hydrology on the physical and chemical characteristics of glacial runoff. Hydrol. Process. 10, 509–521. doi:10.1002/(sici)1099-1085(199604)10:4<509::aid-hyp389>3.0.co;2-3

Fountain, A.G., Walder, J.S., 1998. Water flow through temperate glaciers. Rev. Geophys. 36, 299–328. doi:10.1029/97rg03579

Gordon, S., Sharp, M., Hubbard, B., Smart, C., Ketterling, B., Willis, I., 1998. Seasonal reorganization of subglacial drainage inferred from measurements in boreholes. Hydrol. Process. 12, 105–133. doi:10.1002/(sici)1099-1085(199801)12:1<105::aid-hyp566>3.0.co;2-#

Hannah, D.M., Brown, L.E., Milner, A.M., Gurnell, A.M., McGregor, G.R., Petts, G.E., Smith, B.P.G., Snook, D.L., 2007. Integrating climate–hydrology–ecology for alpine river systems. Aquatic Conserv: Mar. Freshw. Ecosyst. 17, 636–656. doi:10.1002/aqc.800

Hasnain, S.I., Jose, P.G., Ahmad, S., Negi, D.C., 2001. Character of the subglacial drainage system in the ablation area of Dokriani glacier, India, as revealed by dye-tracer studies. J. of Hydrol. 248, 216–223. doi:10.1016/S0022-1694(01)00404-8

Hawkings, J., Wadham, J., Tranter, M., Telling, J., Bagshaw, E., Beaton, A., Simmons, S.-L., Chandler, D., Tedstone, A., Nienow, P., 2016. The Greenland Ice Sheet as a hot spot of phosphorus weathering and export in the Arctic. Global Biogeochem. Cycles 30, 191–210. doi:10.1002/2015GB005237

Hewitt, I.J., 2013. Seasonal changes in ice sheet motion due to melt water lubrication. Earth Planet. Sci. Lett. 371-372, 16–25. doi:10.1016/j.epsl.2013.04.022

Hooke, R.L., 2005. Principles of Glacier Mechanics, second ed. Cambridge Univ. P., Cambridge. doi:10.1017/CBO9780511614231

Hooke, R.L., Laumann, T., Kohler, J., 1990. Subglacial water pressures and the shape of subglacial conduits. J. of Glaciol. 36, 67–71. doi:10.3189/s0022143000005566

Hubbard, B., Sharp, M., Willis, I., Nielsen, M., Smart, C., 1995. Borehole water-level variations and the structure of the subglacial hydrological system of Haut Glacier d'Arolla, Valais, Switzerland. J. Glaciol. 41, 572–583. Doi:10.3189/s0022143000034894

Iken, A., Bindschadler, R.A., 1986. Combined measurements of subglacial water pressure and surface velocity of Findelengletscher, Switzerland: Conclusions about drainage system and sliding mechanism. J. Glaciol. 32, 101–119. doi:10.1017/s0022143000006936

Iken, A., Röthlisberger, H., Flotron, A., Haeberli, W., 2017. The uplift of Unteraargletscher at the beginning of the melt season—A consequence of water storage at the bed? J. Glaciol. 29, 28–47. doi:10.1017/S0022143000005128

Jacobsen, D., Milner, A.M., Brown, L.E., Dangles, O., 2012. Biodiversity under threat in glacier-fed river systems. Nat. Clim. Chang. 2, 361–364. doi:10.1038/nclimate1435

Mair, D., Willis, I., Fischer, U.H., Hubbard, B., Nienow, P., Hubbard, A., 2003. Hydrological controls on patterns of surface, internal and basal motion during three "spring events": Haut Glacier d'Arolla, Switzerland. J. of Glaciol. 49, 555–567. doi:10.3189/172756503781830467

Meierbachtol, T., Harper, J., Humphrey, N., 2013. Basal drainage system response to increasing surface melt on the Greenland ice sheet. Science 341, 777–779. doi:10.1126/science.1235905

Milner, A.M., Khamis, K., Battin, T.J., Brittain, J.E., Barrand, N.E., Füreder, L., Cauvy-Fraunié, S., Gíslason, G.M., Jacobsen, D., Hannah, D.M., Hodson, A.J., Hood, E., Lencioni, V., Ólafsson, J.S., Robinson, C.T., Tranter, M., Brown, L.E., 2017. Glacier shrinkage driving global changes in downstream systems. Proc. Natl. Acad. Sci. USA 114, 9770–9778. doi:10.1073/pnas.1619807114

Moon, T., Joughin, I., Smith, B., Broeke, M.R., Berg, W., Noël, B., Usher, M., 2014. Distinct patterns of seasonal Greenland glacier velocity, Geophys. Res. Lett., 41, 7209–7216, doi:10.1002/2014GL061836

Nghiem, S.V., Hall, D.K., Mote, T.L., Tedesco, M., Albert, M.R., Keegan, K., Shuman, C.A., DiGirolamo, N.E., Neumann, G., 2012. The extreme melt across the Greenland ice sheet in 2012. Geophys. Res. Lett. 39, 165–6. doi:10.1029/2012GL053611

Nienow, P., Sharp, M., Willis, I., 1998. Seasonal changes in the morphology of the subglacial drainage system, Haut Glacier d'Arolla, Switzerland. Earth Surf. Process. Landf. 23, 825–843. doi:10.1002/(SICI)1096-9837(199809)23:9<825::AID-ESP893>3.0.CO;2-2

Nye, J.F., 1976. Water flow in glaciers: jökulhlaups, tunnels and veins. J. Glaciol. 17, 181–207. doi:10.3189/s002214300001354x

Röthlisberger, H., 1972. Water pressure in intra- and subglacial channels. J. Glaciol. 11, 177–203. doi:10.1017/s0022143000022188

Schoof, C., 2010. Ice-sheet acceleration driven by melt supply variability. Nature 468, 803–806. doi:10.1038/nature09618

Shiklomanov, I.A., 1993. World fresh water resources, in: Gleick, P.H. (Ed.), Water in crisis: A guide to the world's fresh water resources. Oxford Univ. Press, New York, pp. 13 – 24.

Stone, D.B., Clarke, G.K.C., 1996. *In situ* measurements of basal water quality and pressure as an indicator of the character of subglacial drainage systems. Hydrol. Process. 10, 615–628. doi:10.1002/(SICI)1099-1085(199604)10:4<615::AID-HYP395>3.0.CO;2-M

Tranter, M., Sharp, M.J., Brown, G.H., Willis, I.C., Hubbard, B.P., Nielsen, M.K., Smart, C.C., Gordon, S., Tulley, M., Lamb, H.R., 1997. Variability in the chemical composition of *in situ* subglacial meltwaters. Hydrol. Process. 11, 59–77. doi:10.1002/(SICI)1099-1085(199701)11:1<59::AID-HYP403>3.0.CO;2-S

Vaughan, D.G., J.C. Comiso, I. Allison, J. Carrasco, G. Kaser, R. Kwok, P. Mote, T. Murray, F. Paul, J. Ren, E. Rignot, O. Solomina, K. Steffen and T. Zhang, 2013: Observations: Cryosphere. In: Climate Change 2013: The physical science basis. Contribution of working group I to the fifth assessment report of the Intergovernmental Panel on Climate

Change [Stocker, T.F., D. Qin, G.-K. Plattner, M. Tignor, S.K. Allen, J. Boschung, A. Nauels, Y. Xia, V. Bex and P.M. Midgley (eds.)]. Cambridge Univ. Press, Cambridge, United Kingdom and New York, NY, USA.

Weertman, J., 1972. General theory of water flow at the base of a glacier or ice sheet. Rev. Geophys. 10, 287–333. doi:10.1029/RG010i001p00287

WGMS, 2017. Global Glacier Change Bulletin No. 2 (2014-2015) 1–257.

Zwally, H.J., Abdalati, W., Herring, T., Larson, K., Saba, J., Steffen, K., 2002. Surface melt-induced acceleration of Greenland ice-sheet flow. Science 297, 218–222. doi:10.1126/science.1071795

Chapter II. ^{222}Rn as a Subglacial Water Residence Time Proxy: Importance of Sampling Location for Proglacial Melt

Abstract

Proglacial meltwater samples are used to reconstruct the subglacial environment, making sampling location and strategy critical to ensure samples, and subsequent interpretation, represent the subglacial environment. Proglacial outflow, especially when sampled near the glacial terminus, is assumed to consist solely of glacial melt with negligible input from other water sources. Field measurements of radiogenic ^{222}Rn activity concentrations in meltwater from Kiattuut Sermiat (KS), an outlet glacier from the southern Greenland Ice Sheet, reveal potential groundwater incursion into a proglacial stream. Measured in-field ^{222}Rn activity concentrations were compared to activity concentrations generated from laboratory slurry experiments using sediments collected from KS, revealing high in-field measurements cannot be generated by sediments collected at the glacier terminus. However, measured ^{222}Rn activity concentration from presumed groundwater collected near the sampling sites yielded values ~8x higher than proglacial waters sampled from the terminus, suggesting a mixing of the two waters.

When combined with laboratory measurements of maximum possible ^{222}Rn activity concentrations using glacial sediments, in-field ^{222}Rn activity concentration measurements may be used to qualitatively evaluate subglacial water residence times. As illustrated by samples collected from the southwestern Greenland Ice Sheet, this method is applicable only if the subglacial lithology contains ^{226}Ra, the parent atom of ^{222}Rn. Finally, comparisons of elemental concentrations between Kiattuut Sermiat samples collected in 2013, 2015, and 2018 with leachate waters derived from laboratory slurry experiments reveal effects on measurements due to pore size

of filters used (0.45 μm versus 0.2 μm). As elemental concentrations in glacial meltwater are used to calculate fluxes of nutrients to the ocean, filter size used should be an important consideration in the design of future glaciochemical research.

Introduction

Polar amplification of global warming (e.g. Bekryaev et al., 2010; Holland and Bitz, 2003; Screen and Simmonds, 2010) has accelerated glacial melting. Much recent effort has focused on understanding meltwater routes and storage within the Greenland Ice Sheet (GrIS) (Chu, 2014; Nienow et al., 2017). Availability, distribution, and volume of GrIS meltwater is positively correlated with glacial velocity, resulting in inter-annual rates of mass loss dependent on extent of melting (Davison et al., 2019; Schoof, 2010). The generated meltwater can flow over the ice surface, or through englacial and subglacial conduits. This water may be rapidly discharged to the ocean, stored within the glacial system, or refrozen into the glacier.

Tracing en- and subglacial hydrologic systems is complicated by their size and large volumes of water flowing through the systems, in addition to their obstruction from view. Thus investigations of subglacial water fluxes often use tracers (e.g. Chandler et al., 2013; Cowton et al., 2013), measurements of subglacial water pressure (e.g. L. C. Andrews et al., 2014; Meierbachtol et al., 2013), and both measurements and models of ice velocity (e.g. Bartholomew et al., 2010; Zwally et al., 2002). Frequently utilized introduced tracers include fluorescent dyes and sulfur hexafluoride gas. These compounds yield breakthrough curves that can be used to evaluate connectivity of the subglacial hydrologic network: short, broad peaks indicate inefficient distributed networks and tall, sharp peaks indicate efficient channelized networks capable of quickly evacuating water (Chandler et al., 2013).

Evaluations of subglacial hydrologic systems require access to the subglacial environment, which can be achieved through moulins and drilled boreholes. Moulins are used for both tracer injections and to measure subglacial water pressure through hydraulic head fluctuations (e.g. L. C. Andrews et al., 2014). A GrIS subglacial hydrologic network was found to develop throughout the melt season toward a moulin 41 km up-ice (Chandler et al., 2013). Initial "slow" water velocity of 0.25 m s^{-1} in this study is still an order of magnitude faster than water velocities measured from tracer injections into a distributed subglacial drainage system at an alpine glacier (South Cascade Glacier, Washington, USA) in 1987 (Fountain, 1993), suggesting moulins may connect to an already partially channelized network (Gulley et al., 2009). Diurnal variations in borehole hydraulic head reveal variations in subglacial channel pressure, but hydraulic head is correlated with increases in subglacial pressure in some boreholes and anti-correlated in others (Gordon et al., 1998), complicating interpretations. While methods relying on moulins and boreholes are naturally limited in spatial distribution, glacial surface velocity measurements integrate velocity-influencing hydrologic changes across the entirety of the glacier. Field studies have correlated surface velocity changes to surface melting rates (e.g. Bartholomew et al., 2010; Shepherd et al., 2009) supporting computational studies showing increased subglacial water volumes increase ice surface velocity (e.g. Parizek and Alley, 2004; Schoof, 2010). Neither field nor computation studies however directly address the residence time of subglacial water.

Subglacial water residence time is a function of subglacial hydrologic network configuration: well-connected, arborescent drainages can accommodate large volumes of meltwater, efficiently routing it to the terminus. Conversely, poorly-connected drainages are distributed over larger areas of the bed, routing smaller volumes of water less efficiently and more slowly, requiring longer residence times to reach the terminus. Thus, subglacial water residence time may serve as a proxy for the degree of connectivity of the subglacial network, with implications

for sliding velocity. Subglacial residence time can be qualitatively evaluated through varying concentrations of chemical weathering products. Ice melt initially has low concentrations of solute and thus is typically undersaturated with respect to minerals in comminuted sediment in subglacial environments. Mineral weathering imparts chemical signatures to melt depending upon minerals present and length of reaction time (e.g. Anderson et al., 1997; Hatton et al., 2019; Yde et al., 2014). This dependence on mineralogical composition as well as grain size and starting meltwater compositions complicates the process of using weathering reactions as a tracer for subglacial water residence time. An ideal tracer for residence time would behave conservatively, is ubiquitous in the subglacial environment, and delivered to subglacial water at rates that depend solely on residence time.

Uranium (U) is one such conservative tracer as a common radioactive trace element in Earth's crust (Rudnick and Gao, 2003). Its highest abundance isotope (^{238}U), decays through a series of short-lived daughter products to stable ^{206}Pb. One daughter isotope, ^{222}Rn is a short lived radioactive noble gas ($t_{1/2}$ = 3.82146 ± 0.00020 days) (Bellotti et al., 2015) derived from the radioactive decay of ^{226}Ra ($t_{1/2}$ = 1600 ± 7 years) (Duchemin et al., 1994). Secular equilibrium with ^{226}Ra will thus occur in ~20 days. As a noble gas, ^{222}Rn is not bound by chemical reactions. Therefore its concentration in outflow water should depend only on residence time and the concentration of ^{226}Ra, making it a potentially powerful tracer for subglacial water residence time.

The dependence of ^{222}Rn concentration on parent ^{226}Ra concentration limits its ability to provide absolute values of residence times. However, ^{222}Rn activity concentration (hereafter referred to as ^{222}Rn concentration) in outflow water from a specific glacier should increase in a more distributed network with long residence times and decrease in a more channelized network with short residence times. Therefore, ^{222}Rn concentrations in glacial outflow can provide qualitative information about subglacial water residence times up to ~20 days (e.g. Arendt et al.,

2015; Bhatia et al., 2011; Linhoff et al., 2017). Subglacial water requires contact with ^{226}Ra bearing sediment to dissolve ^{222}Rn and may exsolve ^{222}Rn when in contact with the atmosphere, ensuring measured ^{222}Rn concentrations reflect subglacial, not englacial, storage. Measured ^{222}Rn concentrations will depend on (1) water-rock contact time, (2) ^{226}Ra concentrations in subglacial bedrock and sediments, and (3) water-rock contact area.

Previous work has used ^{222}Rn to trace groundwater inputs to larger water bodies (e.g. Burnett and Dulaiova, 2003; Dimova et al., 2013) as ^{222}Rn in present in groundwater in concentrations frequently 1000x or greater than ^{222}Rn concentrations in surface waters (Burnett and Dulaiova, 2003) As such, aqueous ^{222}Rn concentrations in glacial outflow can reveal groundwater input that may not be discernable through other measurements. Water sample collected at glacial termini are presumed to consist of only glacial meltwater with chemical interpretations then used to reconstruct the subglacial environment. Identifying a groundwater component has implications for conclusions made about water history in the subglacial environment. In this paper we use aqueous ^{222}Rn concentrations from multiple glaciers in addition to results from laboratory experiments to evaluate the use of ^{222}Rn to qualitatively record subglacial water residence time, and investigate potential groundwater contributions to glacial outflow.

Methods

Sampling Locations

^{222}Rn concentrations were measured in the headwaters of the outflow river at the terminus of Kiattuut Sermiat (KS), an outlet glacier from the GrIS in south Greenland, in 2013, 2015, and 2018 with electronic radon detectors (Figure II-1B). Concentrations were measured with Durridge RAD7 instruments equipped with a RAD H_2O. All RAD7s had been calibrated by the Durridge company 2-3 months prior to field sampling.

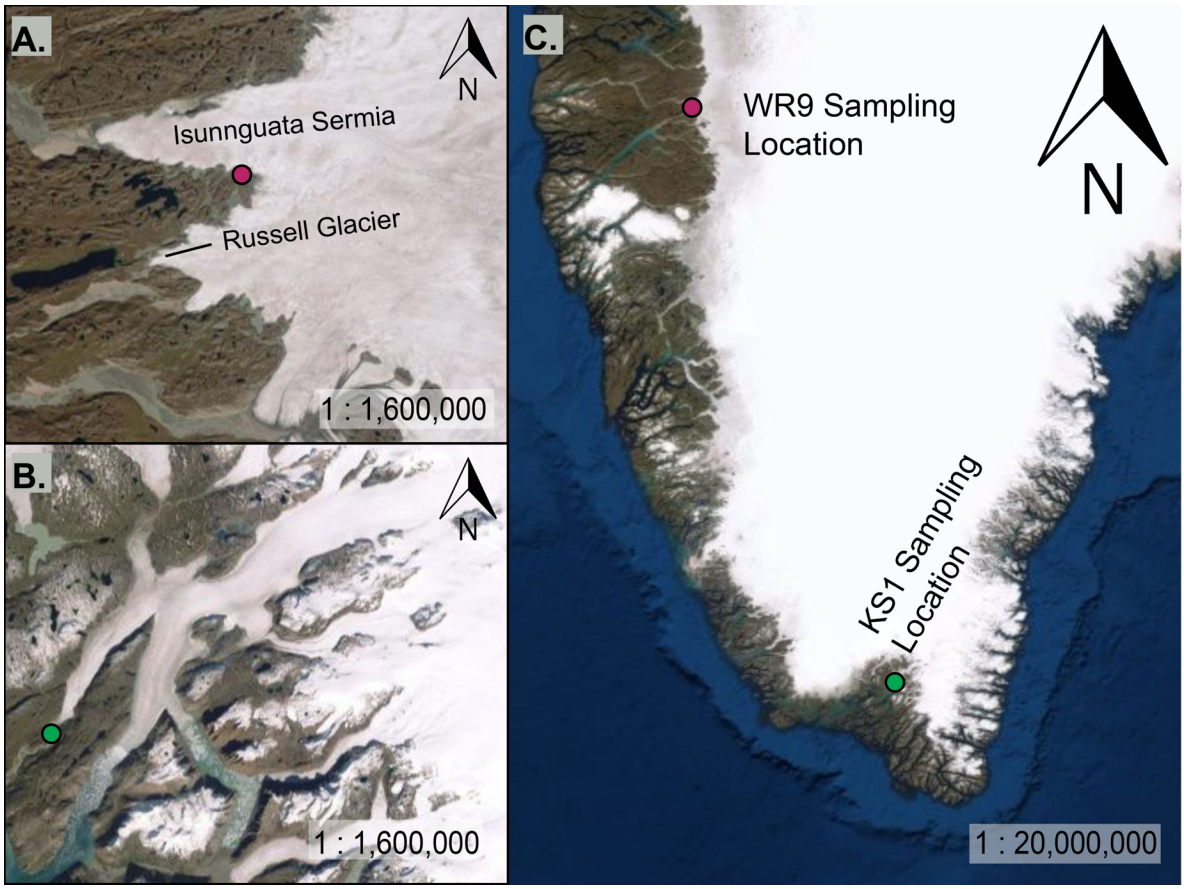

Figure II-1: Location map of southern Greenland (C.). Pink circle marks 2018 WR9 sampling location; inset (A.) shows location between outlet glaciers Isunnguata Sermia and Russell Glacier. Green dot marks KS1 sampling location used in 2013, 2015, and 2018; inset (B.) shows location at the terminus of Kiattuut Sermiat.

2013 samples were collected on days of year (DOY) 200, 201, 202, 203, and 205 from 61.20777°N, 45.32942°W and published in (Arendt et al., 2018). The sampling location was the closest shoreline access point to the glacial terminus (pers. comm. with Dr. Emily Stevenson). Samples from 2015 are comprised of 15 measurements collected between DOY 217 and 266 from a rock in the middle of the river (61.20932°N, 45.3299°W) accessed by boat. 2018 samples were collected on DOY 209, 210, 211, 213, and 216 from site KS1 (61.20646°N, 45.33051°W) at the river bank as close to the KS terminus as possible. Replicate samples were collected on DOY 209, 213, and 216; time of collection was noted and delayed analyses were multiplied by a ^{222}Rn time-

dependent decay correction factor to account for radioactive decay between collection and analysis.

Water samples for ^{222}Rn analysis were collected from a ~2.5 km long transect down the Kiattuut Sermiat river on July 29 & 30, 2018 (DOY 210 & 211). Sampling occurred at KS1-Toe, a sample site as far upstream as physically possible but removed from the thalweg (61.20708°N, 45.32980°W), KS1 (61.20646°N, 45.33051°W) ~100 m downstream, KS2 (61.19977°N, 45.33097°W) ~0.75 further km downstream, and KS3 (61.19656°N, 45.35685°W), ~ 1.6 km downstream from KS2. KS3 was on a point bar in a river meander; the point bar ground surface contained grasses and vegetation. Samples were collected from the bank but as far offshore as possible to reach flowing water. At KS3 (61.19656°N, 45.35685°W), an additional sample (KS3-GW, 61.19656°N, 45.35685°W) was collected as water seeped from the bank into a ~30 cm deep hole which was dug into the river bank. After ~30 minutes of flow the water became clear and was collected for ^{222}Rn analysis.

^{222}Rn was measured on July 15, 16, 18 and August 9, 2018 (DOY 196, 197, 199, 221) in meltwater emanating from the GrIS at sample site WR8 at the headwaters of the Watson River (67.15735°N, 50.05697°W), between outlet glaciers Isunnguata Sermia and Russell Glacier in west Greenland (Figure II-1A).

Sampling and Analytical Protocol

Samples were collected by submerging a 250 mL bottle in the river and capping underwater to prevent ^{222}Rn diffusion. Samples were visually inspected for bubbles, and discarded and recollected if bubbles were present. All analyses began within ~30 minutes of collection. Prior to analysis the RAD7 was purged with dried air until internal relative humidity was <10%, then samples were run using the pre-programmed WAT250 program.

Lab ^{222}Rn Experiments

Slurry experiments (e.g. Hammond and Fuller, 1979) were conducted on sediment from KS and WR to evaluate potential sedimentary contributions to ^{222}Rn concentrations. KS sediments were collected in 2015 as near as possible to the site of the water samples (sample location KS1; 61.20646°N, 45.33051°W). Collected sediments were mostly fine-grained, containing <10 pieces of gravel per kilogram. WR8 sediments were collected in 2018 and were predominately sand-sized. For all experiments, sediment size was constrained by first wet sieving through a 500 µm sieve to remove sparse gravels, then wet sieving <500 µm sediments through a 63 µm sieve. For KS samples, fines (< 63 µm) and sand (63 – 500 µm) fractions were sieved into pre-cleaned Pyrex dishes, then dried in an oven at 80°C. Fine sample mass from WR8 was too small for experiments, so WR8 size fractions used were sand (63 – 500 µm) and bulk (sand plus the small mass of fines present). These fractions, in pre-cleaned Pyrex dishes, were dried in an oven at 80°C. Once dried, each sediment sample was homogenized by mixing and subsequently divided in half: one half remained as-is (specified size fractions) and the other half was crushed in a shatterbox. Prior to use, the shatterbox was brushed out, wiped clean with ethanol, and allowed to air dry. A small subsample of each sediment fraction was crushed and subsequently discarded to ensure no contamination. The remainder of each sample was then crushed to a fine powder.

Approximate 26 g of sediments were added to 250 mL glass bottles, which were then filled with 18.2 MΩ deionized water (Table II-1). Once filled, bottles were placed on a shaker table and left to react for > 20 days, when secular equilibrium with ^{226}Ra was assumed. ^{222}Rn concentrations were then measured in each sample using a RAD7 instrument equipped with a RAD H_2O using the WAT250 program to duplicate methodology for field measurements. Following measurements, water lost during the experiment was replaced with 18.2 MΩ deionized water. The bottles were recapped ensuring no headspace without adding additional sediment (Table II-1). Bottles were again shaken for > 20 days to duplicate the experiment.

Measured ^{222}Rn activity concentrations using the WAT250 program on the RAD7 are reported assuming a sample water volume of 250 mL. As 250 mL glass vessels were used as reaction chambers and therefore contained < 250 mL of water, measured ^{222}Rn concentrations were adjusted to reflect the volume of water present in each bottle. Measured concentrations were scaled by the volume of water in each bottle calculated by mass difference (Table II-1), and reported as pCi L^{-1}.

Table II-1: Comparison of experiment design for ^{222}Rn generation from sediments collected at southern Greenland outlet glacier KS and sampling location WR8.

Sample	**Sieved Sediment Size (μm)**	**Sediment Mass (g)**	**Water Mass (g)**	**Total Mass (g)**
KS-Fines	<63	26.68	239.09	265.77
KS-Sand	63 – 500	26.32	238.71	265.03
KS-Crushed Sand	63 – 500	26.78	239.28	266.06
WR8-Bulk	< 500	26.25	240.27	266.52
WR8-Crushed Bulk	< 500	26.35	239.83	266.18
WR8-Crushed Sand	63 – 500	26.25	240.53	266.78
Experiment 2 – no change in sediments from Experiment 1			**Water Mass Added (g)**	
KS-Fines			7.79	265.45
KS-Sand			7.93	265.56
KS-Crushed Sand			7.53	265.90
WR8-Bulk			7.32	266.58
WR8-Crushed Bulk			6.77	266.53
WR8-Crushed Sand			7.35	266.96
WR8-Sand	63 – 500	26.56	240.00	266.56

Elemental Concentration Measurements

2013 field samples were filtered in-field through 0.2 μm filters and acidified with distilled HCl (Aciego et al., 2015). Elemental concentrations were measured from 3 mL samples on a Thermo Scientific ELEMENT2 ICP-MS at the University of Michigan, as described in Aciego et al., (2015). 2015 samples were also filtered in the field through 0.2 μm filters and acidified to pH <2 with distilled HCl. Elemental concentrations were then measured at Cambridge University on

a Perkin Elmer Nexion 350D quadrupole-based ICP-MS. Samples were run multiple times on subsequent days to ensure replication; bracketing standards and acid blanks were used to ensure accurate measurements. 2018 field samples were filtered through 0.45 μm trace metal grade canister filters and acidified with Optima HNO_3 to pH < 2. Cation concentrations were then measured at the University of Florida on a Dionex ICS-1600 ion chromatograph. Calibration curves were determined using repeated analyses of a diluted Dionex multi-element standard and custom multi-element standards. Results from duplicate samples measured within 5%.

Elemental concentrations were measured on water derived from the slurry experiments. Slurry water was filtered through two distinct filter sizes: 0.45 μm filters, similar to 2018 field samples, and 0.2 μm filters, similar to 2013 and 2015 field samples. Elemental analysis of leachate waters from laboratory experiments were measured at the University of Michigan MEAL lab on a Thermo Scientific iCAPQ ICP-MS. Subsamples were filtered with either 0.45 μm Millex PVDF Durapore filters or 0.22 μm Restek PVDF filters, then acidified with 2% Optima grade nitric acid. Samples were analyzed using a collision cell in KED mode with He gas. Mass drift was corrected with bracketing standards.

Results

^{222}Rn Concentrations in Stream Water

^{222}Rn activity concentrations from 2013, 2015, and 2018 vary by an order of magnitude, with the lowest average and smallest range measured in 2015 mid-river samples (mean = 7.29 pCi L^{-1}) and the highest average and largest range from 2018 river edge samples (mean = 106.65 pCi L^{-1}) (Figure II-2). 2013 river edge measurements fall between the two other years with a mean of 25.14 pCi L^{-1} and an intermediate range (Figure II-2; Table II-2). River transect ^{222}Rn concentrations decrease from 106.7 to 104.5 pCi L^{-1} between KS1-Toe and KS1 and to 92.7 pCi L^{-1} downstream

at sampling location KS2 (Figure II-3). However, ^{222}Rn increased to 244.0 pCi L^{-1} at KS3 (Figure II-3, Table II-3) and 809.0 pCi L^{-1} at KS3-GW (Figure II-3). ^{222}Rn concentrations at WR8 were low with at least one sample measuring 0 pCi L^{-1} within one standard deviation (Figure II-4A).

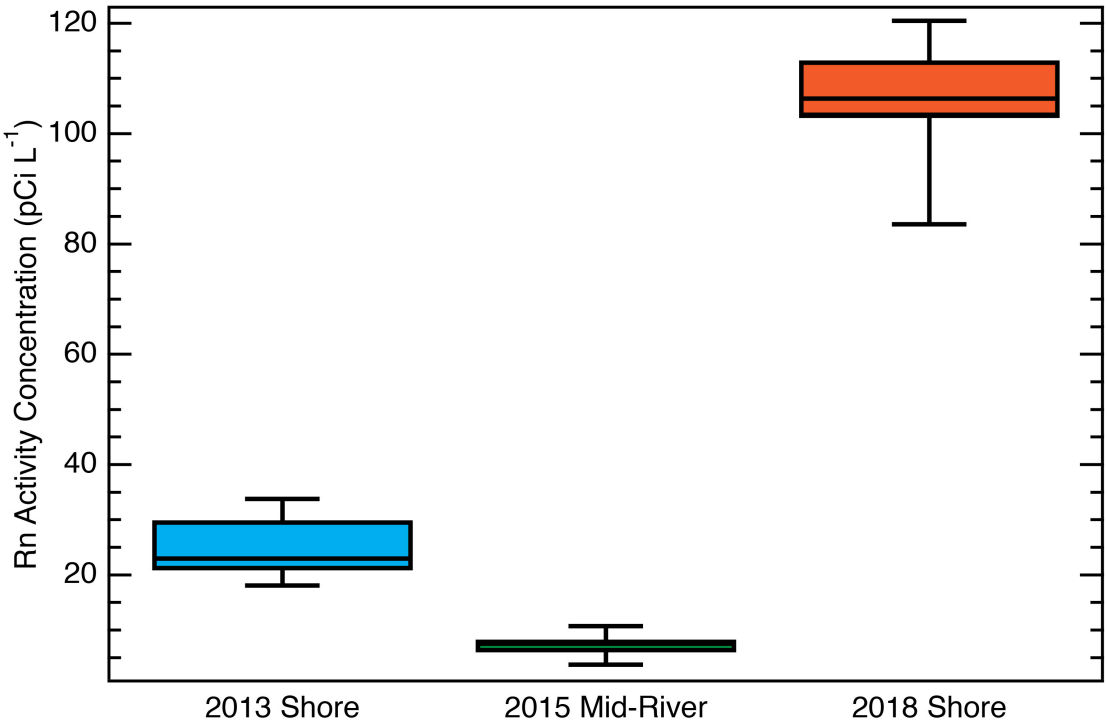

Figure II-2: Boxplot with ^{222}Rn concentrations from KS outflow. Lower box bounds are drawn at the first quartile and upper bounds at the third quartile; mean values are represented by horizontal lines within boxes. Whiskers below and above boxes represent the minimum and maximum data values, respectively. 2013 data reproduced from Arendt et al., (2018). 2013 data (n = 5, collected from DOY 200 – 205) have a mean value of 25.1 pCi L^{-1}, 2015 (n = 15, collected from DOY 217 – 266) mean is 7.25 pCi L^{-1}, and 2018 (n = 10, collected from DOY 209 – 216) mean is 106.7 pCi L^{-1}. Samples were collected from the river edge in 2013 and 2018, and from the center of the outflow river in 2015.

Table II-2: Measured 222Rn activity concentrations at the KS terminus from 2013, 2015, and 2018. 2013 data published in Arendt et al. (2018).

Year	DOY	Latitude (° N)	Longitude (° W)	^{222}Rn Activity Concentration (pCi L^{-1})	1σ Standard Deviation
2013	200	61.20777	45.32942	21.00	11.5
2013	201	61.20777	45.32942	18.10	9.06
2013	202	61.20777	45.32942	33.80	15.9
2013	203	61.20777	45.32942	23.00	6.1
2013	205	61.20777	45.32942	29.80	12.6
2015	217	61.20932	45.3299	7.55	5.66
2015	221	61.20932	45.3299	8.16	0.29
2015	224	61.20932	45.3299	3.22	1.38
2015	231	61.20932	45.3299	6.15	2.63
2015	234	61.20932	45.3299	6.00	3.35
2015	237	61.20932	45.3299	6.13	2.96
2015	240	61.20932	45.3299	6.13	2.17
2015	243	61.20932	45.3299	7.24	4.3
2015	246	61.20932	45.3299	11.10	4.83
2015	248	61.20932	45.3299	8.00	4.06
2015	252	61.20932	45.3299	10.30	6.05
2015	256	61.20932	45.3299	8.16	4.41
2015	262	61.20932	45.3299	4.45	2.36
2015	264	61.20932	45.3299	8.32	2.83
2015	266	61.20932	45.3299	7.86	4.42
2018	209-A	61.20708	45.3298	103.00	6.94
2018	209-B	61.20708	45.3298	113.17	11.2
2018	209-C	61.20708	45.3298	118.99	10.1
2018	210	61.20646	45.33051	103.00	10.2
2018	211	61.20646	45.33051	104.57	8.44
2018	213-A	61.20646	45.33051	108.66	14
2018	213-B	61.20646	45.33051	120.48	25.8
2018	214	61.20646	45.33051	108.20	18.6
2018	216-A	61.20646	45.33051	83.60	4.91
2018	216-B	61.20646	45.33051	102.81	2.08

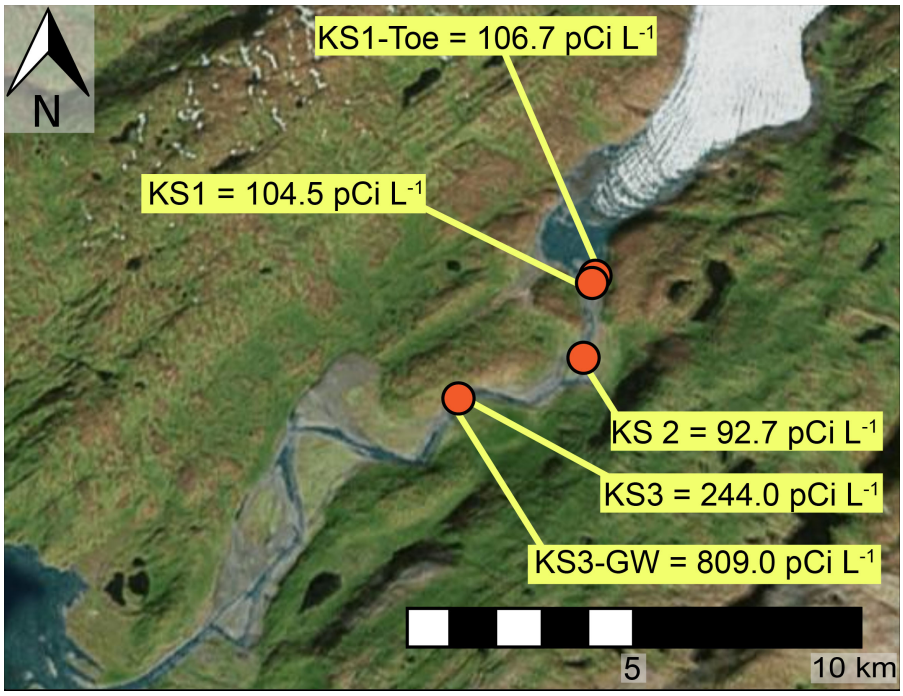

Figure II-3: Location map showing the KS terminus with locations marked for both near-terminus (KS1 and KS1-Toe) and down river (KS2, KS3, and KS3-GW) sampling locations. ^{222}Rn concentrations measured at each location are marked; reported concentrations are averages for sites with multiple measurements (KS1, KS1-toe, and KS2).

Table II-3: ^{222}Rn activity concentrations measured at KS terminus and down a transect of the KS proglacial river.

Sample*	Date (m/d/y)	1σ Standard Deviation	^{222}Rn Activity Concentration (pCi L^{-1})	Daily average ^{222}Rn Activity Concentrations (pCi L^{-1})
KSToe-1_A	7/28/18	6.94	103.0	111.7
KSToe-1_B	7/28/18	11.2	113.2	
KSToe-1_C	7/28/18	10.1	119.0	
KS1-1	7/29/18	10.2	103.0	103.0
KS1-2	7/30/18	8.44	104.6	104.6
KS1-3_A	8/1/18	14.0	108.7	114.6
KS1-3_B	8/1/18	25.8	120.5	
KS1-4	8/2/18	18.6	108.2	108.2
KS1-5_A	8/4/18	4.91	83.6	93.2
KS1-5_B	8/4/18	2.08	102.8	
KS2-1	7/29/18	7.94	105.0	105.0
KS2-2	8/2/18	11.1	80.4	80.4
KS3-1	7/30/18	26.3	244.0	244.0
KS3-GW	7/30/18	89.9	809.0	809.0

*Naming convention: Sample Location – Sample Number_A,B,C for duplicate samples collected concurrently

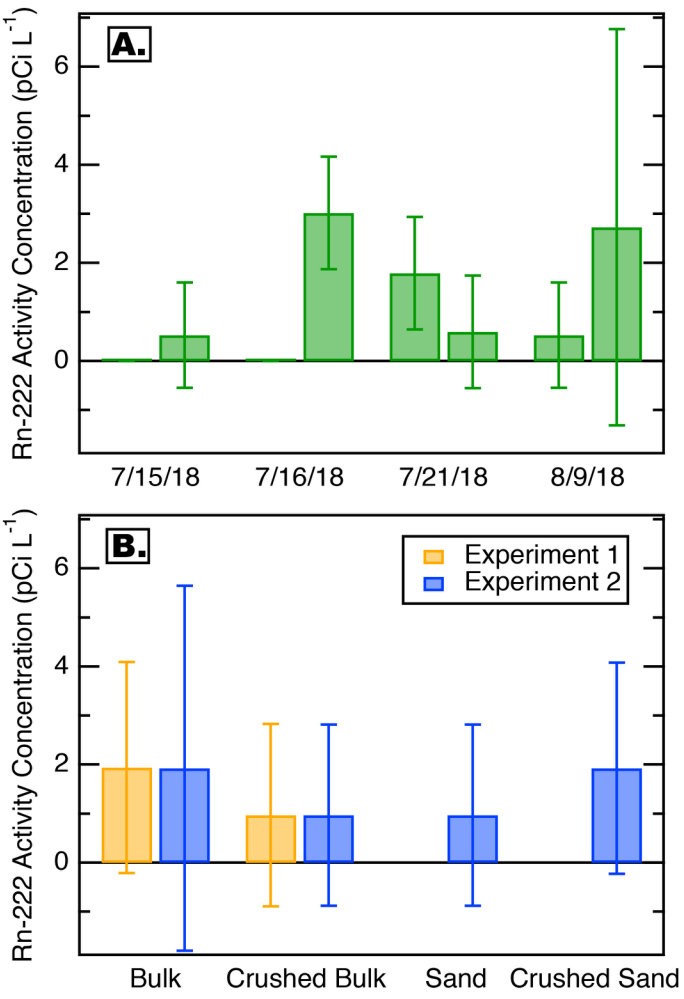

Figure II-4: A.) ^{222}Rn concentrations measured at sampling location WR8 in 2018; duplicate samples were measured each day. Bar tops mark measured concentrations, error bars designate one standard deviation. B.) Results from ^{222}Rn laboratory experiments using sediments collected at WR8 on August 9, 2018. Bar tops mark measured concentrations, error bars designate one standard deviation. Field sediments were predominately sand sized with few fines. Sieved sizes used in experiments were bulk sediments, crushed bulk sediments, sand (63 – 500 µm), and crushed sand. Results of the first experiment for bulk and crushed bulk sediments are plotted as yellow bars; results from crushed sand were discarded (see text) and no sand fraction was analyzed in experiment one. Results from a repeat experiment are plotted as blue bars; no changes were made to sediments used from the first experiment but a new vessel was set up to evaluate the sieved sand fraction.

^{222}Rn Concentrations in Slurry Experiments

^{222}Rn concentrations produced during the slurry experiments vary as a function of grain size (Table II-4). Fines (< 63 µm) generated the highest ^{222}Rn concentrations (Figure II-5) with a mean value of 41.96 pCi L^{-1} and a standard deviation of 19.8. Crushed sand generated the lowest ^{222}Rn concentrations (Figure II-5) (mean value 10.19 pCi L^{-1}; standard deviation 4.2). Whole sand (63 – 500 µm) generated ^{222}Rn concentrations similar to crushed sand values (Figure II-5), but was marginally higher with a mean concentration of 13.60 pCi L^{-1}; standard deviation 6.8).

Table II-4: Comparison of results from ^{222}Rn generation experiments using different grainsizes from the southern Greenland outlet glacier, KS and sample location WR8 adjacent to the GrIS.

Sample	Days Reacted	^{222}Rn (pCi L^{-1})	1σ Standard Deviation
KS-Fines	33	43.92 40.00*	10.7 25.9*
KS-Sand	33	13.61 13.58*	6.42 7.08*
KS-Crushed Sand	33	10.66 9.72*	3.58 4.81*
WR8-Bulk	33	1.94 1.93*	2.15 3.72*
WR8-Crushed Bulk	33	0.97 0.97*	1.86 1.85*
WR8-Sand	33	0.97	1.85
WR8-Crushed Sand	33	~~30.04~~† 1.93	~~12.8~~† 2.15

* Second reaction experiment run to compare duplicate results
† Values excluded; see text

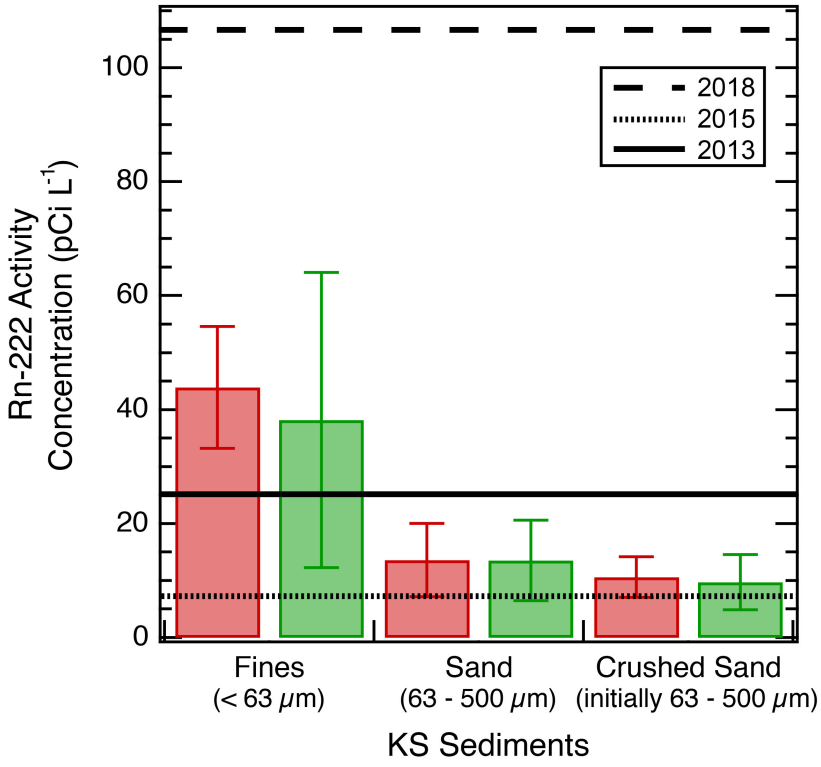

Figure II-5: Histogram results from ^{222}Rn generation laboratory experiments 2015 KS sediments. Top of bars note measured ^{222}Rn concentrations, error bars show one standard deviation. Red bars are results from the first experiment, green bars are results from repeat experiment; no change in sediments used between experiments. Sediment sizes used are fines (< 63 μm), sand (63 – 500 μm), and freshly crushed sand. Mean ^{222}Rn concentrations measured at the KS terminus are plotted as horizontal lines: 2018 (106.7 pCi L^{-1}, dashed line), 2015 (7.25 pCi L^{-1}, dotted line), and 2013 (25.1 pCi L^{-1}, solid line).

Excluding the first crushed sand slurry experiment with WR8 sediment, all WR8 ^{222}Rn equilibration experiments generated little ^{222}Rn regardless of sediment size fraction (Figure II-4B). The first crushed sand experiment generated ^{222}Rn concentrations of 30.04 pCi L^{-1} but the same sediment during the repeat experiment generated concentrations of only 1.93 pCi/L. We have excluded this anomalous sample from further analyses. Bulk sediments and crushed sand (63 – 500 μm) size fractions had the highest ^{222}Rn concentrations at 1.93 pCi L^{-1}; crushed bulk sediments and the sand fraction contained half as much ^{222}Rn with concentrations of 0.97 pCi L^{-1} (Figure II-4B). All experimental concentrations were less than one standard deviation from 0 pCi L^{-1} (Figure II-4B).

Stream Water and Leachate Solute Concentrations

Elemental concentrations of meltwater (n = 4) collected in 2013 are more variable than meltwater (n = 17) collected in 2015 (Figure II-6), but ratios of different elements are similar (Figure II-6). Greatest variations in concentrations occur with Al, P and Fe, which also have the lowest concentrations (Figure II-6). Experimental leachate waters display different proportions of elements depending on grain size used in each experiment, and differ from proportions observed in natural waters (Figure II-6, Table II-5). Ca and Sr concentrations from sand and crushed sand experiments are lower than concentrations measured from field samples while other elements in all size fractions exhibit higher concentrations than natural waters (Figure II-6).

Elemental concentrations in leachate water are greater when filtered through 0.45 μm than when filtered through 0.2 μm for both the sand and the crushed sand size fractions (Figure II-7). Variation in filter size does not appear to greatly affect elemental concentrations in the fine (<63 μm) size fraction (Figure II-7). < 0.2 μm elemental concentration derived from the crushed sand are up to six times greater than the uncrushed sand experiments and even larger when filtered through 0.45 μm filters (Figure II-7, Table II-5).

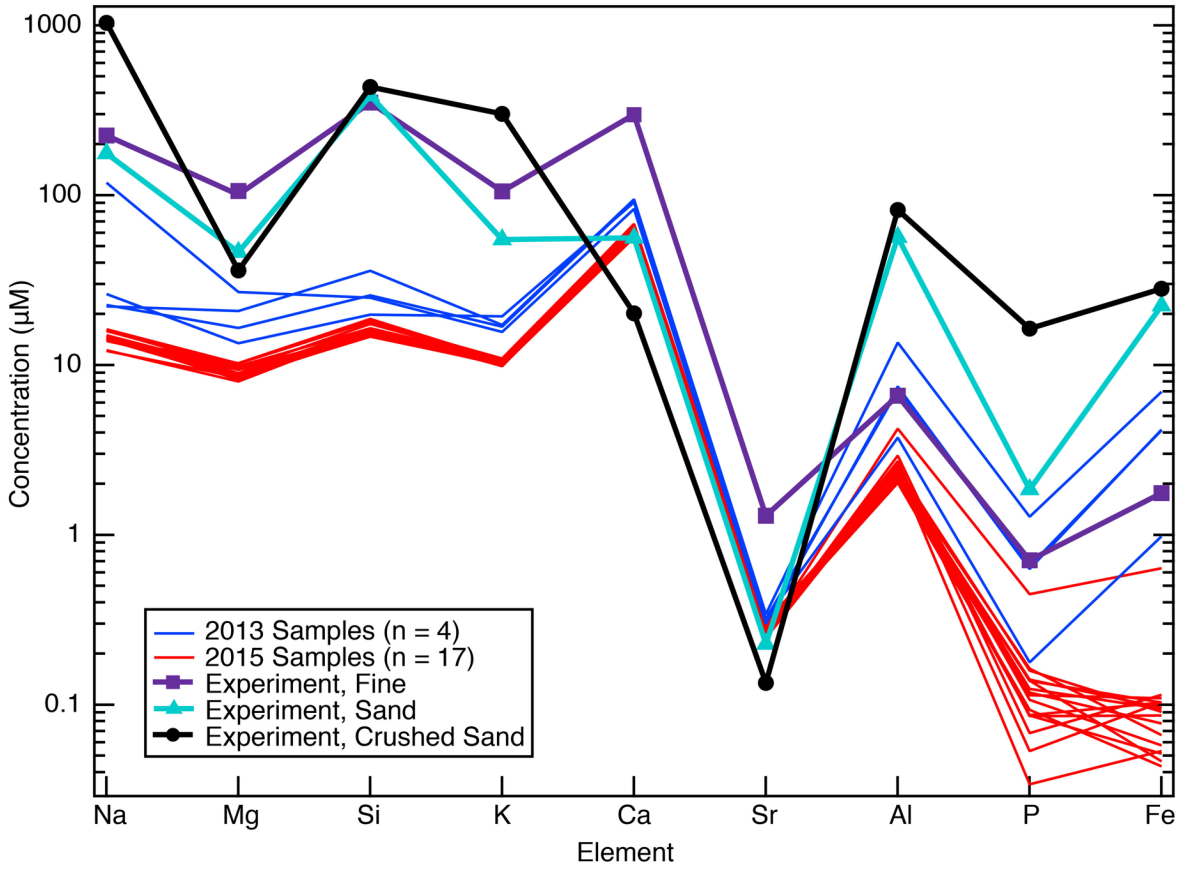

Figure II-6: Concentrations of Na, Mg, Si, K, Ca, Sr, Al, P, and Fe from 2013 (blue lines) and 2015 (red lines) are plotted along with concentrations of same elements from leachate waters after laboratory ^{222}Rn generation experiments. Leachate water from experiment vessel with fine sediment fraction (< 63 µm) marked in purple with square markers, sand sediment fraction (63 – 500 µm) in teal with triangle markers, and crushed sand in black with circle markers. 2013 data is reproduced from Aciego et al., (2015). All samples were filtered through 0.45 µm filters prior to analysis.

Table II-5: Elemental concentrations in leachate waters from ^{222}Rn generation experiments and KS proglacial samples collected in 2013, 2015, and 2018.

Sample Name*	Na (uM)	Mg (uM)	Al (uM)	Si (uM)	P (uM)	K (uM)	Ca (uM)	Fe (uM)	Sr (uM)
Exp 2015 Sand (0.45)	158.1	56.9	77.7	438.3	2.1	75.8	59.5	28.7	0.2
Exp 2015 Crushed Sand (0.45)	1097.4	71.9	180.3	837.9	18.7	354.5	39.5	56.6	0.3
Exp 2015 Fines (0.45)	176.9	106.1	20.7	362.9	1.1	109.5	296.6	7.1	1.3
Exp 2015 Sand (0.2)	175.9	46.3	56.5	385.1	1.8	54.8	56.0	22.3	0.2
Exp 2015 Crushed Sand (0.2)	1033.5	36.0	81.9	434.0	16.4	300.5	20.2	28.1	0.1
Exp 2015 Fines (0.2)	224.3	100.8	6.6	351.3	0.7	105.5	297.9	1.8	1.3
Field 2013-201 (0.2)	22.1	20.8	13.6	36.0	1.3	17.2	94.6	7.0	0.3
Field 2013-202 (0.2)	26.2	13.5	3.7	19.8	0.2	19.4	90.8	1.0	0.3
Field 2013-203 (0.2)	22.5	16.5	7.1	25.7	0.6	16.9	93.3	4.2	0.3
Field 2013-205 (0.2)	118.3	26.9	7.5	24.9	0.7	15.6	83.1	4.1	0.3
Field 2015-217 (0.2)	12.1	8.5	2.4	16.3	0.1	9.8	60.8	0.1	0.2
Field 2015-221 (0.2)	14.6	8.9	2.4	14.7	0.0	10.1	64.1	0.1	0.3
Field 2015-224 (0.2)	14.2	8.4	2.7	15.5	0.1	10.2	59.5	0.1	0.3
Field 2015-231 (0.2)	13.9	9.4	4.2	14.9	0.4	10.0	61.1	0.6	0.3
Field 2015-234 (0.2)	14.4	8.2	2.3	15.5	0.1	10.1	57.2	0.1	0.3
Field 2015-237 (0.2)	14.5	8.4	2.9	15.4	0.1	10.0	59.2	0.1	0.3
Field 2015-240 (0.2)	14.5	8.5	2.3	14.7	0.2	10.3	59.9	0.1	0.3
Field 2015-243 (0.2)	14.8	9.0	2.5	16.4	0.2	10.3	61.3	0.1	0.3
Field 2015-246 (0.2)	14.5	8.6	2.6	16.3	0.1	10.3	61.4	0.1	0.3
Field 2015-248 (0.2)	14.1	8.4	2.6	14.9	0.1	10.1	57.8	0.1	0.3
Field 2015-252 (0.2)	12.2	8.0	2.3	15.9	0.1	9.9	56.4	0.1	0.3
Field 2015-256 (0.2)	14.4	8.9	2.2	15.6	0.1	10.1	61.3	0.1	0.3
Field 2015-258 (0.2)	16.0	9.5	2.1	15.3	0.1	10.9	63.0	0.0	0.3
Field 2015-260 (0.2)	15.0	9.4	2.2	17.4	0.1	10.7	61.9	0.1	0.3
Field 2015-262 (0.2)	15.9	9.8	2.2	16.5	0.1	10.8	63.1	0.1	0.3
Field 2015-264 (0.2)	16.2	10.2	2.2	18.0	0.1	10.9	67.2	0.1	0.3
Field 2015-266 (0.2)	14.2	10.2	2.0	18.7	0.1	10.7	67.7	0.0	0.3
Field 2018-210 (0.45)	17.9	13.6				13.9	80.8		

* Naming Conventions: Exp(erimental) samples, year collected, size fraction (filter pore size). Field data; year collected – DOY collected (filter size in μm).

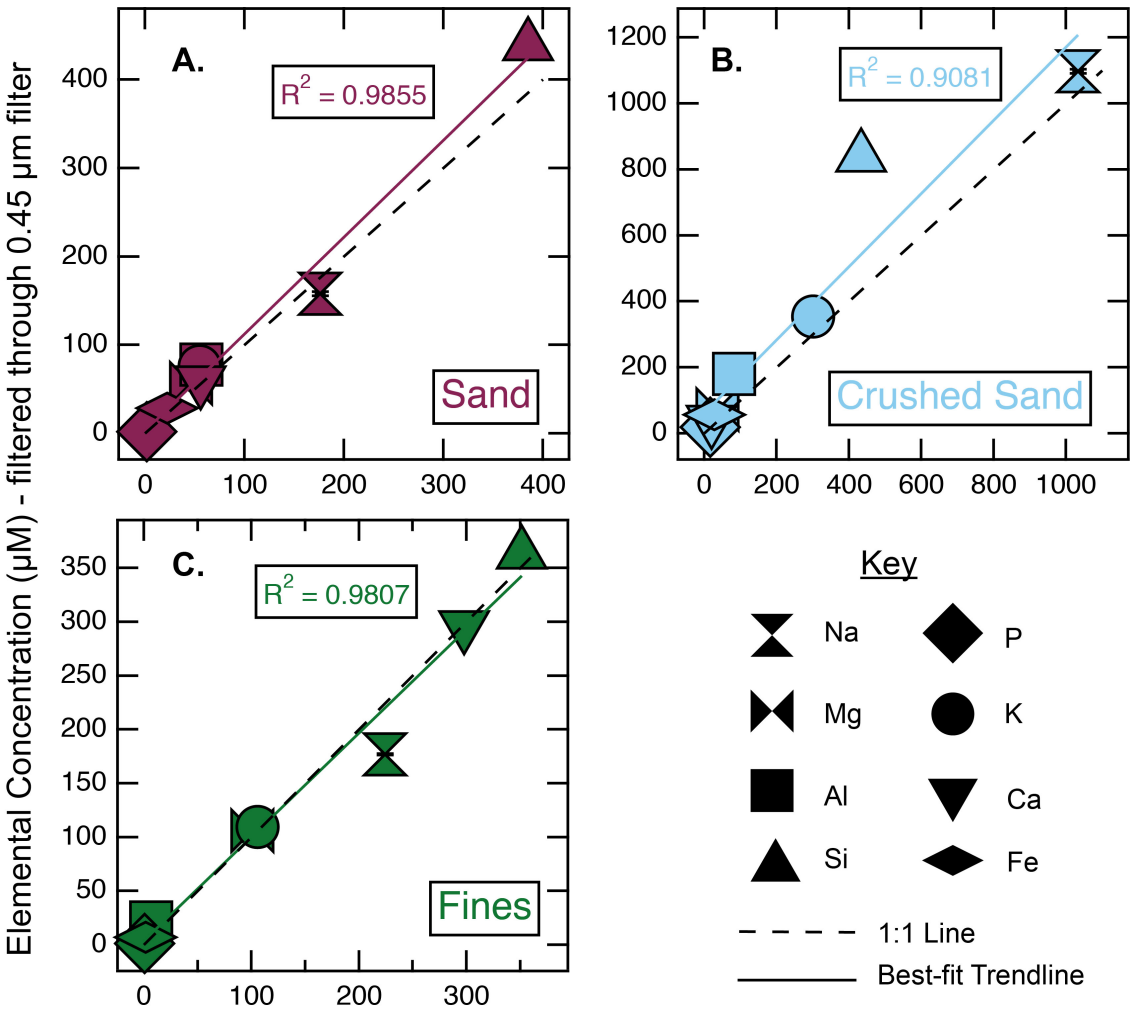

Figure II-7: Elemental concentrations of leachate waters from ^{222}Rn generation experiments using KS sediments. A.) Leachate results from experiment with sand-sized sediments (63 – 500 µm) – maroon, B.) results from experiment with crushed sand – blue, C.) results from experiment with fine sediments (< 63 µm) – green. Elements plotted are Na (hourglasses), Mg, (bow ties), Al (squares), Si (point-up triangles), P (wide diamonds), K (circles), Ca (point-down triangles), and Fe (diamonds). Error bars representing relative standard deviation for both X and Y axes are plotted but are smaller than marker size. X-axes represent concentrations with waters filtered through 0.2 µm filters; y-axes represent concentrations with waters filtered through 0.45 µm filters. Linear regression lines and corresponding R^2 values are provided in each graph and match the color corresponding various sediment size-fractions used in experiments. Black dashed lines are 1:1 lines for comparison.

Discussion

Evidence of Groundwater in Proglacial Rivers Illustrates Importance of Sampling Location Selection

The geochemistry of proglacial rivers can provide information about subglacial processes such as residence times, assuming correlations exist between reaction rates and concentrations of

solutes/isotopic ratios (e.g. Graly et al., 2017; Hatton et al., 2019; Stevenson et al., 2017; Yde et al., 2014). These relationships may be complicated by water delivered to proglacial rivers from other sources (e.g. ground water) or modified by reactions within the stream channels (Deuerling et al., 2017).

^{222}Rn concentration in glacial outflow water is commonly used to estimate subglacial water residence time (e.g. Arendt et al., 2018; Bhatia et al., 2011; Kies et al., 2011). Previous analyses of ^{222}Rn concentrations across multiple GrIS outlet glaciers showed the highest concentrations at the KS outflow (Arendt et al., 2018), which was interpreted to reflect longer residence times at KS than elsewhere. Thus at the relatively slow-moving KS (Morlighem et al., 2014), the potential existed for a source of meltwater with a longer subglacial residence time, warranting further investigation (Arendt et al., 2018). The lower average ^{222}Rn concentrations found in 2015 samples relative to 2013 samples (Figure II-2) could imply shorter residence times in 2015 than 2013. However, specific conductivity (SPC) is similar between the two sample times, averaging 22.7 µS cm^{-1} (SD = 0.6, n = 5) in 2013 and 21.5 µS cm^{-1} (SD = 2.2, n = 16) in 2015, suggesting comparable residence time (e.g. Collins, 1979; Graly et al., 2017; Stone and Clarke, 1996). The highest ^{222}Rn concentrations were measured in 2018 and suggest a substantial increase in subglacial water residence time from 2015. Measured SPC at the same collection site was 25.6 µS cm^{-1}, ~4 µS cm^{-1} higher than in 2013 or 2015, also supporting a longer water residence time.

The fine (<63 µm) sediment fraction in the slurry experiments produced a maximum 42.0 pCi L^{-1}, or about half the value of the 2018 maximum outlet water ^{222}Rn concentration; values from crushed and uncrushed sand were even lower at 10.2 and 13.6 pCi L^{-1}, respectively (Figure II-5). The elevated KS outlet water ^{222}Rn concentrations suggest a source of ^{222}Rn in addition to the sampled KS sediments. Average 2013 in-field ^{222}Rn concentration was also higher than

possible from 63 – 500 μm sized sediments, although this concentration is attainable from the fine size fraction (Figure II-5).

The different concentrations generated in experiments can be explained by different size fractions likely containing different dominant minerals due to size separation and mineral weatherability. ^{222}Rn can only escape mineral lattices to accumulate in water if the parent ^{226}Ra atom is located near the mineral surface (Kies et al., 2011), therefore the size of the sediment grains may be important. Glacially derived sediment is poorly sorted and contains a significant portion of fine-grained glacial flour. Mineral composition differences may occur in different size fractions as mineral hardness plays a role in the physical weathering. Equivalent measurements within error for whole sand and crushed sand (Figure II-5) compared to the fine fraction measurement support mineral composition differences as the primary driver in laboratory determined ^{222}Rn concentrations, not ^{226}Ra location within the mineral lattice. However, these mineral composition differences in subglacial sediment cannot explain the very high ^{222}Rn measurement during the 2018 field season.

Experimental results reveal 2018 in-field ^{222}Rn measurements are higher than possible if generated from collected KS sediments alone, requiring another source. ^{222}Rn concentrations were observed to increase downstream in the KS outflow river (Figure II-3), even though concentrations were expected to decrease downriver due to no additional input, radioactive decay of ^{222}Rn, and evasion from water. The downstream increase in ^{222}Rn concentration may be linked to high ^{222}Rn concentration groundwater (^{222}Rn concentration = 809.0 pCi L^{-1}) discharging into the proglacial river. ^{222}Rn concentrations are frequently elevated in groundwater in relative to surface water due to exposure to large total mineral surface areas and limited potential for evasion to the atmosphere. This makes ^{222}Rn concentration ideal for tracing groundwater input to larger water bodies (e.g. Cecil and Green, 2000; Burnett and Dulaiova, 2003; Dimova et al., 2013).

Thus, the additional source is likely groundwater: we did not identify any other potential high ^{222}Rn water sources that could mix with glacial outflow, and KS3-GW contained high ^{222}Rn concentrations. Groundwater could flow into the pro-glacial river from the bed, making sampling location an important factor in future experimental designs. 2018 and 2013 samples were collected from the river edge, and thus likely also included a groundwater contribution in addition to the pro-glacial river water. The 2013 in-field ^{222}Rn concentrations (Table II-2), while attainable from the fine size fraction, are still elevated relative to what the larger size fraction is capable of producing. Variability between 2013 and 2018 KS ^{222}Rn measurements (Table II-2) may reflect different groundwater inflow, owing to differences in the water table relative to river stage in each year. In contrast, low 2015 in-field results (Table II-2) – measured from water collected at the river surface in the middle of the channel as far from the wetted perimeter as possible – would be unlikely to contain a groundwater contribution.

Comparisons of elemental concentrations in slurry experiment waters with river water elemental concentrations show differing trends depending on grain size (Figure II-6). In the fine sediment fraction slurries, variations in elemental concentrations are similar to those from field samples, although field sample concentrations are much lower. In contrast, water from sand-sized (63 – 500 μm) experiments (both intact and crushed) had lower Ca and Sr concentration than field samples while all other elements were higher (Figure II-6). These results imply that chemical weathering of fine sediments is the dominant contribution to elemental concentrations in meltwater. Different mineral fractions are apt to exist in different size fractions due to cleavage and susceptibility to physical weathering in the glacial environment. This idea is supported though different ^{222}Rn concentrations generated in slurry experiments. Concentrations of soluble elements (Na, Mg, Si, and K) measured in experimental waters are higher than in field samples, likely due

to a combination of longer water-rock interaction time and decreased dilution from melted solute-free ice.

^{222}Rn concentrations reveal a likely groundwater contribution to the KS proglacial river which is not identifiable via elemental concentrations contained in meltwater. In river edge samples, 2018 measurements indicate a definite groundwater component while 2013 samples are inconclusive. Mid-stream samples from 2015 contain lowest measured ^{222}Rn, in concentrations constrained as subglacially feasible from experiments with KS sediments. A groundwater contribution to the 2013 field samples remains the most likely explanation for the differences between years. These results highlight the potential for compromising estimates of residence time through groundwater contributions to meltwater discharge at glacier termini, particularly if ^{222}Rn measurements are used. Future work in proglacial environments should carefully consider sampling location with thoughts for possible groundwater contamination of discharge.

Despite Prevalence of U in Crustal Material, ^{222}Rn is Not Always Useful

Because of the connection between parent and daughter isotope compositions, bedrock and subglacial sediment composition must be considered when Rn is used to estimate subglacial water residence time. As WR8 is next to the edge of the GrIS and not at an outlet glacier, water sampled was inferred to come from under the GrIS itself. The discharge point was characterized by an ~50 cm tall stream boil, suggesting elevated pressure within the sub-ice system. All samples exhibited lower ^{222}Rn concentrations than at KS (Figure II-4A), suggesting very brief residence times for these glacial waters. Short residence times could result from flow into a moulin immediately up ice which then emerged essentially instantaneously from the outlet. Under this scenario the sediment load of the melt should also be low, as the melt would not have been exposed to the subglacial environment from which sediment carried in glacial outflow is sourced. However, water emerging from the ice sheet at this location was turbid, suggesting non-negligible residence time.

Alternatively, water with a long residence time may have low ^{222}Rn concentrations if sediment present does not contain its parent radioisotope, ^{226}Ra, and this provides the best explanation for our low ^{222}Rn measurements.

Slurry experiments using WR8 sediment show limited production of ^{222}Rn (Figure II-4B). That these results also occur in crushed sediment experiments indicate lack of diffusion is not the cause of low ^{222}Rn concentrations. These results reveal a second potential problem with employing ^{222}Rn as a subglacial residence time proxy: subglacial sediments may not contain ^{226}Ra if the bedrock sediment source does not contain appreciable ^{238}U. In this scenario sediments would be unable to generate ^{222}Rn and meltwater concentration measurements will indicate erroneous short subglacial residence times. These results illustrate a drawback to the use of ^{222}Rn as a proxy for subglacial water residence times, particularly if the bedrock under the glacier is unknown. As U is a common trace element in Earth's crust, this proxy has value at most glacial locations, however precautions should be taken before use. Laboratory experiments using locally derived glacial sediments should be performed to evaluate the maximum ^{222}Rn concentrations possible for individual glaciers studied. Additional proxies for residence time estimation should be employed alongside Rn to robustly support results from this proxy.

Filter Pore Size Effects on Measured Elemental Concentrations

As sampling location selection within an outflow river may have important implications for interpreted glacial chemistry, so too does filter pore size matter for measured elemental concentrations. 0.45 μm filters are conventionally used to filter suspended particles from water, with all filter-passing species then assumed to be aqueous. There are known problems with this assumption, as colloids – particles existing in size between suspension and solution – are smaller than 0.45 μm and as such are filter-passing (Eby, 2004). Oxyhydroxides, as well as clays and silica, commonly exist in colloidal form (Eby, 2004), and as all of these species exist in glacial

environments, colloids and subsequent adsorption of metal cations to colloidal surfaces should be considered when interpreting geochemical concentrations in glacial meltwater studies. Colloids exist in a range of sizes, and as such their presence as suspended or gravitationally settled particles is a function of water velocity (Atteia et al., 1998). Subglacial water velocity can vary considerably as water may flow quickly through well-connected channels or percolate through linked cavities with slow velocities (L. C. Andrews et al., 2014; Bartholomew et al., 2010; Schoof, 2010), possibly affecting the size and quantity of colloids present (Atteia et al., 1998).

Studies of elemental or nutrient fluxes from the GrIS use filtered water samples passed through a range of filter sizes from 0.45 μm filters (e.g. M. G. Andrews and Jacobson, 2018; Deuerling et al., 2019; Meire et al., 2016), to 0.2 μm filters (e.g. Arendt et al., 2018; Hawley et al., 2017; Hindshaw et al., 2014), and 0.1 μm filters (e.g. Graly et al., 2017). Explanations are rarely provided for the choice of particular pore size. Tepe and Bau (2015) examined distributions of high field strength elements from the western GrIS, filtering most samples through a 0.2 μm filter, but included one ultra-filtered Watson River sample that was passed through a 10 kDa filter. Rare earth element + Y distribution for the ultra-filtered (<10 kDa) sample displayed a different trend in enrichment than either the <0.2 μm or the 0.2 μm – 10 kDa fractions (Tepe and Bau, 2015). Many major element concentrations were below the lower limit of determination (Tepe and Bau, 2015), making comparisons between their results and slurry experiment elemental concentrations measured through different filter impossible, however, the different trends in relative particle-reactive element concentrations for differently filtered subsamples illustrate the effects filter selection may have on measured elemental concentrations.

Elemental concentrations from waters used in KS sediment ^{222}Rn experiments were analyzed to compare elemental signatures to measured concentrations from field samples. 2013 and 2015 samples were filtered through 0.2 μm filters while 2018 samples were filtered through

0.45 μm filters, so subsamples from each experiment were filtered through 0.2 and 0.45 μm filters prior to analysis to identify variability associated with filter size. If all elements measured were truly aqueous species, there should be no difference in concentrations from different filter sizes and they should plot on a 1:1 line. However, elemental concentrations from each experiment do not plot on a 1:1 line (Figure II-7). Best-fit trendlines for sand and crushed sand experiments deviate from a 1:1 line; waters filtered through 0.45 μm filters have higher elemental concentrations. If differences in elemental concentrations are due to colloidal contributions, it is reasonable that more colloids could pass through the larger filter pores, explaining observed results. Elements deriving from the fine size fraction were well correlated (R^2 = 0.9807) and more elements had relatively higher concentrations than in the sand experiments. However, the trendline closely matched the 1:1 line, deviating only slightly within analytical error towards the 0.2 μm axis.

Increased elemental concentrations trends in 0.45 μm filtered samples are not observed in particle reactive elements (Al, P, and Fe) as some 2013 field-sample concentrations are higher than experimental leachate concentrations (Figure II-6). Furthermore, Fe concentrations are variable, both between sample years and from field to experimental data: 2013 samples contain more Fe than P, but in 2015 65% of the samples contained more P than Fe. All experimental waters contained higher concentrations of Fe relative to P (Figure II-6). These discrepancies between 2013, 2015, and experimental samples may derive from groundwater input to the sampling location, the range of possible filter-passing Fe sizes (aqueous, nanoparticulate, and colloidal) (Raiswell and Canfield, 2012), differences in Fe-flux from the KS glacier, or a combination of any of these possibilities.

Results reveal differences in measured elemental concentrations from using filters with different pore sizes to be considerable. As these data were generated from leaching experiments, concentrations measured are much higher than concentrations commonly seen in glacial outflows

which are frequently diluted during intervals of high flow. At low concentrations, the presence of more or fewer colloids in a water sample may have an even greater effect on measured concentrations and elemental ratios, especially when fluxes are extrapolated to ice sheet- elemental or nutrient fluxes. Future research in glaciochemistry should carefully consider filter pore size prior to measurement to ensure measured values truly reflect intended parameters, taking into consideration the impact of expected filter passing particles on elemental concentrations.

Conclusion

This study reveals higher concentrations of ^{222}Rn gas present in proglacial outflow from the KS glacier in south Greenland than collected KS sediments are capable of producing. In-field sampling indicates groundwater may be the source of the high ^{222}Rn concentrations. Groundwater appears to contribute to outflow from the KS glacier in south Greenland even at the sampling site nearest the glacial terminus, raising questions about nutrient and elemental fluxes previously assumed to be derived solely through subglacial weathering. Measuring ^{222}Rn concentrations in proglacial meltwaters may help ensure future researchers select sampling locations with minimum groundwater input.

Use of ^{222}Rn concentrations as a proxy for subglacial water residence time remains a promising application as shown in Bhatia et al. (2011) and Kies et al. (2011). However, the method can be improved through the addition of laboratory sediment/water ^{222}Rn equilibration experiments like those presented here. Experimental results place in-field concentrations in a broader context by resolving the maximum ^{222}Rn concentration possible from sediments collected at glaciers of interest. Thus in-field measurements can be quantitatively assessed. Furthermore, experiment results will reveal if sediments are unable to produce ^{222}Rn, as at sample site WR8 in this study. This information will inform future researchers to disregard field measurements

implying negligible subglacial water residence time, and to instead find additional residence time proxies. Furthermore, laboratory experiments create leachate waters which may then be analyzed for elemental concentrations to compare with the composition of proglacial waters. By combining these methods, researchers may better understand the complete chemistry of the subglacial environment, allowing for more comprehensive interpretations and predictions of the impact of ice melt.

Finally, this study reveals the necessity carefully selecting filter pore size for sample filtration prior to undertaking glaciochemical field work. Filter-passing colloids – and adsorbed metals – may be measured as aqueous species, when in actuality these species are not aqueous and as such may behave differently in downstream environments. The chemical composition of glacial meltwaters has been studied to evaluate the change in potential nutrient fluxes to the ocean with ongoing climate change; considering filter pore size in future work will improve scaled-up estimates of oceanic nutrient fluxes. Thus this study uses laboratory experiments to evaluate the robustness and application of some glaciochemical field measurements to constrain future field sampling methodology. By adopting some of the suggestions provided here, researchers will be able to improve field sampling strategies and subsequently strengthen conclusions drawn from their results.

References

Aciego, S.M., Stevenson, E.I., Arendt, C.A., 2015. Climate versus geological controls on glacial meltwater micronutrient production in southern Greenland. Earth Planet. Sci. Lett. 424, 51–58. doi:10.1016/j.epsl.2015.05.017

Anderson, S.P., Drever, J.I., Humphrey, N.F., 1997. Chemical weathering in glacial environments. Geology 25, 399–402. doi:10.1130/0091-7613(1997)025<0399:cwige>2.3.co;2

Andrews, L.C., Catania, G.A., Hoffman, M.J., Gulley, J.D., Lüthi, M.P., Ryser, C., Hawley, R.L., Neumann, T.A., 2014. Direct observations of evolving subglacial drainage beneath the Greenland Ice Sheet. Nature 514, 80–83. doi:10.1038/nature13796

Andrews, M.G., Jacobson, A.D., 2018. Controls on the solute geochemistry of subglacial discharge from the Russell Glacier, Greenland Ice Sheet determined by radiogenic and stable Sr isotope ratios. Geochim. Cosmochim. Acta 239, 312–329. doi:10.1016/j.gca.2018.08.004

Arendt, C.A., Aciego, S.M., Hetland, E.A., 2015. An open source Bayesian Monte Carlo isotope mixing model with applications in Earth surface processes. Geochem. Geophys. Geosystems 16, 1274–1292. doi:10.1002/2014gc005683

Arendt, C.A., Aciego, S.M., Sims, K.W., Das, S.B., Sheik, C., Stevenson, E.I., 2018. Influence of glacial meltwater on global seawater δ234U. Geochim. Cosmochim. Acta 225, 102–115. doi:10.1016/j.gca.2018.01.007

Atteia, O., Perret, D., Adatte, T., Kozel, R., Rossi, P., 1998. Characterization of natural colloids from a river and spring in a karstic basin. Environ. Geol. 34, 257–269. doi:10.1007/s002540050277

Bartholomew, I., Nienow, P., Mair, D., Hubbard, A., King, M.A., Sole, A., 2010. Seasonal evolution of subglacial drainage and acceleration in a Greenland outlet glacier. Nat. Geosci. 3, 408–411. doi:10.1038/ngeo863

Bekryaev, R.V., Polyakov, I.V., Alexeev, V.A., 2010. Role of polar amplification in long-term surface air temperature variations and modern Arctic warming. J. Climate 23, 3888–3906. doi:10.1175/2010JCLI3297.1

Bellotti, E., Broggini, C., Di Carlo, G., Laubenstein, M., Menegazzo, R., 2015. Precise measurement of the ^{222}Rn half-life: A probe to monitor the stability of radioactivity. Phys. Lett. B 743, 526–530. doi:10.1016/j.physletb.2015.03.021

Bhatia, M.P., Das, S.B., Kujawinski, E.B., Henderson, P., Burke, A., Charette, M.A., 2011. Seasonal evolution of water contributions to discharge from a Greenland outlet glacier: insight from a new isotope-mixing model. J. Glaciol. 57, 929–941. doi:10.3189/002214311798043861

Burnett, W.C., Dulaiova, H., 2003. Estimating the dynamics of groundwater input into the coastal zone via continuous radon-222 measurements. J. Environ. Radioact. 69, 21–35. doi:10.1016/S0265-931X(03)00084-5

Cecil, L.D., Green, J.B., 2000. Radon-222, in: Cook, P.G., Herczeg, A.L. (Eds.), Environmental tracers in subsurface hydrology, New York, pp. 175-194.

Chandler, D.M., Wadham, J.L., Lis, G.P., Cowton, T., Sole, A., Bartholomew, I., Telling, J., Nienow, P., Bagshaw, E.B., Mair, D., Vinen, S., Hubbard, A., 2013. Evolution of the subglacial drainage system beneath the Greenland Ice Sheet revealed by tracers. Nat. Geosci. 6, 195–198. doi:10.1038/ngeo1737

Chu, V.W., 2014. Greenland ice sheet hydrology: A review. Prog. Phys. Geog. 38, 19–54. doi:10.1177/0309133313507075

Collins, D.N., 1979. Hydrochemistry of meltwaters draining from an Alpine glacier. Arct. Alp. Res. 11, 307–324. doi:10.1080/00040851.1979.12004139

Cowton, T., Nienow, P., Sole, A., Wadham, J., Lis, G., Bartholomew, I., Mair, D., Chandler, D., 2013. Evolution of drainage system morphology at a land-terminating Greenlandic outlet glacier. J. Geophys. Res. Earth Surf. 118, 29–41. doi:10.1029/2012JF002540

Davison, B.J., Sole, A.J., Livingstone, S.J., Cowton, T.R., Nienow, P.W., 2019. The influence of hydrology on the dynamics of land-terminating sectors of the Greenland Ice Sheet. Front. Earth Sci. 7, 1–24. doi:10.3389/feart.2019.00010

Deuerling, K.M., Martin, J.B., Martin, E.E., Abermann, J., Myreng, S.M., Petersen, D., Rennermalm, A.K., 2019. Chemical weathering across the western foreland of the Greenland Ice Sheet. Geochim. Cosmochim. Acta 245, 426–440. doi:10.1016/j.gca.2018.11.025

Deuerling, K.M., Martin, J.B., Martin, E.E., Scribner, C.A., 2017. Hydrologic exchange and chemical weathering in a proglacial watershed near Kangerlussuaq, west Greenland. J. Hydrol. 556, 220-232. doi:10.1016/j.jhydrol.2017.11.002

Dimova, N.T., Burnett, W.C., Chanton, J.P., Corbett, J.E., 2013. Application of radon-222 to investigate groundwater discharge into small shallow lakes. J. Hydrol. doi:10.1016/j.jhydrol.2013.01.043

Duchemin, B., Coursol, N., Bé, M., 1994. The re-evaluation of decay data for the U-238 chain. Nuclear Inst. and Methods in Physics Research, A 339, 146–150. doi:10.1016/0168-9002(94)91795-7

Eby, N.G., 2004. Principles of Environmental Geochemistry. Brooks/Cole, Belmont, CA.

Fountain, A.G., 1993. Geometry and flow conditions of subglacial water at South Cascade Glacier, Washington State, USA; an analysis of tracer injections. J. Glaciol. 39, 143–156. doi:10.1017/S0022143000015793

Gordon, S., Sharp, M., Hubbard, B., Smart, C., Ketterling, B., Willis, I., 1998. Seasonal reorganization of subglacial drainage inferred from measurements in boreholes. Hydrol. Process. 12, 105–133. doi:10.1002/(sici)1099-1085(199801)12:1<105::aid-hyp566>3.0.co;2-#

Graly, J., Harrington, J., Humphrey, N., 2017. Combined diurnal variations of discharge and hydrochemistry of the Isunnguata Sermia outlet, Greenland Ice Sheet. Cryosphere 11, 1131–1140. doi:10.5194/tc-11-1131-2017

Gulley, J.D., Benn, D.I., Screaton, E., Martin, J., 2009. Mechanisms of englacial conduit formation and their implications for subglacial recharge. Quat. Sci. Rev. 28, 1984–1999. doi:10.1016/j.quascirev.2009.04.002

Hammond, D.E., Fuller, C., 1979. The use of Radon-222 to estimate benthic exchange and atmospheric exchange rates in San Francisco Bay, in: Conomos, T.J. (Ed.), San Francisco Bay: the Urbanized Estuary. Am. Assoc. Adv. of Sci., San Francisco, pp. 213–231.

Hatton, J.E., Hendry, K.R., Hawkings, J.R., Wadham, J.L., Kohler, T.J., Stibal, M., Beaton, A.D., Bagshaw, E.A., Telling, J., 2019. Investigation of subglacial weathering under the Greenland Ice Sheet using silicon isotopes. Geochim. Cosmochim. Acta 247, 191–206. doi:10.1016/j.gca.2018.12.033

Hawley, S.M., von Strandmann, P.A., Burton, K.W., Williams, H.M., Gíslason, S.R., 2017. Continental weathering and terrestrial (oxyhydr)oxide export: Comparing glacial and non-glacial catchments in Iceland. Chem. Geol. 462, 55–66. doi:10.1016/j.chemgeo.2017.04.026

Hindshaw, R.S., Rickli, J., Leuthold, J., Wadham, J., Bourdon, B., 2014. Identifying weathering sources and processes in an outlet glacier of the Greenland Ice Sheet using Ca and Sr isotope ratios. Geochim. Cosmochim. Acta 145, 50–71. doi:10.1016/j.gca.2014.09.016

Holland, M.M., Bitz, C.M., 2003. Polar amplification of climate change in coupled models. Clim. Dyn. 21, 221–232. doi:10.1007/s00382-003-0332-6

Kies, A., Nawrot, A., Tosheva, Z., Jania, J., 2011. Natural radioactive isotopes in glacier meltwater studies. Geochem. J. 45, 423–429. doi:10.2343/geochemj.1.0141

Linhoff, B.S., Charette, M.A., Nienow, P.W., Wadham, J.L., Tedstone, A.J., Cowton, T., 2017. Utility of 222Rn as a passive tracer of subglacial distributed system drainage. Earth Planet. Sci. Lett. 462, 180–188. doi:10.1016/j.epsl.2016.12.039

Meierbachtol, T., Harper, J., Humphrey, N., 2013. Basal drainage system response to increasing surface melt on the Greenland ice sheet. Science 341, 777–779. doi:10.1126/science.1235905

Meire, L., Meire, P., Struyf, E., Krawczyk, D.W., Arendt, K.E., Yde, J.C., Juul Pedersen, T., Hopwood, M.J., Rysgaard, S., Meysman, F.J.R., 2016. High export of dissolved silica from the Greenland Ice Sheet. Geophys. Res. Lett. 43, 9173–9182. doi:10.1002/2016GL070191

Morlighem, M., Rignot, E., Mouginot, J., Seroussi, H., Larour, E., 2014. High-resolution ice-thickness mapping in South Greenland. Ann. Glaciol. 55, 64–70. doi:10.3189/2014aog67a088

Nienow, P., Sole, A., Slater, D., Cowton, T., 2017. Recent advances in our understanding of the role of meltwater in the Greenland Ice Sheet system. Curr. Clim. Chang. Rep. 3, 330–344. doi:10.1007/s40641-017-0083-9

Parizek, B.R., Alley, R.B., 2004. Implications of increased Greenland surface melt under global-warming scenarios: ice-sheet simulations. Quat. Sci. Rev. 23, 1013–1027. doi:10.1016/j.quascirev.2003.12.024

Raiswell, R., Canfield, D.E., 2012. The iron biogeochemical cycle past and present. Geochem. Perspect. 1, 1–220. doi:10.7185/geochempersp.1.1

Rudnick, R., Gao, S., 2003. Composition of the continental crust. Treatise on Geochemistry, 1–64. doi:10.1016/b0-08-043751-6/03016-4

Schoof, C., 2010. Ice-sheet acceleration driven by melt supply variability. Nature 468, 803–806. doi:10.1038/nature09618

Screen, J.A., Simmonds, I., 2010. The central role of diminishing sea ice in recent Arctic temperature amplification. Nature 464, 1334–1337. doi:10.1038/nature09051

Shepherd, A., Hubbard, A., Nienow, P., King, M., McMillan, M., Joughin, I., 2009. Greenland ice sheet motion coupled with daily melting in late summer. Geophys. Res. Lett. 36, 33773–5. doi:10.1029/2008GL035758

Stevenson, E.I., Fantle, M.S., Das, S.B., Williams, H.M., Aciego, S.M., 2017. The iron isotopic composition of subglacial streams draining the Greenland ice sheet. Geochim. Cosmochim. Acta 213, 237–254. doi:10.1016/j.gca.2017.06.002

Stone, D.B., Clarke, G.K.C., 1996. *In situ* measurements of basal water quality and pressure as an indicator of the character of subglacial drainage systems. Hydrol. Process. 10, 615–628. doi:10.1002/(SICI)1099-1085(199604)10:4<615::AID-HYP395>3.0.CO;2-M

Tepe, N., Bau, M., 2015. Distribution of rare earth elements and other high field strength elements in glacial meltwaters and sediments from the western Greenland Ice Sheet:

Evidence for different sources of particles and nanoparticles. Chem. Geol. 412, 59–68. doi:10.1016/j.chemgeo.2015.07.026

Yde, J.C., Knudsen, N.T., Hasholt, B., Mikkelsen, A.B., 2014. Meltwater chemistry and solute export from a Greenland Ice Sheet catchment, Watson River, West Greenland. J. Hydrol. 519, 2165–2179. doi:10.1016/j.jhydrol.2014.10.018

Zwally, H.J., Abdalati, W., Herring, T., Larson, K., Saba, J., Steffen, K., 2002. Surface melt-induced acceleration of Greenland ice-sheet flow. Science 297, 218–222. doi:10.1126/science.1071795

Chapter III. Hydrochemical Changes in Bulk Glacial Melt Throughout the Summer to Autumn Transition, Athabasca Glacier, Alberta, Canada

Abstract

Solutes contained within glacial meltwater establish the initial chemistry for downstream fluvial systems. Accordingly, understanding how concentrations of solutes change in response to fluctuating glacial conditions on times scales from diurnal to annual improves predictions of the environmental impacts of climate change on downstream locations. Glacial seasonal field studies are difficult to undertake as many glaciers exist in remote and inaccessible environments. The Athabasca Glacier, an outlet glacier from the Columbia Icefield, Alberta, Canada is more easily accessible, allowing novel investigation into alpine glacial hydrochemistry during the summer to autumn transition. Glacial meltwater samples and *in situ* data [glacial outflow discharge, water conductivity, water pH, dissolved oxygen concentration in outflow, and ^{222}Rn activity] were collected at the glacial terminus from August through October, 2014. Changes in observed cation concentrations track the evolution of the subglacial drainage network in response to seasonal cooling, elucidating chemical weathering trends from summer to early wintertime conditions in mid-autumn.

This study reveals that although dilution primarily controls meltwater hydrochemistry, shifts in chemical reactions occur as subglacial flow transitions from a channelized system to a distributed network with the advent of colder temperatures in autumn. Increased carbonate dissolution relative to silicate weathering early in the study (August) reveals shorter, more efficient water routing, likely through channelized drainages. A shift to distributed drainages and longer water flow paths at the end of the melt season (October) produces increased silicate weathering

and sulfide mineral/organic carbon oxidation, leading to lower dissolved oxygen concentrations, higher elemental concentrations relative to Ca, higher conductivity, and lower water pH. End season conditions are also associated with the highest concentrations of metals. This hydrologic network reorganization is immediately observable within the glacial hydrochemistry, highlighting the sensitivity the subglacial hydrologic system to seasonal changes.

Introduction

Anthropogenic climate change drives increasing air temperatures around the globe, with pronounced increases at high latitudes (IPCC, 2013) where ice sheets, ice caps, and glaciers are vulnerable to melting. Changes in timing of meltwater delivery (e.g. Barnett et al., 2005; Singh and Kumar, 1997), sediment flux (e.g. Hallet et al., 1996; Wada et al., 2011), water temperature (e.g. Brown and Hannah, 2008; Milner and Petts, 1994), river channel stability (e.g. Huisink, 1997), and chemical constituents transported by glacial melt (e.g. Hood and Berner, 2009) are all anticipated effects, with impacts to downstream aqueous environments ranging from large-scale river morphology to microscopic biogeochemistry (e.g. Milner et al., 2017). Understanding how the chemical composition of glacial melt changes as melting rates vary will improve predictions of climate change impacts on glacial and periglacial environments.

Meltwater volumes from alpine glaciers fluctuate on a range of timescales from annual through seasonal to daily as changes in air temperature and solar insolation impact water storage capacity and drainage network efficiency. Although melting rates are highest in summer, glaciers can lose mass throughout the entire year due to geothermal heat flux and frictional heating from both internal ice deformation and basal sliding (Benn and Evans, 2010). Regardless of time of year and volume generated, meltwater is ultimately evacuated from the glacial system. Glacial hydrologic networks include supraglacial, englacial, and subglacial drainages; however as liquid

water is denser than ice, most melt eventually enters the subglacial drainage network (Fountain and Walder, 1998). Subglacial drainage channels exist stably when the hydrostatic pressure of the water within the channel is equal to the pressure of the ice overburden (Hooke et al., 1990; Hubbard and Nienow, 1997; Röthlisberger, 1972).

Alpine glacial subglacial drainage network configuration varies throughout the year to accommodate changing fluxes of glacial melt (Fountain and Walder, 1998; Hubbard and Nienow, 1997). For much of the year, cold air temperatures limit melting such that the network needs only to accommodate small volumes of water. Resultant poorly-connected, circuitous subglacial drainage networks increase water transit times through the network, such that melt takes days to weeks to exit the system (Chandler et al., 2013; Fountain and Walder, 1998; Hasnain et al., 2001). As warming air temperatures in spring generate greater melt, the network reorganizes to accommodate this increased flux (Fountain and Walder, 1998). Cooler autumnal temperatures subsequently reduce flow, contracting efficient conduits in the subglacial network and increasing sub-ice meltwater transit time. Previous glaciological research has focused on the opening (shift from poorly connected to arborescent configurations) of the subglacial drainage network in the spring (e.g. Arendt et al., 2016; Bhatia et al., 2011; Chandler et al., 2013; Meierbachtol et al., 2013; Nienow et al., 1998; Yde et al., 2005). As yet few studies have investigated the return of these networks to low-flow conditions following summer peak melt (e.g. Hindshaw et al., 2011).

Chemical weathering products – elemental concentrations and ratios – reflect the degree of chemical weathering occurring sub-ice and have been used to infer the structure of the subglacial drainage network (S. P. Anderson et al., 2003; Collins, 1989; Hubbard and Nienow, 1997; Kumar et al., 2019; Mitchell et al., 2006; Tranter et al., 1993; 1996). In inefficient, slowly-draining subglacial networks, water is in contact with the subglacial substrate for days to months (Chandler et al., 2013) resulting in increased chemical weathering of the substrate and solute acquisition in

meltwaters (i.e., higher concentrations of cations in meltwaters) (S. P. Anderson et al., 2003; 1997; Graly et al., 2017; Tranter et al., 1993). Efficient drainage networks result in faster meltwater flow (hours to days) (Chandler et al., 2013; Hawkings et al., 2015; Hodgkins et al., 2013; Linhoff et al., 2017; Tranter et al., 1993), therefore in these networks, meltwater cation concentrations are lower due to increased water volume (dilution) and shorter contact time with the substrate (less chemical weathering) (Fountain and Walder, 1998; Tranter and Wadham, 2014). Thus, meltwater elemental concentrations as expressed at the glacial terminus can illuminate general changes in the subglacial drainage network and extent of distributed versus channelized systems (Hubbard and Nienow, 1997; Mitchell et al., 2006; Tranter et al., 1993; 1997).

Glacial chemical weathering reactions and rates are also influenced by sediment grain size, mineral composition, and temperature (Graly et al., 2018; Tranter et al., 1993; Wadham et al., 2010). Glacial discharge contains higher Ca concentrations from calcite dissolution and lower Si concentrations from hydrolysis of silicate minerals relative to nonglacial rivers, likely due to low temperature effects on reaction kinetics (S. P. Anderson et al., 1997; Blum et al., 1998; Singh et al., 2012). However, although associated with cold environments, the extremely small particles and large surface area of finely ground glacial flour leads to enhanced chemical weathering relative to the global mean weathering rates, on par with similarly sized non-glacial catchments (S. P. Anderson, 2005; S. P. Anderson et al., 1997).

This study investigates seasonal changes at the Athabasca Glacier (AG) in Alberta, Canada from August through October, 2014 through *in situ* hydrochemistry – specifically major and trace elemental concentrations, stable water isotopic composition, and ^{222}Rn concentration. Time-series measurements of these parameters provide an improved understanding of subglacial weathering and drainage processes as the network transforms from a late-summer channelized network to a distributed configuration in autumn with wintertime conditions (frequent snowfall and

temperatures below 0°C). Results reveal nuanced non-linear seasonal changes in expressed glaciochemistry owing to evolution of the subglacial environment. These results have implications for changes in the timing of elemental and nutrient delivery to downstream ecosystems from other alpine glacial systems as climate change affects the seasonal drivers for these hydrochemical changes.

Field Description

The Columbia Icefield, located in the northern end of Banff National Park and the southern end of Jasper National Park in Alberta and British Columbia, Canada, is the hydrologic triple drainage divide in the Canadian Rocky Mountains, dispersing glacial meltwater to the Atlantic, Pacific, and Arctic Oceans. The icefield covers approximately 325 km^2, ranging in elevation from 1900 meters to 3400 meters and has eight outlet glaciers (Figure III-1). The AG drains the Columbia Icefield to the northeast, extending 6 km with an area of 6.34 km^2 (Kucera and Henoch, 1978). It joins the Columbia Icefield at an elevation of 2740 meters and terminates at an elevation of 1990 meters (Hugenholtz et al., 2008).

The AG is a land terminating, warm-based glacier with a maximum thickness of 320 meters (Brugman and Demuth, 1994; Paterson, 1964). Melt generated from the glacier emanates from multiple locations at the terminus into a small glacial lake, subsequently flowing into Sunwapta Lake ~0.25 km from the terminus (Figure III-1). The glacier surface is mostly unmarked by rock debris, while the sides are bordered by ice-cored lateral moraines rising 150 m above the glacier foreland (Hugenholtz et al., 2008). These moraines – reaching >100 m above the present ice surface – resulted from the maximum advance of the AG during the Little Ice Age (circa 1840 CE), 1.6 km beyond its present extent (Luckman, 1988). More recently the AG has been retreating several meters per year (Hart, 2006) resulting in a net mass loss. The glacial ice was snow-free for

the majority of this study (August - October 2014); infrequent snow precipitation melted within 1-2 days until end-October, when snow began to accumulate. The ice surface at the terminus was colored gray due to deposition of morainal sediment and ash from local fires, lowering albedo.

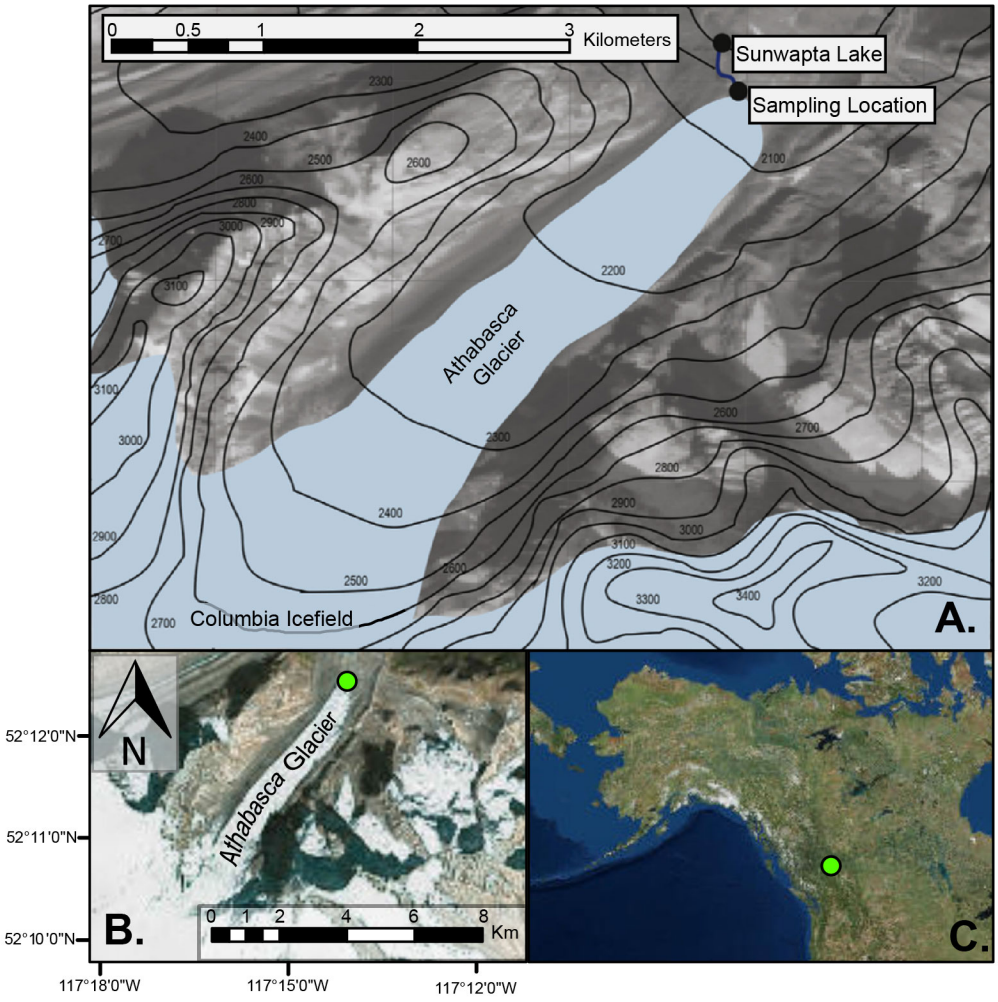

Figure III-1: A.) Schematic drawing of the Athabasca Glacier with topographic information and detailed plot of the sampling location, modified from Arendt et al., (2015). B.) Satellite imagery of the Athabasca Glacier, green circle indicates sampling location. C.) Contextual map of North America, green circle indicates sampling location.

Meltwater under the AG encounters the Middle Cambrian Eldon and Stephen Formations (Charlesworth and Erdmer, 1989). The shallow marine Eldon Fm. consists of limestone and dolostone with interbedded shale layers at the top and bottom of its sequence (Aitken, 1978). Meteoric water intrusion along bedding planes in these carbonates created the Castleguard Cave

karst complex, which exists between the AG and the neighboring Saskatchewan Glacier, another outflow glacier extending to the southeast (Ford et al., 1983; Smart, 1983). The older Stephen Fm. is comprised of shale layers with interbedded thin layers of siltstone, grainstone, and lime-mudstone grading into the base of the Eldon (Aitken, 1978).

Methods

Cleaning of Sampling Equipment and Consumables:

Sample containers and plastic tubing were pre-cleaned in an ISO 7 (class 10,000) clean room in the Glaciochemistry and Isotope Geochemistry Laboratory at the University of Michigan. Plastics were rinsed three times with 18.2 MΩ deionized water, leached for 24 hours with double-distilled 10% nitric acid, rinsed three times with 18.2 MΩ deionized water, leached 24 hours with 10% double-distilled hydrochloric acid, and rinsed again three times with 18.2 MΩ deionized water, as in Arendt et al., (2015).

Discharge Measurements, In Situ Data:

Daily discharge was measured using an Acoustic Doppler Velocimeter (ADV) Flowtracker at ~10:00 AM local time. Discharge was measured at the head of the outflow river (52° 12.366'N, 117° 14.059'W) (Figure III-1) in a section of the channel where water flowed over a single large flat dolostone section with few cobbles or boulders to perturb flow lines. River channel width was measured daily at this location and the ADV Flowtracker sensor was submerged parallel to water flow. Channel width varied from a maximum of 13.41 m on DOY 267 to a minimum of 6.40 m on DOY 298. Once calibrated, water depth and velocity were measured in 30 cm intervals across the channel section. Velocity was measured continuously for 60 s at each interval; average velocity at each interval was used for calculations. Total discharge was calculated using the method of Morlock et al. (2002), then converted to $m^3\ s^{-1}$.

Conductivity, pH, and dissolved oxygen were measured concurrently with a handheld YSI Professional Plus multi-probe at the same location. The pH probe was calibrated to pH 4, 7, and 10, conductivity calibrated with 1413 µS cm^{-1} solution, and DO calibrated with water-saturated air prior to use. pH calibration was checked daily and recalibrated with pH 4, 7, and 10 solutions as required. Complete recalibrations were conducted monthly in the field. Precipitation and air temperature data were downloaded from the Sunwapta Weather Station, located ~30 km north of the sampling location (Government of Alberta). Timing and intensity of precipitation events at the weather station generally match field observations of rainfall events.

Sample Collection for Elemental Data and Stable Water Isotopes:

Water samples were collected every 1 to 3 days in August, September, and October 2014 at 10:00 AM at the same location used to measure discharge, ~15 m downstream from the glacier terminus. Samples were collected from the thalweg of the meltwater stream to ensure a well-mixed sample of all sub-, en-, and supraglacially-routed melt. After rinsing the sample bottle with flowing meltwater from the sample site three times, 250 mL water samples were collected at mid-depth and immediately analyzed for radon concentrations using a Durridge RAD7 instrument. It was outfitted with the RAD H_2O accessory and [^{222}Rn] was determined using the factory programmed WAT250 protocol. The Rad7 instrument was calibrated by Durridge in May 2014.

Water samples for oxygen and hydrogen isotope analysis were collected with new 60 mL luer-lok syringes that were rinsed with meltwater from the sample location three times prior to sample collection. Water was filtered through a 0.45 µm hydrophilic Millex GV PVDF filter directly attached to the syringe. Samples for oxygen and hydrogen isotope analysis were filtered directly into Kimble 20 mL glass screw-thread scintillation vials with cone caps. Vials were initially filled completely without headspace, but temperatures below 0°C and subsequent sample expansion broke a small subset of vials. Succeeding samples were filled mostly full to allow for

expansion due to possible freezing in sub-zero temperatures, tightly closed, and remained sealed until measurement. Vials were stored at 4°C prior to measurement to minimize isotopic fractionation.

Meltwater samples for major/trace element analysis were collected every 1 to 3 days and immediately filtered in the field to prevent further reaction with suspended sediment. Collected meltwater (1 L) was passed through a 0.22 µm Millipore Durapore® membrane filter enclosed in a PTFE filter housing via a Masterflex modular peristaltic pump. The water was then stored in pre-cleaned HDPE plastic bottles and acidified with Optima grade hydrochloric acid on-site to pH < 2.

Major and trace elemental concentrations were measured in 2 mL field-acidified, filtered water samples at the University of Michigan on a Thermo Scientific ELEMENT2 high resolution ICP-MS operating in pulse counting mode. Baseline acid blank measurements determined detection limits; values are published in (Aciego et al., 2015). A three-point calibration curve was used to calculate concentrations. Standards were diluted to bracket the lowest and highest sample concentrations and analyzed at the beginning and end of each run. In addition, an acid blank and a standard of known concentration were analyzed as unknowns every five samples; acid blanks measured below detection limits and standards reproduced within error of the calibration curve. Samples were measured in triplicate, and internal analytical errors were <1% with external accuracy and reproducibility ensured by recurring measurement of an international reference standard (NIST1640a). Reference standard measurements are published in Aciego et al. (2015).
Oxygen and hydrogen isotopes were measured on a Picarro L2120-I Cavity Ringdown Spectrometer with an A0211 high-precision vaporizer, autosampler, and ChemCorrect software in the University of Michigan Water Isotopes Laboratory. The water $\delta^{18}O$ and δD values were

calibrated to VSMOW/VSLAP using three internal laboratory standards. Typical analytical precision is better than 0.1‰ for $\delta^{18}O$ and 1‰ for δD.

Results

During the sampling period from August through October 2014 daily average air temperature decreased from ~20 to 0°C at the Athabasca Glacier (Figure III-2A). Three intervals where the daily average air temperature fell below 0°C are marked by purple bars (Figure III-2A). Precipitation fell as both rain and snow (reported in water equivalency and marked by blue overlays) during the study period (Figure III-2B). There were instances of snow at the field site not recorded in data from the weather station; these dates are marked with blue overlays, but not accompanied by liquid water-equivalency (Figure III-2B). Measured discharge (Q) at the sampling site decreased from ~3.5 to 0.1 $m^3 s^{-1}$ over the study period (Figure III-2E, Table III-1) although precipitation events and warm periods led to stochastically increased discharge (Figure III-2). Colder air temperatures correlate with decreasing discharge ($R^2 = 0.53$), with lowest Q associated with air temperatures below 0°C (Figure III-2). As expected, rain events generated increased discharge, as did periods of warmer temperatures. Suspended sediment concentrations averaged 0.039 g L^{-1} (standard deviation 0.022 g L^{-1}), punctuated by order-of-magnitude increases coincident with rapidly warming air temperatures, immediately following low discharge intervals on DOY 258 and 280 (associated with freezing air temperatures) (Figure III-2F, Table III-1). Water isotopes become more enriched over the course of the study; the precipitation event (rain changing to snow) on day 284 was associated with a 2‰ increase in $\delta^{18}O$ and a 15‰ increase in δD of the glacial meltwater (Figure III-2C, D; Table III-1).

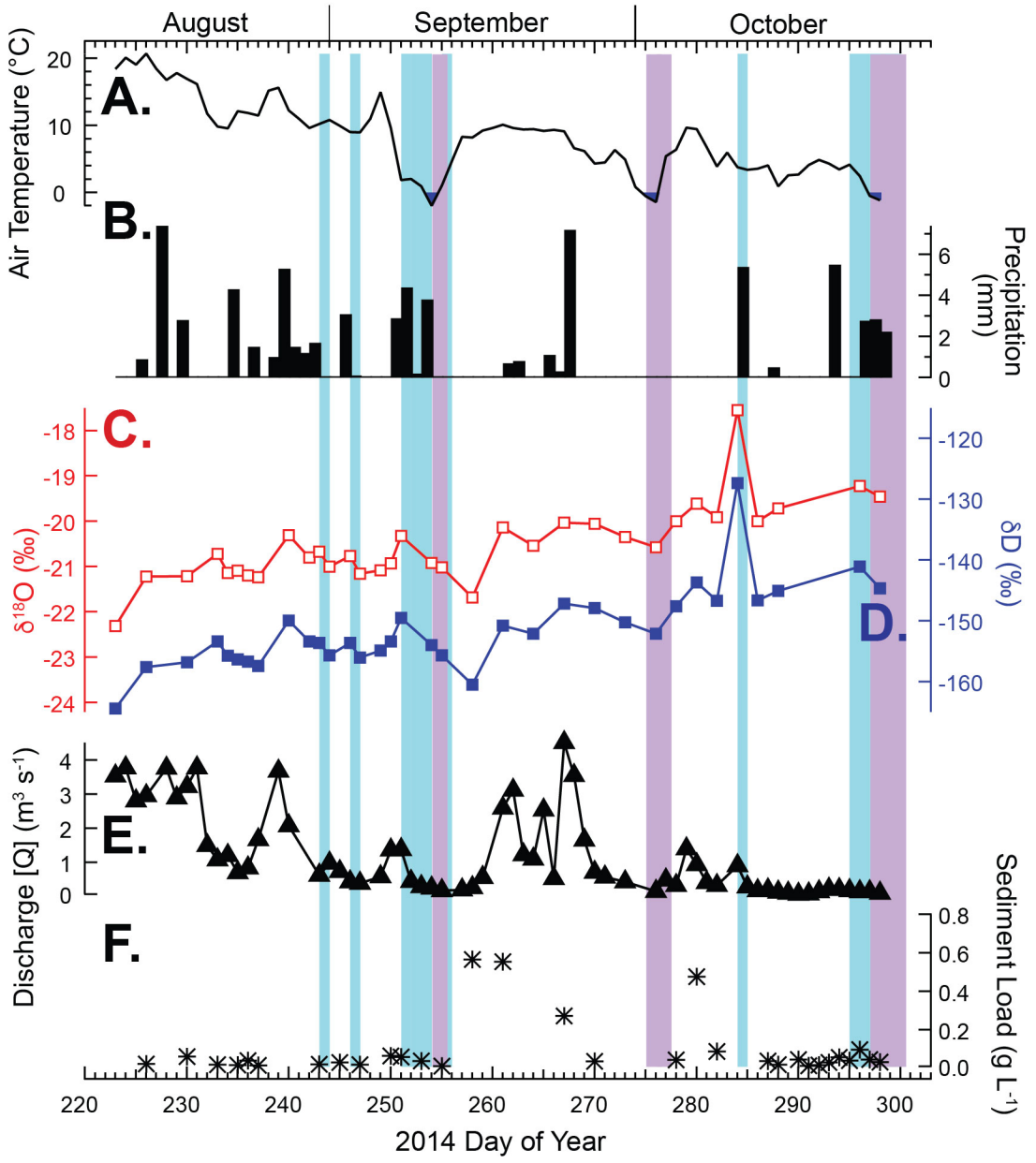

Figure III-2: 2014 hydroclimate data from the Athabasca glacier. A.) Daily mean air temperature as measured at Environment Canada's Sunwapta Falls weather station, ~30 km from the sampling location. Temperatures below freezing are in-filled and marked with purple bars. B.) mm of accumulated precipitation, rain or snow-water equivalency, measured at Sunwapta Falls weather station. Overlaid blue bars denote observed instances of in-field snow, including cases not recorded at the weather station. C.) $\delta^{18}O$ and D.) Deuterium isotopic composition of meltwater collected for sampling. E.) Glacial discharge measured at 10 am concurrent with sample collection. F.) Mass of sediment filtered from water sample normalized by number of liters filtered.

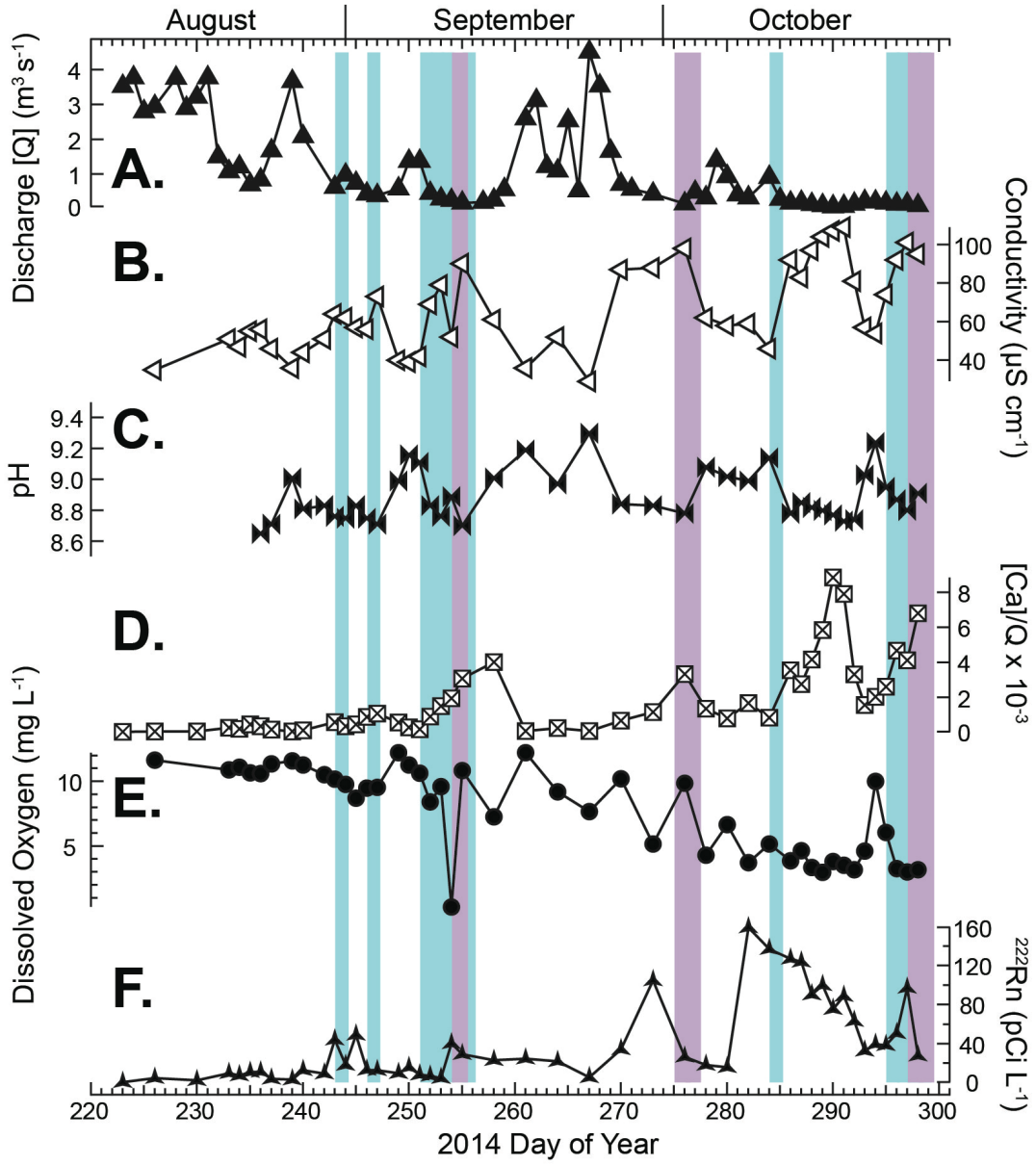

Figure III-3: 2014 geochemical data from the Athabasca glacier. A.) Repeat of discharge data from Figure 2. B.) Measured conductivity, C.) pH, and E.) dissolved oxygen from the glacial outflow channel. D.) Calcium concentrations normalized to daily discharge. F.) ^{222}Rn concentrations measured immediately after collecting a sample.

A first-order increase in conductivity is observed from August through October (40 to 200 µS cm^{-1}), with fluctuations that are in phase with Ca/Q and antiphase to discharge (Figure III-3A, B, D; Table III-1). pH varied between 8.7 and 9.3 (Figure III-3C; Table III-1) and is anti-correlated with conductivity. Dissolved oxygen (DO) decreased from 11.64 mg L^{-1} in mid-August to 3.19 mg L^{-1} in end-October, with greater scatter in the first-order trend observed between mid-September

and mid-October (DOY 258 – 289) (Figure III-3E; Table III-1). DO is saturated at approximately 11 mg L^{-1} and reaches those concentrations when Q > ~1 m^3 s^{-1} (Figure III-3E). Water temperatures remained at 0-0.1°C over the course of the study, eliminating temperature effects on saturation as the cause for varying levels of DO. ^{222}Radon activity concentrations ranged between 10 and 159 pCi L^{-1}; high Rn occurred with low Q (Figure III-3f). Radon concentrations were low (< 20 pCi L^{-1}) when Q was regularly > 1 m^3 s^{-1} (Figure III-3F; Table III-1).

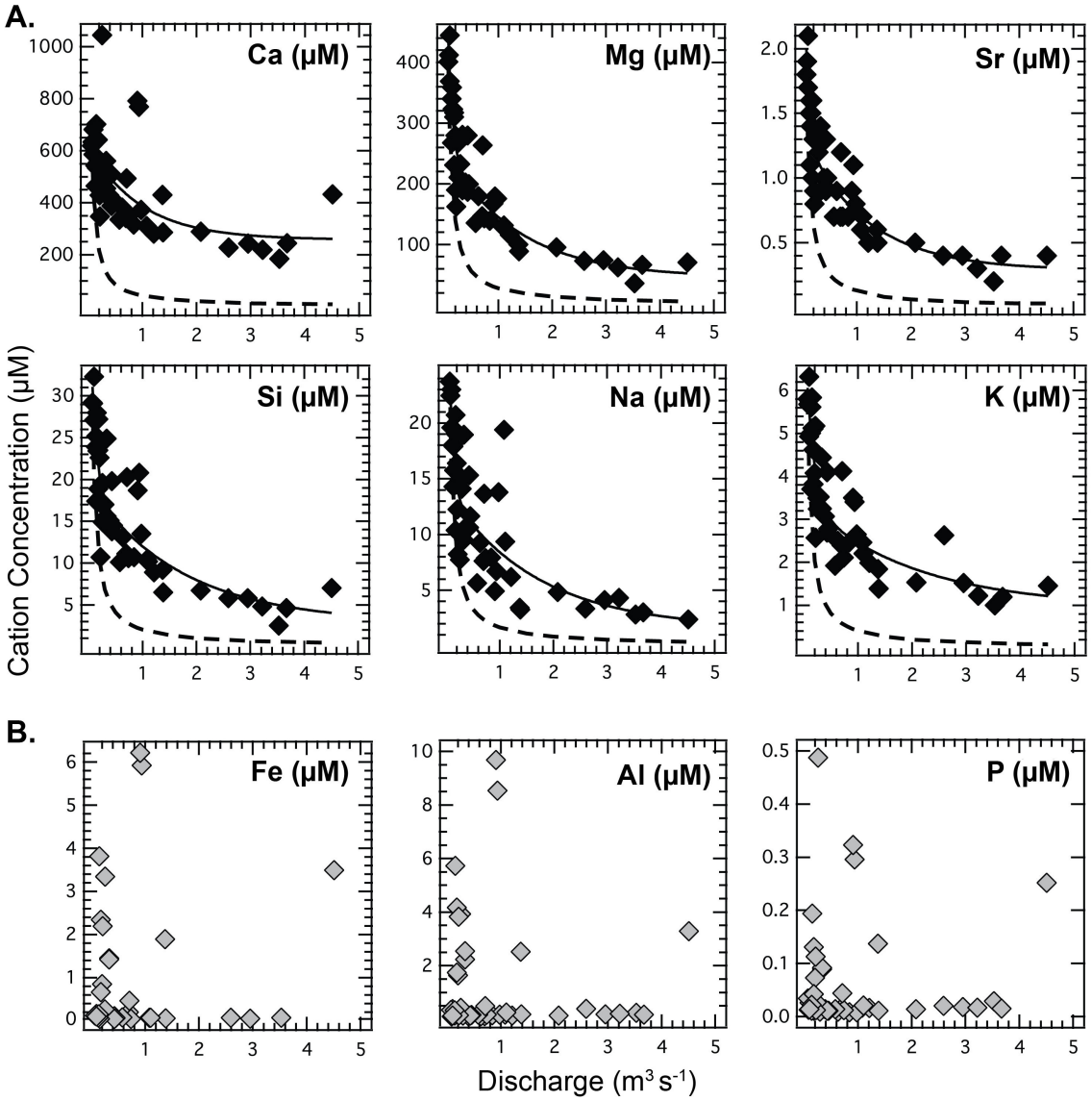

Figure III-4: A.) Concentrations as a function of glacial discharge of six soluble cations: calcium, magnesium, strontium, silicon, sodium, and potassium. Solid lines show trends of measured concentrations, dashed lines show calculated concentrations from pure mathematical dilution of the most concentrated value. B.) Concentrations as a function of glacial discharge of three insoluble cations: iron, aluminum, and phosphorous.

Table III-1: in situ hydrological parameters (Q, EC, pH, DO), ^{222}Rn activity concentration, $\delta^{18}O$, δD, and suspended concentration measurements by 2014 DOY.

2014 DOY	Q ($m^3\ s^{-1}$)	EC ($\mu S\ cm^{-1}$)	pH	DO ($mg\ L^{-1}$)	^{222}Rn ($pCi\ L^{-1}$)	$\delta^{18}O$ (‰)	δD (‰)	S. Sed ($mg\ L^{-1}$)
223	3.53	—	—	—	0.72	-22.31	-164.41	
226	2.95	35	—	11.64	4.94	-21.22	-157.61	24
230	3.22	—	—	—	2.75	-21.21	-156.80	62
233	1.08	51	—	10.90	9.75	-20.72	-153.35	20
234	1.21	47	—	11.11	7.41	-21.14	-155.74	—
235	0.70	55	—	10.66	10.9	-21.09	-156.35	18
236	0.84	56	8.65	10.62	11.5	-21.20	-156.71	41
237	1.67	46	8.71	11.37	4.06	-21.24	-157.39	16
239	3.67	36	9.01	11.60	3.2	—	—	—
240	2.08	44	8.81	11.26	13	-20.31	-149.91	—
242	—	51	8.83	10.52	9.46	-20.80	-153.35	—
243	0.63	64	8.76	10.17	44.1	-20.67	-153.60	22
244	0.98	62	8.75	9.78	18.3	-21.00	-155.64	—
245	0.74	57	8.83	8.70	49	—	—	30
246	0.43	56	8.75	9.48	13.4	-20.77	-153.59	—
247	0.39	73	8.71	9.53	12.8	-21.16	-156.03	20
249	0.58	40	8.99	12.22	9.71	-21.08	-154.88	—
250	1.37	39	9.16	11.27	16	-20.93	-153.35	65
251	1.38	42	9.11	10.63	8.3	-20.32	-149.51	60
252	0.45	69	8.83	8.43	7.28	—	—	—
253	0.29	79	8.76	9.59	5.07	—	—	39
254	0.25	52	8.89	0.30	40.2	-20.92	-153.99	—
255	0.18	90	8.70	10.84	29.2	-21.02	-155.64	12
258	0.26	61	9.01	7.26	23.2	-21.68	-160.51	566
261	2.59	36	9.19	12.21	24.7	-20.14	-150.81	555
264	1.10	52	8.97	9.20	21.9	-20.54	-152.10	—
267	4.51	29	9.30	7.68	5.77	-20.03	-147.19	272
270	0.71	87	8.84	10.21	34.2	-20.06	-147.87	36
273	0.43	88	8.83	5.18	105	-20.35	-150.25	—
276	0.16	98	8.78	9.86	26.8	-20.57	-152.12	—
278	0.33	62	9.08	4.31	18.4	-20.00	-147.58	44
280	0.94	58	9.02	6.67	16	-19.61	-143.67	477
282	0.33	59	8.99	3.74	159	-19.91	-146.67	89
284	0.91	46	9.14	5.16	137	-17.55	-127.37	—
286	0.18	92	8.78	3.88	127	-20.00	-146.63	—
287	0.20	83	8.85	4.65	124	—	—	39
288	0.13	97	8.82	3.35	90.3	-19.72	-145.04	20
289	0.10	104	8.80	2.99	99.9	—	—	—
290	0.07	107	8.77	3.80	75.4	—	—	46
291	0.08	109	8.73	3.53	88.7	—	—	14
292	0.14	81	8.74	3.19	63.2	—	—	18
293	0.22	57	9.03	4.62	32.9	—	—	30
294	0.21	54	9.24	9.99	39.6	—	—	58

295	0.18	74	8.95	6.07	38.3	—	—	41
296	0.15	92	8.87	3.27	50.6	-19.22	-141.07	97
297	0.14	101	8.80	3.00	97.2	—	—	47
298	0.10	95	8.91	3.17	27.9	-19.46	-144.64	32

Soluble major and trace cations (Na, Mg, Si, K, Ca, Sr) show lowest measured concentrations during high discharge periods and highest measured concentrations with low discharge (Figure III-4a). Consequently, as Q decreased from August through October, these soluble elements show an inverse trend. Insoluble elements (Fe, Al, P) do not correlate with discharge or day of year (Figure III-4b), although concentrations correlate with one another (Figure III-5a). Concentrations of insoluble elements also correlate with suspended sediment concentration (Figure 5b).

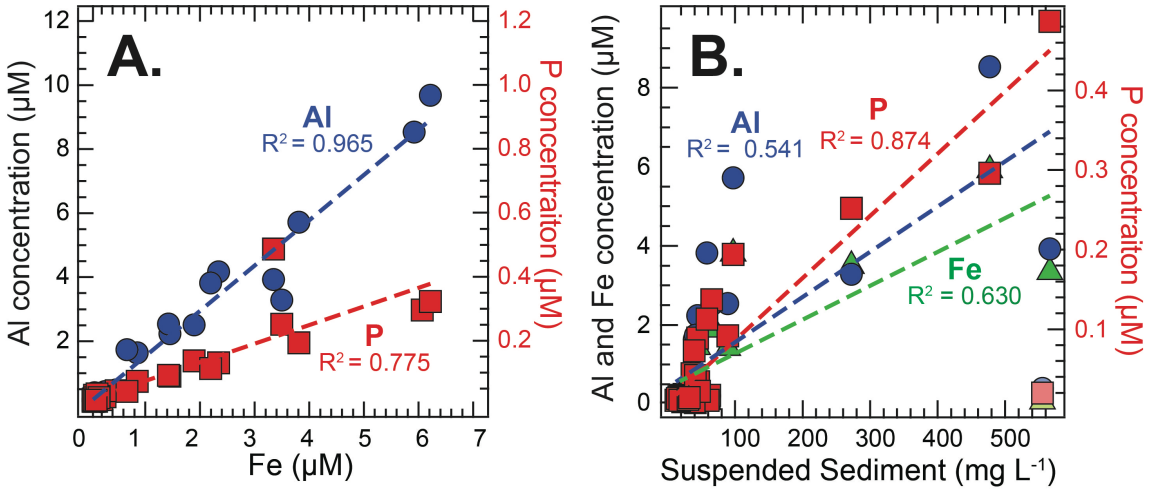

Figure III-5: A.) Correlations of insoluble elements. Aluminum concentration is plotted as a function of iron concentration in blue (R^2 = 0.965) and phosphorous concentration is plotted as a function of iron concentration in red (R^2 = 0.775). B.) Correlations of insoluble elements plotted as a function of suspended sediment concentration. Aluminum in blue (R^2 = 0.541), phosphorous in red (R^2 = 0.874), and iron in green (R^2 = 0.630). The three lighter colored points with high sediment concentration and low elemental concentrations were from the same day immediately following another day with high sediment concentrations and were not included in regression calculations.

Table III-2: Measured elemental concentrations (Na, Mg, Al, Si, P, K, Ca, Fe, and Sr) in 2014 collected outflow samples, organized by 2014 DOY.

2014 DOY	Na µM	Mg µM	Al µM	Si µM	P µM	K µM	Ca µM	Fe µM	Sr µM
223	2.83	35.72	0.24	2.55	0.03	1.00	185.37	0.07	0.22
226	4.12	73.97	0.19	5.78	0.02	1.52	242.57	0.04	0.40
230	4.31	62.29	0.20	4.82	0.02	1.22	220.44		0.34
233	19.39	129.21	0.18	10.43	0.02	2.46	310.19	0.07	0.64
234	6.18	115.75	0.13	8.91	0.02	1.99	281.92		0.54
235	7.63	146.67	0.12	11.13	0.02	2.40	340.77	0.19	0.67
236	7.91	138.86	0.15	10.66	0.01	2.47	316.40		0.67
237	6.28	123.05	0.12	9.03	0.01	1.95	291.52		0.61
239	3.02	66.21	0.17	4.63	0.01	1.19	244.17		0.36
240	4.84	95.54	0.14	6.67	0.01	1.53	289.05		0.47
242	6.73	131.92	0.13	9.75	0.01	2.08	326.11		0.63
243	9.24	179.78	0.12	13.14	0.01	2.50	381.29		0.87
244	13.80	175.60	0.17	13.49	0.01	2.65	373.05		0.85
245	7.86	142.91	0.17	10.59	0.01	2.11	347.25	0.04	0.73
246	10.63	186.65	0.14	13.77	0.01	2.69	388.26	0.10	0.89
247	10.75	201.95	0.13	15.13	0.01	3.07	429.45		0.97
249	5.63	135.33	0.17	10.06	0.01	1.92	335.79	0.08	0.65
250	3.42	100.12	2.51	9.17	0.14	1.84	430.47	1.89	0.57
251	3.27	88.70	0.18	6.50	0.01	1.39	286.33	0.06	0.47
252	11.64	199.44	0.16	14.55	0.01	2.78	412.50	0.06	1.01
253	14.10	232.22	0.14	17.05	0.01	3.52	438.39		1.19
254	14.78	267.44	0.43	19.63	0.02	3.49	489.32	0.26	1.29
255	20.71	310.23	0.21	23.48	0.01	4.62	555.24		1.41
258	7.72	210.37	3.93	14.88	0.49	3.24	1044.27	3.34	1.31
261	3.35	72.95	0.39	5.84	0.02	2.63	228.02	0.07	0.43
264	9.37	131.50	0.25	10.23	0.02	2.20	303.77	0.07	0.72
267	2.37	70.33	3.29	6.97	0.25	1.45	432.05	3.49	0.45
270	13.67	263.23	0.49	20.28	0.04	4.12	493.42	0.46	1.23
273	15.31	279.77	0.14	19.76	0.01	4.10	508.69	0.04	1.27
276	19.40	322.92	0.20	23.42	0.02	5.12	534.28	0.04	1.51
278	9.52	189.05	2.24	15.58	0.09	3.25	455.04	1.45	0.93
280	6.70	179.22	8.53	20.85	0.30	3.41	769.02	5.92	1.05
282	18.96	280.54	2.54	24.89	0.09	4.44	559.89	1.42	1.44
284	4.93	167.26	9.68	18.66	0.32	3.50	791.56	6.21	0.94
286	19.02	317.35	4.17	27.23	0.13	5.11	641.85	2.34	1.57
287	16.38	279.43	1.64	22.59	0.07	4.08	554.12	0.85	1.33
288	18.04	339.79	0.20	23.87	0.01	5.01	542.67	0.07	1.50
289	19.58	369.15	0.38	27.12	0.03	4.93	585.55	0.16	1.70
290	23.73	401.10	0.35	29.22	0.03	5.80	619.24	0.11	1.83
291	22.46	412.31	0.10	29.12	0.01	5.68	632.95		1.87
292	14.28	267.22	0.13	17.36	0.01	3.70	464.99		1.14
293	8.22	162.08	0.15	10.67	0.01	2.57	348.18		0.77

294	12.25	189.75	3.83	17.22	0.11	5.17	429.05	2.19	0.88
295	10.38	230.73	1.74	18.88	0.04	3.82	471.21	0.66	1.03
296	15.76	323.19	5.72	28.04	0.19	5.84	701.86	3.81	1.42
297	17.91	359.02	0.33	25.16	0.02	5.61	578.31	0.15	1.59
298	23.00	444.55	0.13	32.27	0.01	6.32	680.84	0.10	2.10

Discussion

Effects of Dilution on Measured Hydrochemistry

Measured elemental concentrations are strongly tied to glacial discharge through mixing and dilution of different water masses (e.g. Raiswell, 1984; Sharp et al., 1995; Tranter et al., 1997; 1993). In this multi-month study of AG melt, concentrations of water-soluble elements (Na, Mg, Si, K, Ca, Sr) are primarily controlled by dilution with highest concentrations occurring at low discharge (Figure III-4a). Chemical weathering reactions (e.g. carbonation, reduction-oxidation, and hydrolysis) add solutes to meltwater in the subglacial environment (S. P. Anderson et al., 1997; Raiswell, 1984; Tranter et al., 1993). As the AG has predominately carbonate bedrock, the most common weathering reactions are carbonation of carbonate minerals and carbonate hydrolysis, releasing Ca and Mg. Elements associated with silicate minerals (Na, Si, K) enter AG meltwater (Figure III-4a) via chemical weathering of shale layers interbedded with the carbonate bedrock.

AG ice originates as inland meteoric snow, and therefore contains few solutes. Surface water, supraglacial melt and rainfall, enters the en-/subglacial drainage system via moulins which dot the ice surface. As discharge varies with temperature trends and rainfall events (Figure III-2), the extent to which subglacial waters and weathering products are subsequently diluted also varies. Dilution is evidenced by decreasing elemental concentrations (Figure III-4a) and bulk conductivity measurements concurrent with increasing discharge (Figure III-3).

If solute production from chemical weathering is constant, it is possible that changing solvent (water) volume is the only mechanism affecting cation concentrations. To test this

hypothesis, the highest measured concentrations of six soluble elements (Ca, Mg, Sr, Si, Na, K) were mathematically diluted (Figure III-4a). The duplicate shape of the measured concentration best-fit (solid) lines and the calculated concentration best-fit (dashed) lines reveals dilution to be a primary control on elemental concentrations, yet measured concentrations do not reach the minima predicted from pure dilution (Figure III-4a). The concentrations measured in AG meltwater can be produced by increasing the amount of chemical weathering during intervals of low discharge to generate higher solute concentrations (e.g. Mitchell et al., 2006; Mitchell and Brown, 2008; Tranter et al., 1993).

Other Factors Influencing Chemical Weathering

Chemical weathering product concentrations are affected by: (1) water-rock interaction times, (2) availability of reactants (commonly protons and oxygen), (3) freshness of reactive mineral surfaces, (4) amount of exposed mineral surface area, and (5) type of minerals present in the environment in addition to dilution (Blum et al., 1998; Raiswell, 1984; Tranter et al., 1996; 1993). Water-rock interaction time is an important parameter controlling the extent of chemical weathering but is difficult to quantify in the obscured subglacial environment. Subglacial water residence time approximates water-rock interaction time, or length of time liquid water is present in the subglacial system and capable of reacting with sediment. Longer residence in the subglacial system provides more time for chemical reactions, allowing a greater number of fast reactions to occur and for more kinetically slow reactions to approach equilibrium. Bulk conductivity, water turbidity, and geochemical tracers are often used to estimate subglacial water residence time (Hubbard and Nienow, 1997; Nienow et al., 1998; Stone and Clarke, 1996). However, high meltwater volume dilutes bulk electrical conductivity (EC) making determination of volumes of fast- and slow-flow waters impossible (Tranter et al., 1997). Furthermore, EC is not conservative in glacial environments, making its use as a defining parameter for a mixing model a poor choice

(Bhatia et al., 2011; Sharp et al., 1995). Turbidity is limited by the availability of fine sediment and may produce erroneous residence time estimates if previously hydrologically isolated portions of the bed are suddenly flushed or if glacial grinding and sediment generation has been minimal. Tracer studies measure direct transit time but are limited spatially by moulin location, human access, and ability to detect the tracer at the terminus.

Subglacial water residence time may be revealed by changing ^{222}Rn activity concentrations in meltwater (Arendt et al., 2017; Bhatia et al., 2011; Kies et al., 2011). ^{222}Rn is formed by alpha decay of ^{226}Ra ($t_{1/2}$ = 1600 years), an intermediary in the uranium decay series. ^{222}Rn is radioactive ($t_{1/2}$ = 3.8 days), and as such reaches secular equilibrium with ^{226}Ra in five half-lives (> 20 days). Prior to secular equilibrium, ^{222}Rn produced in the subglacial environment dissolves into meltwater, increasing its concentration as a function of water residence time. ^{222}Rn activity concentration ([^{222}Rn]) is useful as a proxy for water residence time as: (1) it ultimately derives from ^{238}U – a ubiquitous isotope, (2) it is a noble gas and therefore unreactive, and (3) a short half-life means its presence establishes recent water-sediment interaction (Bhatia et al., 2011; Kies et al., 2011). At the AG, [^{222}Rn] was low (<50 pCi L^{-1}) through mid-September (DOY 267) while discharge was high, reaching a maximum of 159 pCi L^{-1} in late October concurrent with low discharge (Figure III-3), suggesting increased subglacial water residence time.

Previous work investigated the seasonal 'opening' of alpine subglacial drainage networks in spring as slow-flowing disconnected networks shift to efficiently connected, rapidly-flowing channelized networks (Fountain and Walder, 1998; Hubbard and Nienow, 1997). This process is well documented in alpine glaciers (R. S. Anderson et al., 2004; Iken and Bindschadler, 1986; Mair et al., 2003), and has been observed to occur at the AG (Arendt et al., 2015). As subglacial drainage networks evolve from slow, inefficient configurations to quick arborescent (channelized) networks each spring, a subsequent shift in configuration back to an inefficient (distributed) network logically

occurs at a later season. Subglacial drainage channels at alpine glaciers shrink and become less efficient as frictional heating driven by liquid water flux decreases, eventually closing through ice creep when no longer held open by flowing water (Hubbard and Nienow, 1997; Nye, 1976; Röthlisberger, 1972; Shreve, 1972). Subglacial water residence time is therefore hypothesized to increase over the study period as air temperatures cooled from 21°C on August 14 to -2°C on October 28 and discharge decreased (Figure III-2).

Unlike spring events where an initial meltwater pulse from melting surface ice overwhelms the subglacial drainage network, lubricates the glacial bed, and causes a substantial, measurable increase in ice surface velocity for hours to days (R. S. Anderson et al., 2004; Iken and Bindschadler, 1986; Mair et al., 2003), subglacial hydrologic network closure is slower and less pronounced. Individual air temperature measurements do not follow seasonal trends and precipitation events add water stochastically to the system both quickly (rain) and slowly (snow), so gradual trends can be obscured in daily noise. Less melt in the system also lowers the liquid pressure experienced by melt water, so it does not receive the same 'push' through the system as in peak melt. Coding the data by DOY reveals that as discharge decreased from August through October, [^{222}Rn] increased, DO concentration decreased, and conductivity increased; all parameters supporting a transition to a disconnected system with increased water residence time (Figure III-6). However, as temperature and discharge vary over the study period, daily EC and ^{222}Rn activity measurements also fluctuate, reflecting a dynamic subglacial system.

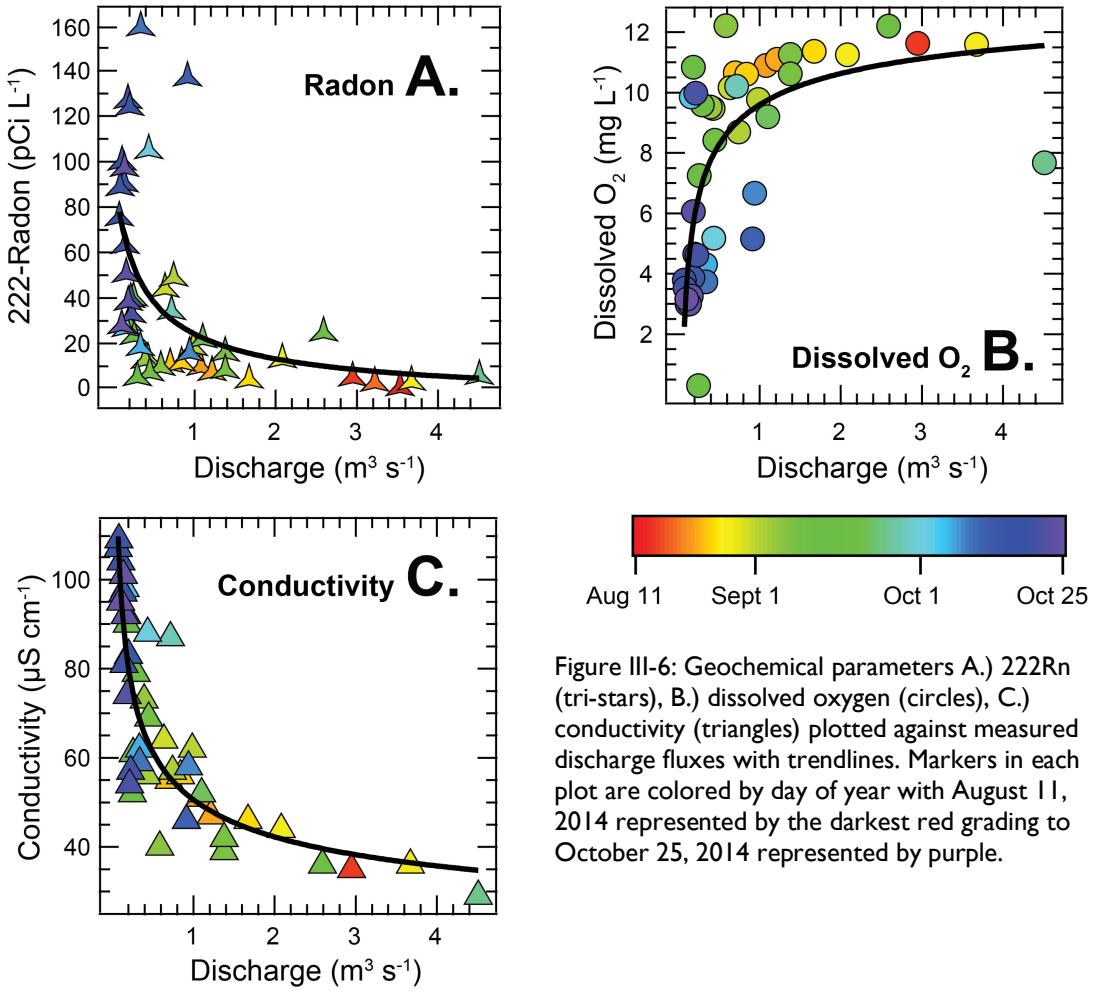

Figure III-6: Geochemical parameters A.) 222Rn (tri-stars), B.) dissolved oxygen (circles), C.) conductivity (triangles) plotted against measured discharge fluxes with trendlines. Markers in each plot are colored by day of year with August 11, 2014 represented by the darkest red grading to October 25, 2014 represented by purple.

Suspended sediment concentrations can reveal changes in hydrologic configuration (Gordon et al., 1998; Swift et al., 2005; Haritashya et al., 2010), specifically showing the non-linearity of the shutdown process and providing context for variability seen in EC and ^{222}Rn activity. Abrupt reorganization of subglacial drainage networks at alpine glaciers is frequently accompanied by increases in sediment flux (Collins, 1989; 1990; Gordon et al., 1998; Swift et al., 2005): as subglacial drainage networks become established in a channelized configuration, preferential flushing of sediments within channels occurs. At the AG, suspended sediment concentrations generally ranged from 10-60 mg L^{-1} but were an order of magnitude higher on DOY 258-261 (566 mg L^{-1}) and 280 (477 mg L^{-1}). These dates are noteworthy as they are both

associated with warmer air temperatures and increased discharge immediately following days with air temperatures < 0°C (Figure III-2). Gordon et al. (1998) observed changes in hydrologic connectivity between boreholes drilled at Haut Glacier d'Arolla, Switzerland, finding smaller, isolated hydrologic sub-networks disconnected from, then reconnected to, main drainage as water input volumes changed. Additional meltwater had the ability to reconnect some of these isolated sections back to a more comprehensive configuration as daily temperature and precipitation volumes varied (Gordon et al., 1998). This process likely occurred at the AG during this 2014 study as air temperature and discharge fluctuated (Figure III-2). DOY 254 and 275 were both days when average daily temperature was < 0°C, EC was high, discharge was low, and [^{222}Rn] was above background (Figure III-3). DOY 258 and 280, in contrast just 4-5 days later, exhibited positive daily temperatures, high discharge, and lower [^{222}Rn] (Figure III-3). If cold air temperatures led to isolation of some parts of the bed and consequently a less efficient drainage network, then subsequent warmer temperatures generated increased melt, reconnected the isolated sections, and forced the network back to an efficient configuration before a final shutdown. These data illustrate the non-linearity of subglacial hydrologic network shutdown.

Abrasion of entrained sediments in glacial ice produces very fine, high surface area–low volume rock flour (Benn and Evans, 2010); constant availability of fresh, reactive mineral surfaces in subglacial sediment leads to enhanced chemical weathering relative to non-glacial environments at similarly cold temperatures. Acidity – a necessary reactant to dissolve carbonate minerals – is commonly derived by dissolution of CO_2 into water but can be limited by slow kinetics (Fairchild et al., 1994). With carbonate bedrock, water pH at the AG is controlled by carbonate equilibrium (Fairchild et al., 1994) whereas EC reflects the concentration of bulk ionic products. Over this three-month study, pH fluctuated within a half unit 8.85 – 9.3 and EC ranged from 29 – 109 μS

cm^{-1}, but there were no occurrences of concurrent high conductivity and low pH (Figure III-7b). High EC only occurred with lower pH values regardless of time of year, potentially indicating a change in the type of chemical reactions occurring in this system.

Closing subglacial hydrologic networks are unable to freely exchange CO_2 with the atmosphere, and as such additional protons may be sourced by pyrite oxidation (Fairchild et al., 1994; Tranter et al., 2002). At the AG, pyrite is a common accessory mineral in the interbedded Stephen Fm. shales (Butterfield, 1995; Gaines et al., 2012); its oxidation is coupled to calcite dissolution in equation 1:

$$4FeS_{2(s)} + 14H_2O + 15O_2 + 16CaCO_3 \rightarrow 4Fe(OH)_{3(s)} + 8SO_4^{2-} + 16Ca^{2+} + 16HCO_3^- \quad (1)$$

DO was saturated (~11 mg L^{-1}) in glacial terminus waters in August but decreased to ~3 mg L^{-1} in October (Figure III-7c), likely due to both decreasing input to the subglacial system and increasing consumption en route. In August, higher average daily temperatures generated increased surface melt which then drained into crevasses or moulins. This flow was turbulent, increasing DO to saturation via diffusion prior to entry into the subglacial network. Once in the subglacial network, DO was removed from subglacial water as a reactant in oxidation reactions. Pyrite and organic carbon oxidation produced protons – lowering pH – and ionic products (sulfate) – increasing EC, explaining the late October observations (Figure III-7b) (Mitchell and Brown, 2008).

DO concentrations as a function of EC (Figure III-7a) reveal a linear relationship both in the beginning and end of the study, with the simple relationship breaking down during September. A more complex relationship coincides with intervals of high suspended sediment concentrations when dynamic change and isolation of sections of the hydrologic system occur (Figure III-2f). Water stored in isolated areas have longer water-rock interaction times, consequently consuming

DO, producing more solutes, and increasing EC (Figure III-7a). Lower water pH at the terminus indicates DO consumption (oxidation) (Figure III-7c), supporting a more distributed drainage configuration. Resultant proton-driven dissolution of carbonates indicated by the calcium flux, normalized to discharge, increases as pH decreases (Figure III-7d). Changing configurations of the hydrologic network relink isolated sections, mixing fast- and slow-flowing subglacial waters prior to exiting the system. Therefore, while there are broad seasonal trends in water quality data (Figures III-6, III-7), daily temperature and weather fluctuations force data from individual days closer to or further away from average trends. Notably, the negligible time lag between the shift from negative to positive air temperatures and resultant differences in hydrochemistry indicates the subglacial hydrologic network is extremely dynamic and responsive to weather fluctuations.

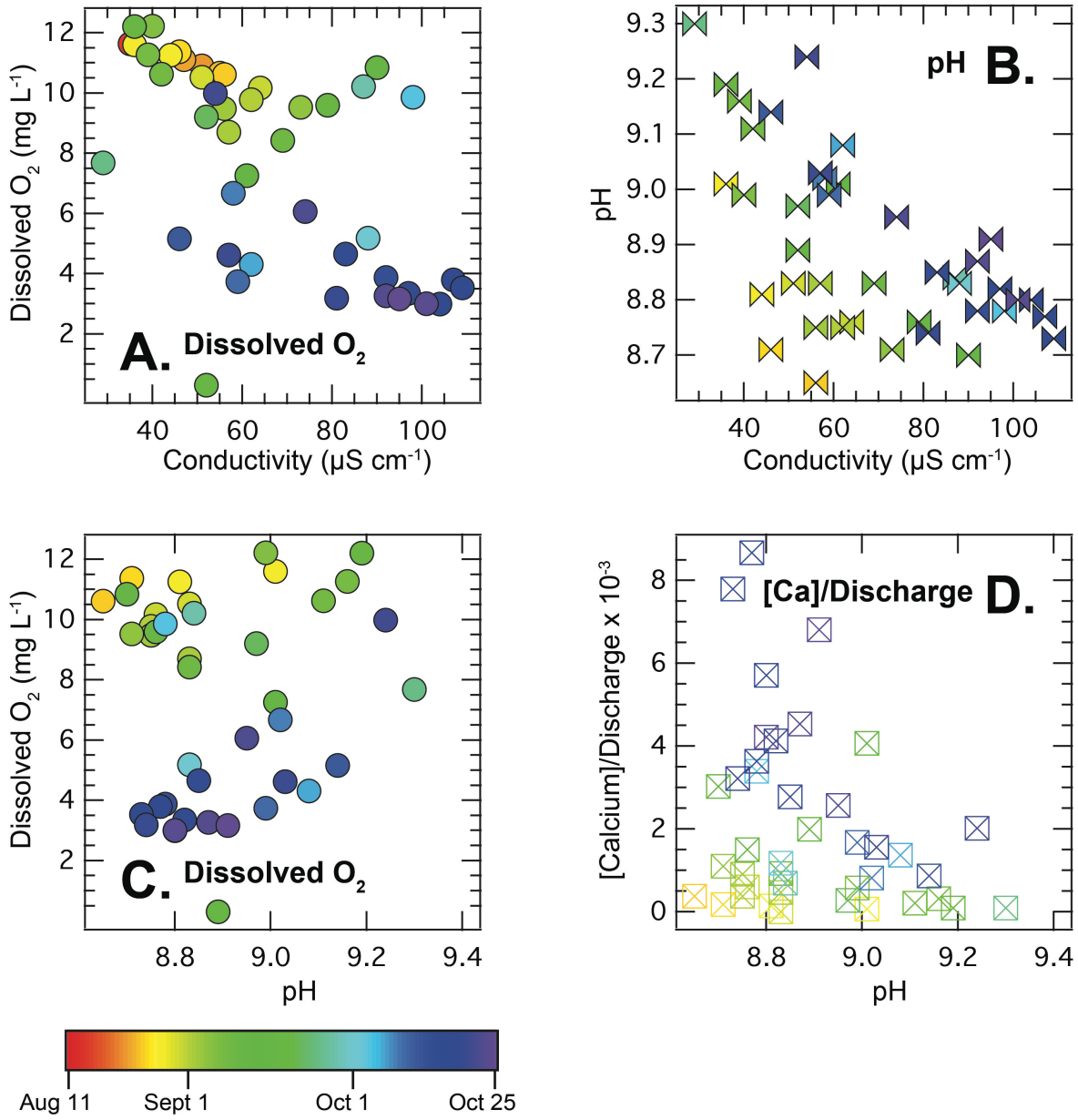

Figure III-7: A.) Dissolved oxygen (circles) plotted as a function of conductivity. B.) pH (bowties) plotted as a function of conductivity. C.) Dissolved oxygen (circles) plotted as a function of pH. D.) Calcium normalized to discharge (X-boxes) plotted as a function of pH. Markers in each plot are colored by day of year with August 11, 2014 represented by the darkest red grading to October 25, 2014 represented by purple.

Shifts in Subglacial Weathering Regimes

Beyond dilution effects and subglacial water residence time, changing the ratio of different types of chemical weathering can also influence measured glacial hydrochemistry. The heterogeneous bedrock at the AG of carbonates with interbedded shales produces Ca and Mg

cations ('CE' – carbonate elements) while hydrolysis of clay minerals in shales contributes elements such as Si, Na, and K ('SE' – silicate elements). Seasonal shifts of these two elemental groups in meltwater resolve the relative contributions of different weathering reactions in the subglacial environment. In addition to the greater relative abundance of carbonates to shales in the AG subglacial environment, the order of magnitude difference in concentration of CE compared to SE (Figure III-8) also results from reaction kinetics: carbonate dissolution occurs much more rapidly than hydrolysis of silicate minerals (Anderson et al., 1997).

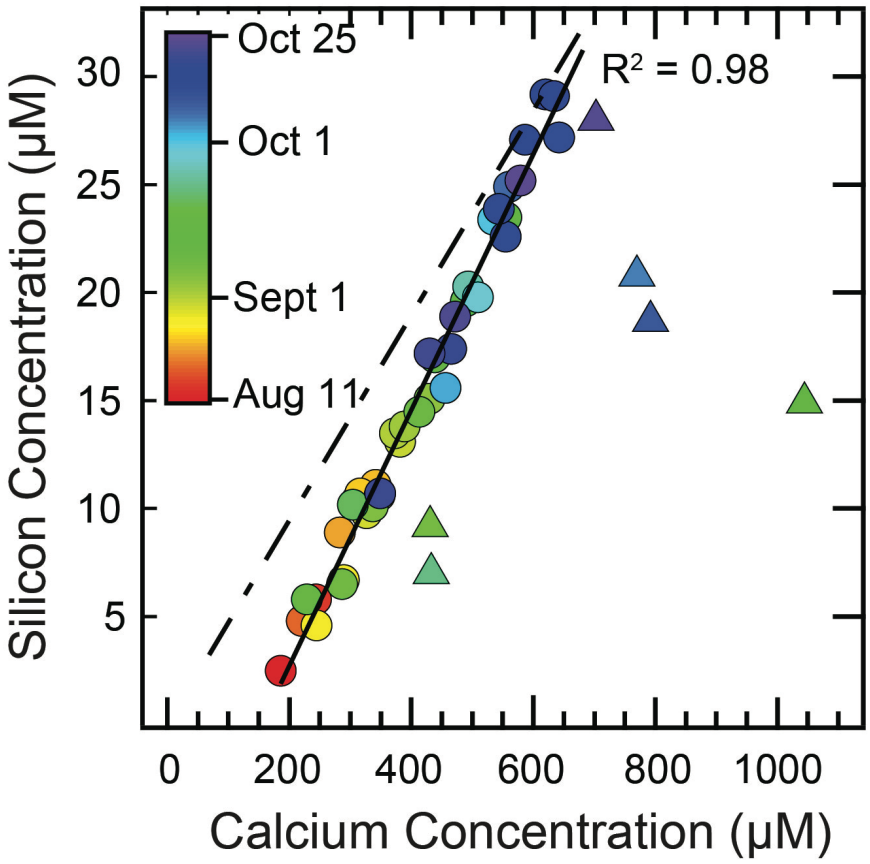

Figure III-8: Silicon concentrations versus calcium concentrations. All points are colored by day of year with August 11, 2014 represented by the darkest red grading to October 25, 2014 represented by purple. Circular points were included in the trendline calculation; six triangular points were excluded. Solid line shows the linear regression (R^2 = 0.98) through the circular points. Dashed line shows pure mathematical dilution of the most concentrated value.

Subglacial water flows through a deformable mixed till layer between the ice and the solid bedrock beneath the AG, effectively homogenizing heterogeneous bedrock (Clinger et al., 2016).

As till is not size sorted, this blended till layer contains a range of silt- to clay-sized particles significantly increasing mineral surface area available for weathering reactions relative to bedrock (S. P. Anderson et al., 1997; Tranter and Wadham, 2014). This homogenized, high surface area layer ensures any observed difference in the proportion of CE to SE within the bulk meltwater is likely due to changes in subglacial chemical reactions and is not merely an artifact of water encountering a different rock type as its path under the ice changes.

CE and SE, represented by Ca and Si respectively, are strongly positively correlated (Figure III-8, $R^2 = 0.98$), reflecting their simultaneous subglacial production from the till layer. Due to dilution, both CE and SE concentrations show exponential decay with increasing discharge (Figure III-4a). The sample with highest Ca and Si concentrations was mathematically diluted (Figure 8, dashed line) to determine if dilution produced the observed trend in concentration. However, the steeper sloped best-fit line of the observed data (Figure III-8, solid line) reveals additional CE relative to SE when concentrations of both are low in times of high discharge. As neither dilution nor increased water-rock interaction time explain this trend, there is a third factor – conceivably reaction kinetics – affecting subglacial chemical concentrations.

Glacial catchments yield similar total cation denudation rates compared to non-glaciated catchments with comparable bedrock (Anderson et al., 1997), but generate a much larger proportion of CE relative to SE regardless of bedrock type (S. P. Anderson et al., 1997; Blum et al., 1998). In subglacial environments, carbonate mineral weathering reactions are enhanced due to high calcite dissolution reaction kinetics and mineral strain caused by glacial abrasion (S. P. Anderson et al., 1997; Blum et al., 1998) while chemical weathering rates of silicate minerals are reduced. These differences in weathering rates are apparent in the concentrations of Ca and Si measured at the AG in this study, but do not explain the divergence of measured concentrations (Figure III-8) from the calculated pure-dilution line during periods of high discharge. High

discharge occurs in late-August/early-September when air temperatures are above freezing and the sub-glacial drainage network is in a well-connected summertime channelized configuration, with minimal water residence times. As mineral surfaces chemically weather, meltwater flow removes both CE and SE products, leaving the drainage network perpetually undersaturated. Undersaturation promotes chemical weathering reactions; faster rates of carbonate weathering result in increased CE concentrations, and accounts for the deviation between the measured cation concentrations and mathematically diluted concentrations (Figure III-8). The difference between CE and SE concentrations decreases in October (Figure III-8) due to lower flow rates and a more distributed network: longer water residence times allow time for consumption of all available reactants and/or allows the subglacial environment to reach saturation.

Within the study period, anomalously high Ca concentrations relative to Si were observed on six days of the 46 sample collection days in the study period (Figure III-8; triangles). These particular samples also displayed higher, but not anomalous, EC measurements, but there are no other environmental characteristics unique to these days. These six samples may have become enriched in Ca relative to Si because of enhanced Ca weathering explained by greater carbonate dissolution – such as may occur within a secondary calcite vein. If subglacial flow paths reorganize such that waters are in contact with many small-sized, high surface area grains of crushed limestone and not dolostone, the characteristic carbonate fast-weathering rates may explain this increase in Ca, but not Mg, concentration. This study is not able to distinguish whether these anomalous Ca concentrations are due to exposure of unweathered mineral surfaces on freshly ground glacial carbonate flour or exposure of water to previously untouched diagenetic calcite, but either possibility may explain these six data points.

Particle Reactive (Fe, Al, P) Weathering Product Trends

Most elemental concentrations within AG meltwater are primarily controlled by dilution (Figure III-4a) along with reaction kinetics and water-rock interaction time (Figures III-6, III-8), but insoluble elements (Fe, Al, and P) display different behavior (Figure III-4b). Concentrations of these elements correlate with each other (Figure III-5a) and with concentrations of suspended sediment (Figure III-5b), but do not correlate with other hydrochemical parameters. Particle reactive elements such as Fe, P, and Al form oxides on the outside of sedimentary particles and thus can be transported as colloids (<1 μm), nanoparticles (<0.1 μm), and in aqueous forms (<0.01 μm) (Hawkings et al., 2014; Raiswell and Canfield, 2012) in meltwater. Previous work shows soluble reactive P sorbs onto reactive Fe (oxy)hydroxide colloids and nanoparticles (Hawkings et al., 2014). Aluminum behaves similarly to Fe in that it exists in a variety of sizes beyond simply 'dissolved' and 'suspended' forms in filtered waters and depends on the presence, abundance, and type of colloidal material (Horowitz et al., 1996). Even though waters were filtered through a 0.22 μm pore size filter, it is possible that a significant fraction of (colloidal or smaller) Fe, P, and Al was filter-passing (Hawkings et al., 2014; Raiswell and Canfield, 2012). Thus, the aqueous fraction collected at the AG may have included some of these smaller particles which were then measured as 'dissolved' forms. Iron, Al, and P concentrations correlate with measured sediment concentrations (Figure III-5b), supporting the hypothesis that elemental concentrations are controlled primarily by colloidal particle availability.

Higher concentration (mg L^{-1}) major weathering products such as Ca are not associated with colloids (Horowitz et al., 1996), and therefore are not expected to correlate with Fe, P, or Al concentrations. However, six samples (Figure III-8, triangles) that show greatly enhanced carbonate weathering relative to silicate weathering occur on DOYs that also have high measured concentrations of Fe, Al, and P. This relationship may be due to exposure of unweathered mineral

surfaces on freshly ground glacial carbonate flour. These six samples may evidence routing changes in the subglacial environment, flushing previously isolated and minimally weathered sediments with accompanying colloids.

Annual Glaciochemical Cycling

Changes in expressed hydrochemistry at the Athabasca Glacier have been observed during the opening of the subglacial drainage network in early spring (Arendt et al., 2017; 2015; Niu et al., 2017). Comparison of 2014 late season to 2011 early season hydrochemistry reveals cyclic trends with implications for downstream aquatic environments. Deuterium isotopes show a seasonal evolution of water source: in May, meltwater initially reflects a mix of ice (-140‰) and snow (-205‰) melt, with δD shifting more negatively towards pure snowmelt as discharge increases in mid-May (Figure III-9) (Arendt et al., 2015). As seasonal snow is not an enduring reservoir, end-May sees δD move more positively, again with increasing discharge, away from snow towards ice melt values (Figure III-9) (Arendt et al., 2015). 2014 initial (August) δD and discharge measurements correspond well with published July 2011 values (Arendt et al., 2015), evolving through September and October 2014 toward pure ice melt isotopic composition as discharge decreases with cooling temperatures (Figure III-9). Here, scatter in isotopic measurements relates to stochastic precipitation with significantly more positive δD values (Figure III-9). The final sample in 2014 did not match the values from the initial 2011 samples; discharge was too high and the δD value more closely resembled ice-, not snow-, melt. We predict as winter transitions to spring, discharge would increase as snow melts and δD would approach May 2011 values (Arendt et al., 2015).

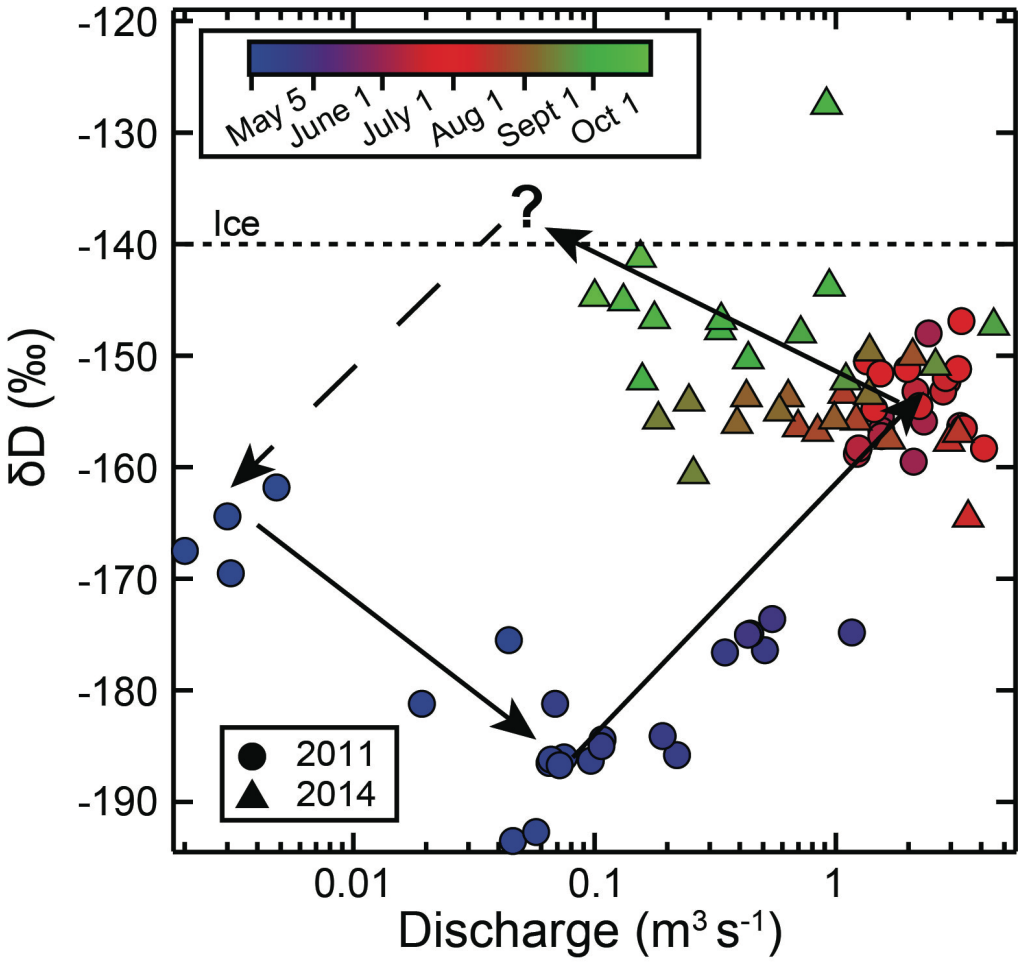

Figure III-9: δD plotted against discharge. 2011 δD data (circles) were published in Arendt et al. (2015) and correlated with discharge data published in Arendt et al. (2017) by day of year. 2014 data (triangles) collected in this study. Ice melt δD (dotted line) value is published in Arendt et al. (2015). Markers are colored by day of year with May 6 (DOY 126) represented by the darkest blue grading to October 25 (DOY 298) represented by green. Solid arrows show seasonal evolution of δD; dashed arrow represents a possible path from DOY 298 to DOY 126 in the subsequent year.

Combining 2011 (Arendt et al., 2015) and 2014 hydrochemistry allows for the reconstruction of an (almost) annual subglacial weathering regime highlighting shifts in proportion of carbonate vs. silicate weathering (Figure III-10). An initial increase in SE relative to CE is observed as springtime discharge increases, associated with an increase in connectivity tied to a spring opening event, flushing out concentrated meltwater previously isolated in winter (Collins,

1989; Iken and Bindschadler, 1986; Mair et al., 2003; Nienow et al., 1998). As rates of carbonate weathering are much faster than silicate weathering in glacial environments (Blum et al., 1998; Jacobson et al., 2002), this observed change in meltwater chemistry likely reflects the evacuation of previously isolated waters that were able to weather silicate minerals for an extended period of time (Figure III-10). Waters measured in May 2011 exhibit higher ^{222}Rn activity (Arendt et al., 2017), further supporting a long residence time under the AG. July 2011 weathering products show a large increase in CE relative to SE when discharge increases and the system is fast-flowing and 'open' to the atmosphere (Figure III-10). Late summer 2014 data then reveal a gradual decrease in CE relative to SE through fall as discharge drops. Closure of the system would limit gas flux to the subglacial environment, limiting reactants for dissolution reactions (Raiswell et al., 2008; Tranter et al., 1993). Late winter/early spring measurements of CE/SE and discharge are predicted to match up with the values measured in 2011 by Arendt et al. (2015).

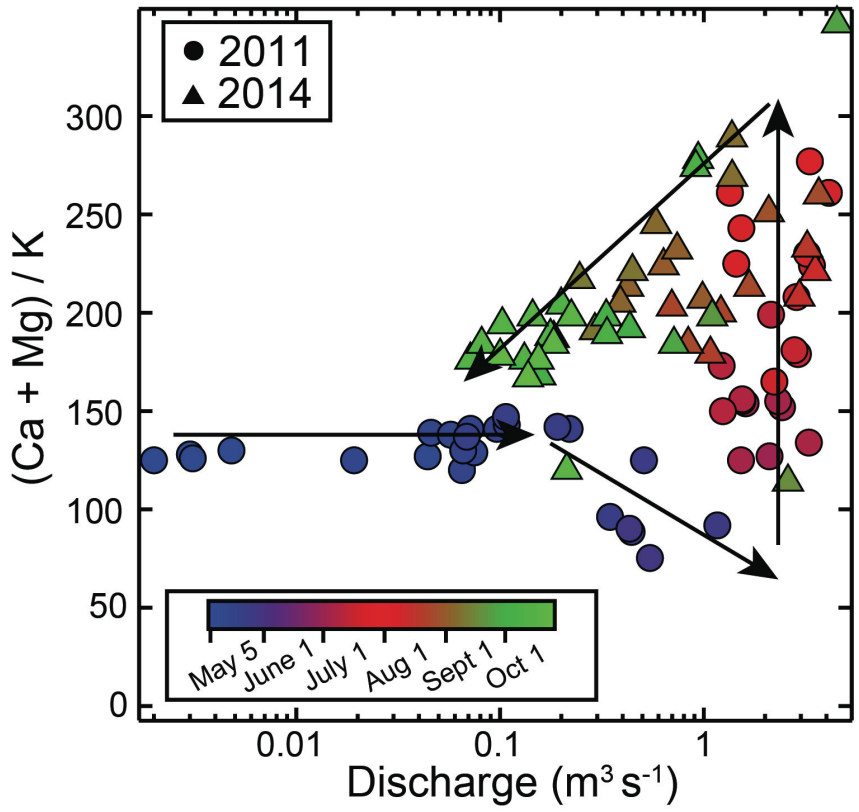

Figure III-10: Carbonate weathering products (Ca + Mg) normalized by a representative silicate weathering product (K) plotted as a function of discharge. 2011 data (triangles) published in Arendt et al. (2017), 2014 data (circles) collected in this study. Markers are colored by day of year with May 6 (DOY 126) represented by the darkest blue grading to October 25 (DOY 298) represented by green. Solid arrows show seasonal progression.

These trends (Figures III-9, III-10) reveal that seasonal changes both in water source at the AG and how meltwater chemically weathers available minerals extend across multiple years. Similarities in the data suggest this cycle repeats annually: relatively lower proportions of CE in early spring when most water is snowmelt (Arendt et al., 2015), followed by a large increase in CE through mid-summer with ice melt greatly contributing to discharge, then a final gradual decrease in the ratio of CE to SE concurrent with the shutdown and freezing of the hydrologic network. Future climate change will adjust the timing of physical changes in the subglacial hydrologic system as wintertime conditions are predicted to occur later in the year.

Conclusion

A three-month geochemical timeseries of meltwater discharged from the Athabasca Glacier in the Columbia Icefield, Canada documents the seasonal transition from a well-connected configuration in August to a poorly-connected, discontinuous subglacial hydrologic system in October. Dilution primarily controls cation concentrations in meltwater collected at the glacial terminus, although chemical weathering rates and reactant availability are also factors. Late August hydrochemistry indicates summertime channelized conditions: high discharge, low elemental fluxes, and relatively high proportions of Ca relative to Si. Significantly cooler average air temperatures, lower discharge, and higher bulk conductivity measurements marked the end of the study in October, suggesting a poorly-connected subglacial hydrologic network.

Varying ratios of carbonate to silicate weathering products illustrate the existence of more nuanced chemistry beyond simple dilution at the AG. Mid-study (September) ratios of Ca to Si, sediment flux, and pH variations anticorrelated with conductivity all suggest a stochastic transition from a primarily channelized drainage network to a more disconnected distributed system. Slow flow waters contained less DO as it was consumed in pyrite and organic matter oxidation;

simultaneously longer water-rock contact time imparted more ^{222}Rn to the water. These changes occurred as immediate responses to freezing temperatures, marking the subglacial hydrologic network as a dynamic environment.

While the hydrochemistry presented here appears to show shutdown of the 2014 AG subglacial drainage network concurrent with the advent of wintertime conditions in autumn, measured discharge did not reach the low values measured at the same location in May 2011 (Arendt et al., 2015). Continued monitoring of the glacier into November and December might have shown further geochemical evidence for changes in the subglacial drainage network, but winter conditions precluded further measurement in 2014. Future work may build on this study by analyzing anion concentrations in addition to cations to better understand the chemical weathering reactions occurring. Increased sampling frequency during freezing events could improve our understanding of the temporal resolution of subglacial channel reorganization. Combined, these approaches could provide a greater understanding of the seasonal evolution of the subglacial drainage network at the Athabasca Glacier and its response to changing air temperatures.

References

Aciego, S.M., Stevenson, E.I., Arendt, C.A., 2015. Climate versus geological controls on glacial meltwater micronutrient production in southern Greenland. Earth Planet. Sci. Lett. 424, 51–58. doi:10.1016/j.epsl.2015.05.017

Aitken, J.D., 1978. Revised models for depositional grand cycles, Cambrian of the southern Rocky Mountains, Canada. Bull. Can. Petrol. Geol. 26, 515–542.

Anderson, R.S., Anderson, S.P., MacGregor, K.R., Waddington, E.D., O'Neel, S., Riihimaki, C.A., Loso, M.G., 2004. Strong feedbacks between hydrology and sliding of a small alpine glacier. J. Geophys. Res. 109, 1–17. doi:10.1029/2004JF000120

Anderson, S.P., 2005. Glaciers show direct linkage between erosion rate and chemical weathering fluxes. Geomorphology 67, 147–157. doi:10.1016/j.geomorph.2004.07.010

Anderson, S.P., Drever, J.I., Humphrey, N.F., 1997. Chemical weathering in glacial environments. Geology 25, 399–402. doi:10.1130/0091-7613(1997)025<0399:cwige>2.3.co;2

Anderson, S.P., Longacre, S.A., Kraal, E.R., 2003. Patterns of water chemistry and discharge in the glacier-fed Kennicott River, Alaska: evidence for subglacial water storage cycles. Chem. Geol. 202, 297–312. doi:10.1016/j.chemgeo.2003.01.001

Arendt, C.A., Aciego, S.M., Hetland, E.A., 2015. An open source Bayesian Monte Carlo isotope mixing model with applications in Earth surface processes. Geochem. Geophys. Geosystems 16, 1274–1292. doi:10.1002/2014gc005683

Arendt, C.A., Aciego, S.M., Sims, K.W.W., Aarons, S.M., 2017. Seasonal progression of uranium series isotopes in subglacial meltwater: Implications for subglacial storage time. Chem. Geol. 467, 42–52. doi:10.1016/j.chemgeo.2017.07.007

Arendt, C.A., Stevenson, E.I., Aciego, S.M., 2016. Hydrologic controls on radiogenic Sr in meltwater from an alpine glacier system: Athabasca Glacier, Canada. Appl. Geochem. 69, 42–49. doi:10.1016/j.apgeochem.2016.04.002

Barnett, T.P., Adam, J.C., Lettenmaier, D.P., 2005. Potential impacts of a warming climate on water availability in snow-dominated regions. Nature 438, 303–309. doi:10.1038/nature04141

Benn, D.I., Evans, D.J.A., 2010. Glaciers & Glaciation, second ed. Routledge, London.

Bhatia, M.P., Das, S.B., Kujawinski, E.B., Henderson, P., Burke, A., Charette, M.A., 2011. Seasonal evolution of water contributions to discharge from a Greenland outlet glacier: insight from a new isotope-mixing model. J. Glaciol. 57, 929–941. doi:10.3189/002214311798043861

Blum, J.D., Gazis, C.A., Jacobson, A.D., Chamberlain, C.P., 1998. Carbonate versus silicate weathering in the Raikhot watershed within the High Himalayan Crystalline Series. Geology 26, 411–414. doi:10.1130/0091-7613(1998)026<0411:CVSWIT>2.3.CO;2

Brown, L.E., Hannah, D.M., 2008. Spatial heterogeneity of water temperature across an alpine river basin. Hydrol. Process. 22, 954–967. doi:10.1002/hyp.6982

Brugman, M.M., Denmuth, M.N., 1994. Surface and basal topography of the Athabasca Glacier: A glaciological interpretation and recommendation for the location of near-ice interpretative facilities. National Hydrology Research Institute, Saskatoon, Saskatchewan.

Butterfield, N.J., 1995. Secular distribution of Burgess-Shale-type preservation. Lethaia 28, 1–13. doi:10.1111/j.1502-3931.1995.tb01587.x

Chandler, D.M., Wadham, J.L., Lis, G.P., Cowton, T., Sole, A., Bartholomew, I., Telling, J., Nienow, P., Bagshaw, E.B., Mair, D., Vinen, S., Hubbard, A., 2013. Evolution of the subglacial drainage system beneath the Greenland Ice Sheet revealed by tracers. Nature Geoscience 6, 195–198. doi:10.1038/ngeo1737

Charlesworth, H., Erdmer, P., 1989. An overview of the Geology of the Rocky Mountains between the Athabasca and North Saskatchewan Rivers. Edmonton Geological Society.

Clinger, A.E., Aciego, S.M., Stevenson, E.I., Arendt, C.A., Robbins, M.J., 2016. Implications for post-comminution processes in subglacial suspended sediment using coupled radiogenic strontium and neodymium isotopes. Geomorphology 259, 134–144. doi:10.1016/j.geomorph.2016.02.006

Collins, D.N., 1989. Seasonal development of subglacial drainage and suspended sediment delivery to melt waters beneath an alpine glacier. Ann. Glaciol. 13, 45–50. doi:10.3189/s026030550000762x

Collins, D.N., 1990. Seasonal and annual variations of suspended sediment transport in meltwaters draining from an Alpine glacier. Hydrol. Mt. Reg. I: Hydrol. Meas.; Water Cycle 193, 439–446.

Fairchild, I.J., Bradby, L., Sharp, M., Tison, J.-L., 1994. Hydrochemistry of carbonate terrains in alpine glacial settings. Earth Surf. Process. Landf. 19, 33–54. doi:10.1002/esp.3290190104

Ford, D., Smart, P., Ewers, R., 1983. The physiography and speleogenesis of Castleguard Cave, Columbia Icefields, Alberta, Canada. Arct. Alp. Res. 15, 437-450. doi:10.2307/1551231

Fountain, A.G., Walder, J.S., 1998. Water flow through temperate glaciers. Rev. Geophys. 36, 299–328. doi:10.1029/97rg03579

Gaines, R.R., Hammarlund, E.U., Hou, X., Qi, C., Gabbott, S.E., Zhao, Y., Peng, J., Canfield, D.E., 2012. Mechanism for Burgess Shale-type preservation. Proc. Natl. Acad. Sci. 109, 5180–5184. doi:10.1073/pnas.1111784109

Gordon, S., Sharp, M., Hubbard, B., Smart, C., Ketterling, B., Willis, I., 1998. Seasonal reorganization of subglacial drainage inferred from measurements in boreholes. Hydrol. Process. 12, 105–133. doi:10.1002/(sici)1099-1085(199801)12:1<105::aid-hyp566>3.0.co;2-#

Government of Alberta. Current and historical Alberta weather station data viewer. Retrieved from http://agriculture.alberta.ca/acis/alberta-weather-data-viewer.jsp (accessed 33 January 2016).

Graly, J., Harrington, J., Humphrey, N., 2017. Combined diurnal variations of discharge and hydrochemistry of the Isunnguata Sermia outlet, Greenland Ice Sheet. Cryosphere 11, 1131–1140. doi:10.5194/tc-11-1131-2017

Graly, J.A., Humphrey, N.F., Licht, K.J., 2018. Two metrics describing the causes of seasonal and spatial changes in subglacial aqueous chemistry. Front. Earth Sci. 6, 195. doi:10.3389/feart.2018.00195

Hallet, B., Hunter, L., Bogen, J., 1996. Rates of erosion and sediment evacuation by glaciers: A review of field data and their implications. Glob. Planet. Chang. 12, 213–235. doi:10.1016/0921-8181(95)00021-6

Haritashya, U.K., Kumar, A., Singh, P., 2010. Particle size characteristics of suspended sediment transported in meltwater from the Gangotri Glacier, central Himalaya — An indicator of subglacial sediment evacuation. Geomorphology 122, 140–152. doi:10.1016/j.geomorph.2010.06.006

Hart, J.K., 2006. Athabasca Glacier, Canada - a field example of subglacial ice and till erosion? Earth Surf. Process. 31, 65–80. doi:10.1002/esp.1233

Hasnain, S.I., Jose, P.G., Ahmad, S., Negi, D.C., 2001. Character of the subglacial drainage system in the ablation area of Dokriani glacier, India, as revealed by dye-tracer studies. J. of Hydrol. 248, 216–223. doi:10.1016/S0022-1694(01)00404-8

Hawkings, J.R., Tranter, M., Raiswell, R., Benning, L.G., Statham, P.J., Tedstone, A., Nienow, P., Lee, K., Telling, J., Wadham, J.L., 2014. Ice sheets as a significant source of highly reactive nanoparticulate iron to the oceans. Nat. Commun. 5, 1–8. doi:10.1038/ncomms4929

Hawkings, J.R., Wadham, J.L., Tranter, M., Lawson, E., Sole, A., Cowton, T., Tedstone, A.J., Bartholomew, I., Nienow, P., Chandler, D., Telling, J., 2015. The effect of warming climate on nutrient and solute export from the Greenland Ice Sheet. Geochem. Persp. Let. 94–104. doi:10.7185/geochemlet.1510

Hindshaw, R.S., Tipper, E.T., Ben C Reynolds, Lemarchand, E., Wiederhold, J.G., Magnusson, J., Bernasconi, S.M., Kretzschmar, R., Bourdon, B., 2011. Hydrological control of stream water chemistry in a glacial catchment (Damma Glacier, Switzerland). Chem. Geol. 285, 215–230. doi:10.1016/j.chemgeo.2011.04.012

Hodgkins, R., Cooper, R., Tranter, M., Wadham, J., 2013. Drainage-system development in consecutive melt seasons at a polythermal, Arctic glacier, evaluated by flow-recession analysis and linear-reservoir simulation. Water Resour. Res. 49, 4230–4243. doi:10.1002/wrcr.20257

Hood, E., Berner, L., 2009. Effects of changing glacial coverage on the physical and biogeochemical properties of coastal streams in southeastern Alaska. J. Geophys. Res. 114, 1–10. doi:10.1029/2009JG000971

Hooke, R.L., Laumann, T., Kohler, J., 1990. Subglacial water pressures and the shape of subglacial conduits. J. Glaciol. 36, 67–71. doi:10.3189/s0022143000005566

Horowitz, A.J., Lum, K.R., Garbarino, J.R., Hall, G.E., Lemieux, C., Demas, C.R., 1996. Problems associated with using filtration to define dissolved trace element concentrations in natural water samples. Environ. Sci. Technol. 30, 954–963. doi:10.1021/es950407h

Hubbard, B., Nienow, P., 1997. Alpine subglacial hydrology. Quat. Sci. Rev. 16, 939–955. doi:10.1016/s0277-3791(97)00031-0

Hugenholtz, C.H., Moorman, B.J., Barlow, J., Wainstein, P.A., 2008. Large-scale moraine deformation at the Athabasca Glacier, Jasper National Park, Alberta, Canada. Landslides 5, 251–260. doi:10.1007/s10346-008-0116-5

Huisink, M., 1997. Late-glacial sedimentological and morphological changes in a lowland river in response to climatic change: the Maas, southern Netherlands. J. Quat. Sci. 12, 209–223. doi:10.1002/(sici)1099-1417(199705/06)12:3<209::aid-jqs306>3.0.co;2-p

Iken, A., Bindschadler, R.A., 1986. Combined measurements of subglacial water pressure and surface velocity of Findelengletscher, Switzerland: Conclusions about drainage system and sliding mechanism. J. Glaciol. 32, 101–119. doi:10.1017/s0022143000006936

IPCC, 2013: Climate Change 2013: The physical science basis. Contribution of working group I to the fifth assessment report of the Intergovernmental Panel on Climate Change [Stocker, T.F., D. Qin, G.-K. Plattner, M. Tignor, S.K. Allen, J. Boschung, A. Nauels, Y. Xia, V. Bex and P.M. Midgley (eds.)]. Cambridge Univ. P., Cambridge, United Kingdom and New York, NY, USA, 1535 pp.

Jacobson, A.D., Blum, J.D., Chamberlain, P.C., Poage, M.A., Sloan, V.F., 2002. Ca/Sr and Sr isotope systematics of a Himalayan glacial chronosequence: carbonate versus silicate weathering rates as a function of landscape surface age. Geochim. Cosmochim. Acta 66, 13–27. doi:10.1016/s0016-7037(01)00755-4

Kies, A., Nawrot, A., Tosheva, Z., Jania, J., 2011. Natural radioactive isotopes in glacier meltwater studies. Geochem. J. 45, 423–429. doi:10.2343/geochemj.1.0141

Kucera, R.E., Henoch, W.E.S., 1978. Glacier and landform features in the Columbia Icefield area, Banff and Jasper National Parks, Alberta, Canada. Environment Canada, Inland Waters Directorate, Glaciology Division, unpublished report carried out for Parks Canada.

Kumar, N., Ramanathan, A., Tranter, M., Sharma, P., Pandey, M., Ranjan, P., Raju, J.N., 2019. Switch in chemical weathering caused by the mass balance variability in a Himalayan glacierized basin: a case of Chhota Shigri Glacier. Hydrol. Sci. J. 64, 179–189. doi:10.1080/02626667.2019.1572152

Linhoff, B.S., Charette, M.A., Nienow, P.W., Wadham, J.L., Tedstone, A.J., Cowton, T., 2017. Utility of 222Rn as a passive tracer of subglacial distributed system drainage. Earth Planet. Sci. Lett. 462, 180–188. doi:10.1016/j.epsl.2016.12.039

Luckman, B.H., 1988. Dating the moraines and recession of Athabasca and Dome glaciers, Alberta, Canada. Arct. Alp. Res. 20, 40. doi:10.2307/1551697

Mair, D., Willis, I., Fischer, U.H., Hubbard, B., Nienow, P., Hubbard, A., 2003. Hydrological controls on patterns of surface, internal and basal motion during three "spring events": Haut Glacier d'Arolla, Switzerland. J. of Glaciol. 49, 555–567. doi:10.3189/172756503781830467

Meierbachtol, T., Harper, J., Humphrey, N., 2013. Basal drainage system response to increasing surface melt on the Greenland ice sheet. Science 341, 777–779. doi:10.1126/science.1235905

Milner, A.M., Khamis, K., Battin, T.J., Brittain, J.E., Barrand, N.E., Füreder, L., Cauvy-Fraunié, S., Gíslason, G.M., Jacobsen, D., Hannah, D.M., Hodson, A.J., Hood, E., Lencioni, V., Ólafsson, J.S., Robinson, C.T., Tranter, M., Brown, L.E., 2017. Glacier shrinkage driving global changes in downstream systems. Proc. Natl. Acad. Sci. USA 114, 9770–9778. doi:10.1073/pnas.1619807114

Milner, A.M., Petts, G.E., 1994. Glacial rivers: physical habitat and ecology. Freshw. Biol. 32, 295–307. doi:10.1111/j.1365-2427.1994.tb01127.x

Mitchell, A.C., Brown, G.H., 2008. Modeling geochemical and biogeochemical reactions in subglacial environments. Arct. Antarct. Alp. Res. 40, 531–547. doi:10.1657/1523-0430(06-075)[mitchell]2.0.co;2

Mitchell, A.C., Brown, G.H., Fuge, R., 2006. Minor and trace elements as indicators of solute provenance and flow routing in a subglacial hydrological system. Hydrol. Process. 20, 877–897. doi:10.1002/hyp.6112

Morlock, S.E., Nguyen, H.T., Ross, J.H., 2002. Feasibility of acoustic doppler velocity meters for the production of discharge records from U.S. Geological Survey streamflow-gaging stations. Water-Resour. Investig. Rep. 01-4157, 1–56. doi:10.3133/wri20014157

Nienow, P., Sharp, M., Willis, I., 1998. Seasonal changes in the morphology of the subglacial drainage system, Haut Glacier d'Arolla, Switzerland. Earth Surf. Process. Landf. 23, 825–843. doi:10.1002/(SICI)1096-9837(199809)23:9<825::AID-ESP893>3.0.CO;2-2

Niu, Y., Castro, M.C., Hall, C.M., Aciego, S.M., Arendt, C.A., 2017. Characterizing glacial meltwater sources in the Athabasca Glacier, Canada, using noble gases as tracers. Appl. Geochem. 76, 136–147. doi:10.1016/j.apgeochem.2016.11.015

Nye, J.F., 1976. Water flow in glaciers: jökulhlaups, tunnels and veins. J. Glaciol. 17, 181–207. doi:10.3189/s002214300001354x

Paterson, W., 1964. Variations in velocity of Athabasca Glacier with time. J. Glaciol. 5, 277–285. doi:10.3189/s0022143000029026

Raiswell, R., 1984. Chemical models of solute acquisition in glacial melt waters. J. Glaciol. 30, 49–57. doi:10.3189/s0022143000008480

Raiswell, R., Benning, L.G., Tranter, M., Tulaczyk, S., 2008. Bioavailable iron in the Southern Ocean: the significance of the iceberg conveyor belt. Geochem. Trans. 9. doi:10.1186/1467-4866-9-7

Raiswell, R., Canfield, D.E., 2012. The iron biogeochemical cycle past and present. Geochem. Perspect. 1, 1–220. doi:10.7185/geochempersp.1.1

Röthlisberger, H., 1972. Water pressure in intra- and subglacial channels. J. Glaciol. 11, 177–203. doi:10.1017/s0022143000022188

Sharp, M., Brown, G.H., Tranter, M., Willis, I.C., Hubbard, B., 1995. Comments on the use of chemically based mixing models in glacier hydrology. J. Glaciol. 41, 241–246. doi:10.3189/s0022143000016142

Shreve, R.L., 1972. Movement of water in glaciers. J. Glaciol. 11, 205–214. doi:10.1017/s002214300002219x

Singh, P., Kumar, Naresh, 1997. Impact assessment of climate change on the hydrological response of a snow and glacier melt runoff dominated Himalayan river. J. Hydrol. 193, 316–350. doi:10.1016/s0022-1694(96)03142-3

Singh, V.B., Ramanathan, A.L., Pottakkal, J.G., Sharma, P., Linda, A., Azam, M.F., Chatterjee, C., 2012. Chemical characterisation of meltwater draining from Gangotri Glacier, Garhwal Himalaya, India. J. Earth Sys. Sci. 121, 625–636. doi:10.1007/s12040-012-0177-7

Smart, C., 1983. The hydrology of the Castleguard karst, Columbia Icefields, Alberta, Canada. Arct. Alp. Res. 15, 471. doi:10.2307/1551234

Stone, D.B., Clarke, G.K.C., 1996. *In situ* measurements of basal water quality and pressure as an indicator of the character of subglacial drainage systems. Hydrol. Process. 10, 615–628. doi:10.1002/(sici)1099-1085(199604)10:4<615::aid-hyp395>3.0.co;2-m

Swift, D.A., Nienow, P.W., Hoey, T.B., 2005. Basal sediment evacuation by subglacial meltwater: suspended sediment transport from Haut Glacier d'Arolla, Switzerland. Earth Surf. Process. Landf. 30, 867–883. doi:10.1002/esp.1197

Tranter, M., Brown, G., Raiswell, R., Sharp, M., Gurnell, A., 1993. A conceptual model of solute acquisition by alpine glacial meltwaters. J. Glaciol. 39, 573–581. doi:10.3189/s0022143000016464

Tranter, M., Brown, G.H., Hodson, A.J., Gurnell, A.M., 1996. Hydrochemistry as an indicator of subglacial drainage system structure: A comparison of alpine and sub-polar environments. Hydrol. Process. 10, 541–556. doi:10.1002/(sici)1099-1085(199604)10:4<541::aid-hyp391>3.0.co;2-9

Tranter, M., Sharp, M.J., Brown, G.H., Willis, I.C., Hubbard, B.P., Nielsen, M.K., Smart, C.C., Gordon, S., Tulley, M., Lamb, H.R., 1997. Variability in the chemical composition of *in situ* subglacial meltwaters. Hydrol. Process. 11, 59–77. doi:10.1002/(sici)1099-1085(199701)11:1<59::aid-hyp403>3.0.co;2-s

Tranter, M., Sharp, M.J., Lamb, H.R., Brown, G.H., Hubbard, B.P., Willis, I.C., 2002. Geochemical weathering at the bed of Haut Glacier d'Arolla, Switzerland—a new model. Hydrol. Process. 16, 959–993. doi:10.1002/hyp.309

Tranter, M., Wadham, J., 2014. Geochemical weathering in glacial and proglacial environments. Treatise Geochem, second ed. 7, 157–173. doi:10.1016/b978-0-08-095975-7.00505-2

Wada, T., Chikita, K.A., Kim, Y., Kudo, I., 2011. Glacial effects on discharge and sediment load in the subarctic Tanana River Basin, Alaska. Arct. Antarct. Alp. Ress 43, 632–648. doi:10.1657/1938-4246-43.4.632

Wadham, J., Tranter, M., Skidmore, M., Hodson, A.J., Priscu, J., Lyons, W.B., Sharp, M., Wynn, P., Jackson, M., 2010. Biogeochemical weathering under ice: Size matters. Glob. Biogeochem. Cycles 24. doi:10.1029/2009gb003688

Yde, J.C., Knudsen, N.T., Nielsen, O.B., 2005. Glacier hydrochemistry, solute provenance, and chemical denudation at a surge-type glacier in Kuannersuit Kuussuat, Disko Island, West Greenland. J. Hydrol. 300, 172–187. doi:10.1016/j.jhydrol.2004.06.008

Chapter IV. Seasonal Evolution in Subglacial Hydrochemistry at Kiattuut Sermiat, South Greenland

Abstract

Here we present data collected in August and September 2015 from a south Greenland outlet glacier, Kiattuut Sermiat (KS), providing quantitative measurements of hydrochemical parameters which imply the existence of a stable subglacial hydrologic system into early autumn. As seen through meltwater elemental concentrations and high-resolution *in situ* hydrochemical data over this two-month period, the existing efficient hydrologic system is capable of routing large volumes of meltwater quickly to the glacial terminus. No discernable seasonal change in configuration is observed through end-September, 2015. Overlap in early August 2015 pH and electrical conductivity data presented here with published 2013 values also measured at KS suggests consistent interannual hydrochemical trends in KS outflow. Water source evolved over the study period from a mixture of both distal and proximal water in August to a mixture with a greater proximal water-source signature in September. Shifts in water source likely derive from changes in up-ice conditions, which are conveyed to the KS terminus through the subglacial hydrologic system. Finally, these data may establish a baseline with which to evaluate future end-summer glaciochemical changes at KS.

Introduction

More perennial ice exists on Earth than the present climate can support; current research suggests previous predictions of ice loss from the Greenland Ice Sheet (GrIS) are likely too conservative and rates of future mass loss will increase (Bevis et al., 2019; Trusel et al., 2018).

Satellite data reveal ice mass loss has been dominated by surface mass balance processes (SMB: accumulation minus ablation) relative to glacial dynamics (deformation due to gravity and subsequent calving) over the past 20 years (Mouginot et al., 2019). As Earth's climate continues to warm, SMB processes – generating vast volumes of meltwater – are predicted to increase ice mass loss from the GrIS (Bevis et al., 2019; Trusel et al., 2018). Exactly how increased meltwater production is coupled to glacial dynamics on/within the GrIS remains an active and debated research topic (e.g. Davison et al., 2019), key to improving current glaciological flow models. As in-field research is limited by accessibility, seasonality, and experimental scale; meltwater residence time (e.g. Aciego et al., 2015; Bhatia et al., 2011), routes to the glacier bed (e.g. Clason et al., 2015; Koziol et al., 2017), and changes in subglacial hydrologic network efficiency (e.g. Chandler et al., 2013; Schoof, 2010) are poorly understood. This study presents hydrochemical data from outflow waters emanating from a south Greenland outlet glacier as summer peak melt season transitions to early autumn, providing baseline chemical parameters with which to compare future hydrological changes.

Meltwater, once generated, is routed through the GrIS supra-, en-, and subglacial hydrologic systems, eventually reaching the Atlantic and Arctic Oceans. Water chemistry within this melt continuously evolves along its route via chemical weathering reactions with freshly comminuted glacial flour. Resultant hydrochemistry is controlled by types of bedrock present, subglacial water storage time, erosion rate, availability of reactants (primarily H+ ions and dissolved oxygen [DO]), and presence of microbial activity (Anderson et al., 1997; 2003; Raiswell, 1984; Tranter et al., 1996; 2002; Tranter and Wadham, 2014; Yde et al., 2014). Elemental composition of glacial meltwater has been used to infer changes in the subglacial hydrologic network configuration as water routed through different conduits is exposed to different minerals with disparate chemical weathering rates (e.g. Graly et al., 2018; Yde et al., 2014; 2005). Glacial

meltwater, initially undersaturated in solutes as pure ice melt, encounters large volumes of freshly comminuted sediment as it flows through the subglacial hydrologic system (Anderson, 2007). Despite cold temperatures, significant chemical weathering occurs in glacial environments when undersaturated water reacts with freshly broken unweathered mineral surfaces produced through glacial grinding, increasing the solute load of the meltwater (Anderson, 2005).

Subglacial hydrologic systems are dynamic, with the degree of connectivity depending on the volumes of water accommodated (Andrews et al., 2014; Bartholomew et al., 2010; Fountain and Walder, 1998). Wintertime cold temperatures generate little meltwater and resultant hydrologic systems exist in poorly-connected, slow, inefficient systems characterized by long water residence times. Increased meltwater volumes in spring from warming temperatures result in an "opening" of the hydrologic system, marked by an increase in ice velocity as the water volume overwhelms the existing hydrologic configuration, lubricating a large area the bed, and enhancing basal ice sliding (Bartholomew et al., 2010; Zwally et al., 2002). This phenomenon is transitory: the subglacial hydrologic system increases in connectivity and channels expand in size to accommodate the melt such that basal water pressure – and subsequently ice velocity – decrease (Bartholomew et al., 2010; 2012; Hoffman et al., 2011). In addition to ice velocity trends, these changes in hydrological configuration are also evident in meltwater elemental trends: increased spring meltwater volumes dilute solute load and subsequently lower both bulk electrical conductivity (EC) and elemental concentrations (Bhatia et al., 2011; Chandler et al., 2013; Moon et al., 2014). With the advent of cooler temperatures as summer transitions to autumn, meltwater volumes decrease. The resultant decrease in hydrostatic pressure within unfilled subglacial channels allows closure via deformation of overlying ice (Shreve, 1972) as part of the transition from an efficient channelized system to an inefficient poorly connected system. Seasonal change of

the subglacial hydrologic system however is poorly documented outside the warmest seasons as harsh glacial environments and difficulty in accessibility frequently prohibit field observation.

This study investigates the chemical properties of meltwater discharging from Kiattut Sermiat (KS): an accessible land-terminating outlet glacier in southern Greenland in August and September 2015. KS has been the site of numerous glaciochemical research studies (e.g. Aciego et al., 2015; Hawkings et al., 2016; Hatton et al., 2019) undertaken earlier in the summer melt season. Here, we present a high-resolution two-month data set of continuous *in situ* proglacial stream monitoring (water temperature, pH, EC, and DO saturation) and regularly sampled major and trace elemental concentrations, water stable isotope values, and radiogenic strontium compositions of both proglacial stream water and suspended sediment following peak summertime melt. Through comparison of this new KS data with data collected in previous years, we identify long-term trends in the hydrochemical behavior of KS and improve the understanding of annual chemical trends in Southern Greenland outlet glaciers.

Site Description

Kiattuut Sermiat (KS; 61.25°N, 45.28 °W) is a land-terminating glacier located in south Greenland (Figure IV-1). It branches from Qooqqup Sermia (QS): a larger, faster-flowing outlet glacier connected to the GrIS (Figure IV-1). KS is contained within a steep walled valley, limiting its possible lateral extent. Differences in digital elevation models reveal a general thinning of the whole glacier between 2001 and 2014 (Mätzler et al., 2015). Mean ice velocity at KS is < 60 m yr^{-1}, with the last few hundred meters closest to the terminus likely dead ice (Rignot and Mouginot, 2012). KS terminates in a proglacial lake (0.5 km^2), which then empties into a braided stream flowing ~10 km southwest through a broad, sandy floodplain to Tunulliarfik fjord. Once the glacial melt season begins in spring, lake turnover is rapid, taking < 24 hours after DOY 157 (Hatton et

al., 2019). Bedrock under KS is primarily 1.8 Ga granite of the Julianehåb Batholith containing complexes of diorite and granodiorite, with basaltic intrusions also present (Henriksen et al., 2009; Greenland Portal).

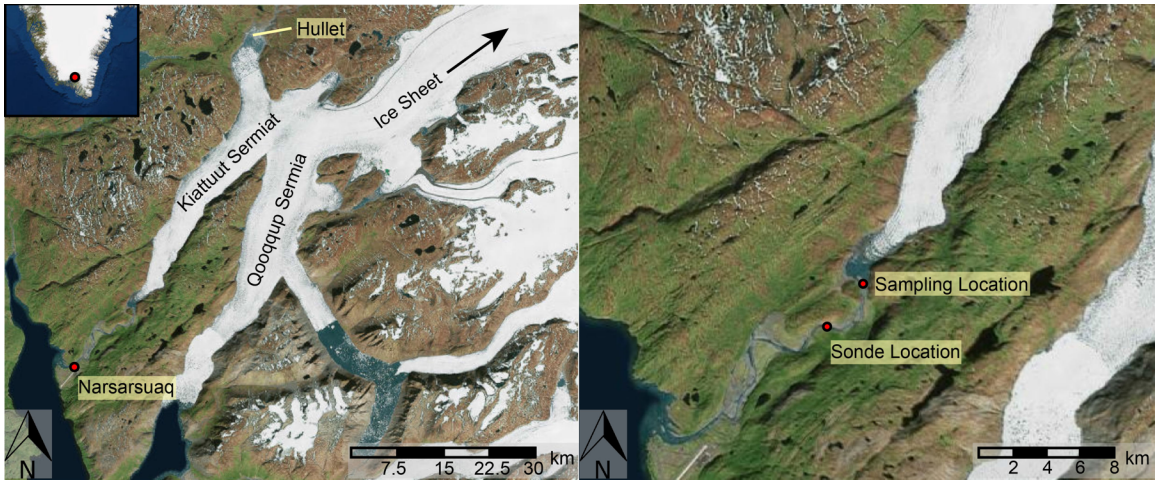

Figure IV-1: Site location maps. Left panel shows the location of Kiattuut Sermiat relative to Qooqquup Sermia and the Greenland Ice Sheet, the town of Narsarsuaq, and glacial lake Hullet. Right panel expands the view of the terminus of Kiattuut Sermiat indicating the position of the sampling location and the YSI EXO2 sonde in the outflow river. Insert indicates position of site (red circle) in Southern Greenland

A small second glacier, Sydgletsjer, branches north from KS near its separation from QS, terminating in ice-dammed Lake Hullet (Figure IV-1). Hullet drains to the south through KS via subglacial outburst floods (Mätzler et al., 2015). Floods usually occur in late summer – typically in August or September – and last for two to three weeks (Mätzler et al., 2015). Landsat 7 imagery shows this flood to be an annual occurrence from 2000 through 2014 (data are missing for 2002 and 2006), and an intensive study in 2014 revealed that the lake-draining flood event that year occurred over a 23-day period (Mätzler et al., 2015).

Methods

Pre-Cleaning Procedures:

HDPE plastic bottles and tubing were pre-cleaned in an ISO 7 (class 10,000) clean room at the University of Michigan prior to the start of the field campaign. Cleaning methodology is

outlined in detail in Arendt et al. (2015). Briefly, all plastics were rinsed three times with 18.2 MΩ deionized water, leached for 24 hours in double-distilled 10% nitric acid, rinsed three additional times with 18.2 MΩ deionized water, leached 24 hours in double-distilled 10% hydrochloric acid, and rinsed three final times with 18.2 MΩ deionized water (Arendt et al., 2015).

Sample Collection for Elemental and Stable Water Isotope Analysis

17 bulk meltwater samples were collected at ~13:00 beginning August 5 and ending September 23, 2015. To sample waters most representative of bulk glacial outflow, a sample location was selected at the origin of the outflow river from the proglacial lake (Figure IV-1). Sampling was conducted by boat at a rock protruding from the center of the glacial outflow river (61° 12.559'N, 45° 19.794'W) to ensure a consistent sampling location. Sample containers were rinsed three times with flowing water immediately prior to sample collection; samples were collected upstream of the rock and immediately capped until filtration. Collection occurred at ~13:00 every 3-4 days from August 5 (DOY 217) to September 9 (DOY 252), and every other day from September 9 through the end of the field campaign on September 23 (DOY 266).

Filtration was completed within three hours post-collection to prevent further chemical reaction with suspended sediment. One liter of 18.2 MΩ deionized water was pumped through a 0.2μm Millipore Durapore® membrane filter held in a PTFE filter housing by a Masterflex modular peristaltic pump to prime the filtration system, then discarded. One L of sample was then collected into a pre-cleaned 1L HDPE plastic bottle and acidified with Optima hydrochloric acid to a pH < 2. HCl was used instead of nitric acid because HCl was required for iron co-precipitation; as Ag was not an element of interest possible Ag-Cl complexes were immaterial. Additionally, sample water was passed directly into Kimble 20mL glass screw-thread scintillation vials with cone

caps for later oxygen and hydrogen isotope analysis. Filled vials were capped tightly and remained sealed until measurement.

Elemental concentrations were run on a Perkin Elmer Nexion 350D quadrupole ICP-MS at Cambridge University. Duplicates were run on subsequent days to ensure replication; bracketing standards and acid blanks were used to ensure accurate measurements. Stable water isotopes were run on a Picarro L2130-I Isotopic Liquid Water Analyzer in the stable isotope lab at Iowa State University. The instrument was equipped with an autosampler and ChemCorrect software. Each sample was measured a total of six times, with only the last three injections used to calculate mean isotopic values to account for memory effects from the previous sample. Reference standards (OH-3, GISP) were used for regression-based isotopic corrections; at least one reference standard was analyzed for every five samples. $\delta^{18}O$ uncertainty is ± 0.06‰ (VSMOW) and δD uncertainty is ± 0.23‰ (VSMOW).

In Situ Data Collection

EC, water temperature, DO concentration, and pH were measured simultaneously with sample collection using a handheld YSI Professional Plus multi-probe at the mid-stream sampling location. The pH probe was calibrated to pH 4, 7, and 10, EC calibrated with 1413 μS cm^{-1} solution, and DO calibrated with water-saturated air prior to use. pH calibration was checked daily and recalibrated with pH 4, 7, and 10 solutions as required. Complete recalibrations were conducted monthly in the field.

Discharge

A site was chosen to measure discharge (Q) approximately 500 m downstream from the start of the outflow river. All water was contained in a single channel at this location with braided channels extending up- and downstream. The far bank was a vertical rock face with a river depth of ~6 m. The near bank was gently-sloping, comprised primarily of rounded cobbles extending 2-

3 meters into the stream, after which the riverbed transitioned to sand and silt. River geometry was obtained by rowing out into the current and simultaneously measuring the river depth using a sonar fish finder and recording the GPS coordinates of each measurement location. Due to river water velocity it was impossible to measure a direct transect; researchers generated a cloud of depth data paired with GPS coordinates. The spatial coordinates were input into ArcGIS and projected using the North Pole Lambert Equal Area projection. A surface representing the river bottom was generated by interpolating between the measured depths using a natural neighbor interpolation tool. The 3D profile tool was then used to create a cross section to calculate cross sectional area.

River stage, and subsequently cross-sectional area, varied throughout the study. To account for these fluctuations, researchers selected and marked a rock at the water's edge (61° 12.239'N, 45° 19.825'W). Each sample day, shoreline deviations from this rock and river depth both 10 and 20 feet away were measured and recorded just before sample collection. The change in river depth was modeled as a rectangle that was either added or subtracted to the calculated cross-sectional area for that day.

Direct, quantitative measurement of Q was impossible during this field campaign: the outflow channel was too deep to take depth and velocity measurements in intervals to calculate Q. River flow was non-turbulent and floats moved downstream with minimal cross channel mixing. Although absolute Q measurements were not collected, relative Q was estimated as follows: Maximum stream surface velocity was measured twice during the field campaign: once on September 3, 2015 and again three weeks later on September 23, 2015. Floats were released into the fastest flowing section of stream, and travel times recorded for distances of 50 and 100 feet. Measured stream surface velocities were multiplied by a factor of 0.85 to more accurately reflect average stream velocities due to friction along the stream bed. Average stream velocity was multiplied by that day's cross-sectional area to calculate discharge. As it was only possible to

measure stream velocity on two days due to extra personnel requirements, the relationship between river stage and discharge was assumed to be linear. An equation computing Q as a function of river stage was then used to calculate discharge for each of the other sample days. Because of all the assumptions employed, Q is reported as relative values rather than as absolute values, and water chemistry is never reported relative to Q. Thus while relative Q is less informative than absolute Q measurements, these values are included so that other variations in other measured parameters may be considered with respect to glacier outflow, allowing for a better understanding of the whole system.

Hullet Sample:

One sample was collected from Lake Hullet, the glacial lake retained by Sydgletsjer north of KS. This sample was collected before the anticipated approximately annual flood expected in late summer/early autumn (Mätzler et al., 2015) to compare to floodwater outflow after flow through KS. The same sampling procedures were used as for KS samples; all samples were also preserved, stored, and analyzed using the same methods.

Continuous Monitoring Sonde

A YSI EXO2 water quality monitoring sonde equipped with pH, temperature/EC, optical DO, and pH/oxidation-reduction potential (ORP) probes was installed in the outflow river from the KS glacier (Figure IV-1). The location was selected because (1.) the outflow river was confined to a single channel, (2.) it was a bedrock-bounded cutbank in the river channel, so waters were well mixed and minimal to no interaction with groundwater was anticipated due to the lack of soil or sediment, and (3.) it was accessible by researchers from the bank. Calibrations with pH 4, 7, and 10 solutions for pH, 1413 µS cm^{-1} standard for EC, and water saturated air for DO were conducted following manufacturer guidelines prior to installation and recalibrated mid-way through the field

campaign. Day and time were set on the instrument and it was programmed to measure and record all parameters every 15 minutes. Data were downloaded and analyzed weekly for quality control.

Instrument consistency was evaluated during recalibrations; the sonde regularly measured DO more accurately than the handheld YSI and as such we use sonde measured values for interpretations. While absolute DO values measured by the handheld YSI are likely incorrect, the trends shown over the study match with sonde trends. DO from both instruments is reported in percent saturation to avoid water temperature effects on absolute concentration, yet diurnal variations are still observable within sonde data (Figure IV-2).

Results

Weather Data

Mean daily air temperature decreased from 12°C on August 5 (day of year [DOY] 217) at the start of the 2015 study period to 3°C on September 23 (DOY 266) at its conclusion (Figure IV-2) (Cappelen et al., 2018). The warmest mean daily temperature was 13°C and occurred on September 3 (DOY 246), mid-way through the study (Figure IV-2). A trendline fit through daily average temperature ($R^2 = 0.62$) produces a slope of -0.14°C day^{-1}. Daily temperatures exhibited strong diurnal cycles, except for a period mid-way through the study (DOY 240 – 249) with consistent regular rain (blue shading in Figure IV-2). This is the longest span of daily rain, although rain events also occurred on DOY 223, 239, 259-260, and 263-266 (Cappelen et al., 2018).

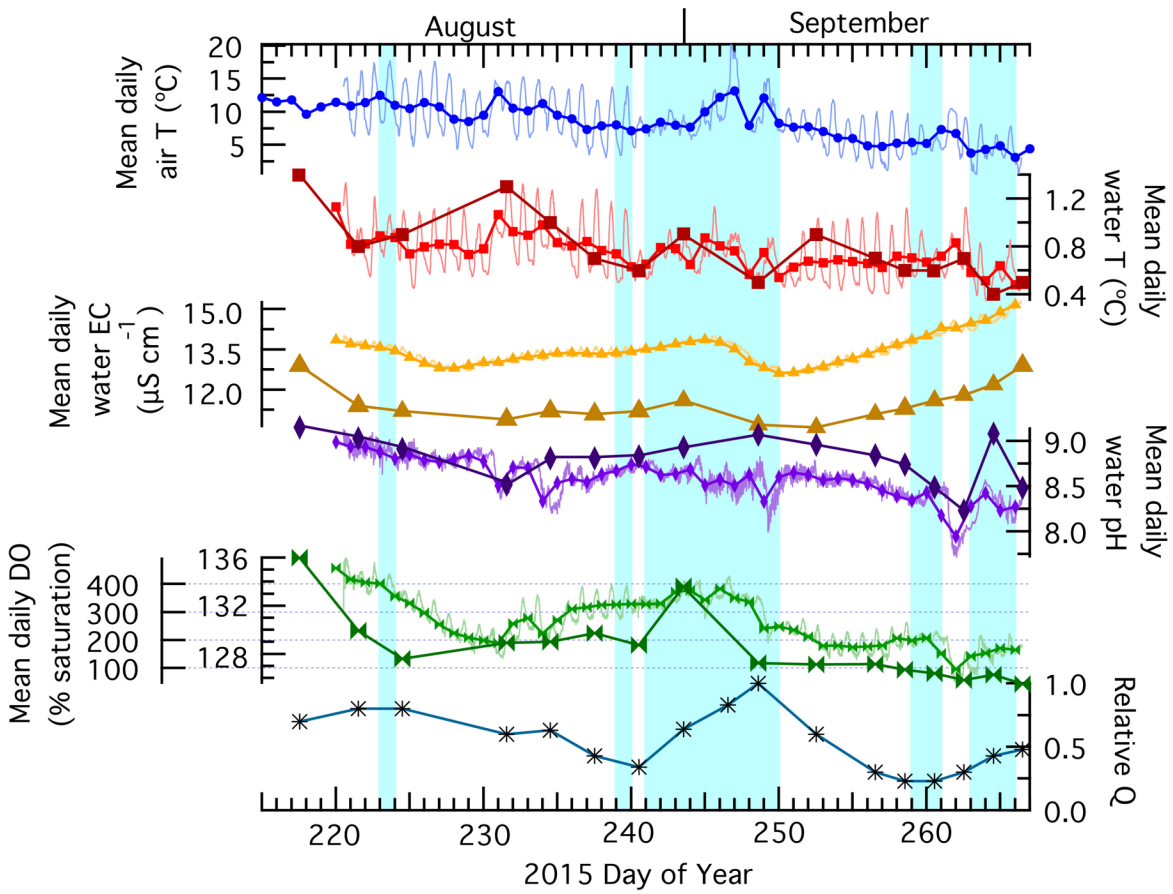

Figure IV-2: *In situ* water quality data recorded at 15-minute intervals (light lines) was used to generate daily averages (smaller markers). Measurements taken concurrently with water sampling are superimposed (larger markers). (A) Air temperature (blue circles) was recorded at the Narsarsuaq weather station (Cappelen et al., 2018). (B),Water temperature (red squares), (C) electrical conductivity (yellow triangles), (D) pH (purple diamonds) and (E) dissolved oxygen in percent saturation (green bowties) were recorded in 15-minute intervals by an emplaced YSI EXO2 water quality monitoring sonde. (F) Estimated relative discharge was calculated (black stars). Vertical blue bars indicate days associated with rainfall.

Hydrochemical Data

Measurements (river stage and shoreline migration) to model Q were taken concurrently; relative Q varied from a high of 1.0 (modeled value 80 m^3 sec^{-1}) on DOY 248 to a low of 0.2 (modeled value 18 m^3 sec^{-1}) on DOY 258 and 260 (Figure IV-2). Modeled absolute Q shows a much larger range of values than seem likely from field observations, so we instead present relative Q for following interpretations of hydrochemical data.

Water temperatures collected concurrently with sample collection match well with contemporaneous water temperatures logged by the sonde, though *in situ* temperatures are spot

measurements and therefore plot off the sonde daily average temperature line (Figure IV-2). Sonde recorded water temperature data reveal diurnal fluctuations in-phase with fluctuations in air temperature (Figure IV-2). Trends in *in situ* EC measurements correlate with sonde-recorded EC values, although absolute *in situ* values are lower ranging from a minimum of 10.6 μS cm^{-1} (DOY 252) to a maximum of 12.9 μS cm^{-1} (DOY 266). Sonde EC measurements initially decreased from 13.9 μS cm^{-1} at the start of monitoring (DOY 220) to 12.8 μS cm^{-1} (DOY 228), then broadly increased over the remainder of the study period (Figure IV-2). The recorded sonde first-order EC increase is divided into two distinct periods separated by a relatively abrupt decrease from DOY 245 – 250, falling from a daily average of 13.9 μS cm^{-1} to 12.6 μS cm^{-1} (Figure IV-2). This drop occurs mid-way through the longest interval of consistent rain (Figure IV-2).

In situ pH decreased from a high of 9.15 (DOY 217) on the first sampling day to a low of 8.23 (DOY 262), with a period of increasing pH mid-study on DOY 231 – 248. Sonde-logged pH shows a similar trend, but higher resolution sampling reveals more subtle fluctuations. Abrupt decreases in pH occur on DOYs 230-231, 233-234, 249, and 261 ranging from -0.5 to -0.8 pH units over 7 – 14 hours (Figure IV-2). These decreases are then followed by more gradual (12 – 46 hour) increases, returning pH to the slowly-decreasing first-order trend (Figure IV-2). Similar to pH, *in situ* DO decreased throughout the study from a high of 494% saturation on DOY 217 to a low of 43% saturation on the last day of sampling (DOY 266), with a period of increase from DOY 224 – 243. DO percent saturation is negatively correlated with DOY ($R^2 = 0.5$). Sonde logged DO mirrors the seasonal trends from *in situ* data, although the magnitude of changes is much smaller. Sonde DO is consistently oversaturated and shows a first-order decrease in saturation from a high of 135% on DOY 220 to a low of 127% on DOY 262 (Figure IV-2). This decreasing trend is interrupted by periods of increasing saturation (DOY 231 – 236) and of relative stability (DOY

236 – 242, 253 – 260) (Figure IV-2). DO increases daily beginning at approximately 08:00 and peaks between 15:00 – 16:00; this trend is in-phase with daily insolation and therefore with both air and water temperatures (Figure IV-2).

Major rock-forming elements (Ca, Na, K, Mg) and trace elements (Al, Fe, P) exhibited slightly different behavior throughout the study (Figure IV-3). Trace elemental concentrations were unchanging except on DOY 231 when Fe and P concentrations increased from an average of 0.1 µM to 0.4 and 0.6 µM respectively, and Al increased from 2.4 µM to 4.2 µM (Figure IV-3). Mg concentration also slightly increased on DOY 231, but not above observed variability (Figure IV-3). Other major elemental concentrations did not increase on this day (Figure IV-3). Rock-associated soluble elements displayed little variability in concentration prior to DOY 252.

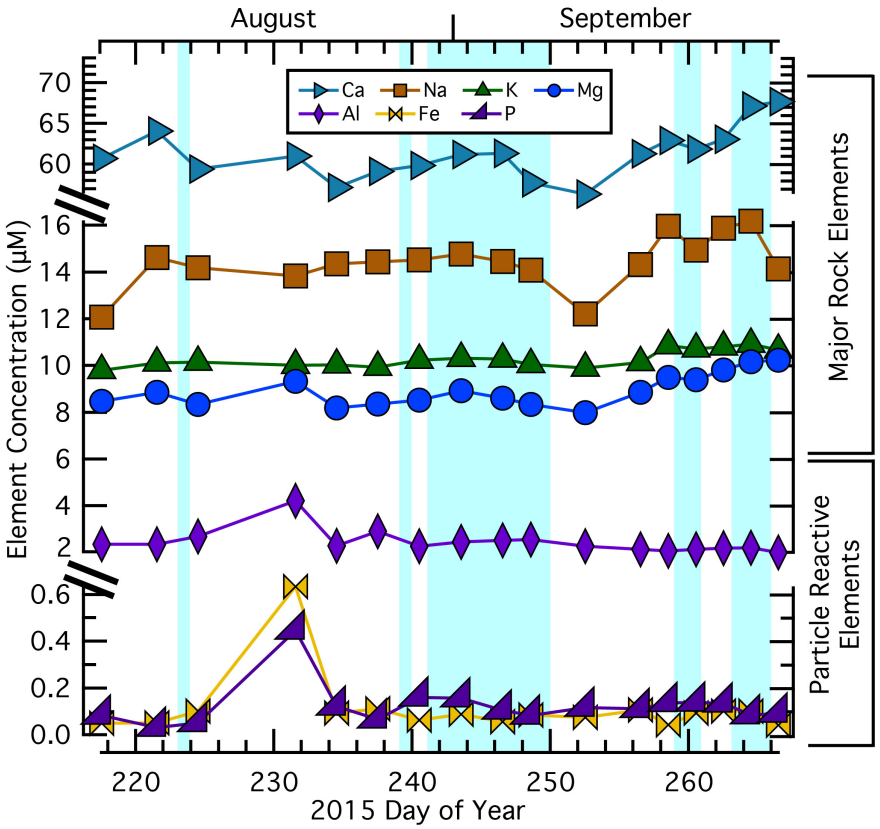

Figure IV-3: Elemental concentrations outflow river samples from the 2015 field study by day of year. Note the discontinuous y-axis. Calcium (teal triangles) is plotted between 65-76 µM. Sodium (brown squares), potassium (green triangles), magnesium (blue circles), and aluminum (purple diamonds) are plotted between 2-16 µM. Iron (yellow bowties) and potassium (purple right triangles) are plotted between 0.0-0.6 µM. Vertical blue bars indicate days associated with rainfall.

Following DOY 252, Ca, Na, K, and Mg all marginally increased in concentration to the end of the study period (Figure IV-3).

Meltwater $\delta^{18}O$ and δD composition changed throughout the season. Initially both $\delta^{18}O$ and δD decreased until DOY 240: $\delta^{18}O$ decreased from -20.9‰ to -21.2‰ and δD decreased from -153‰ to -156‰ (Figure IV-4). After DOY 240, the trend reversed and $\delta^{18}O$ and δD increased throughout the remainder of the field season, with $\delta^{18}O$ reaching a maximum of -20.1‰ and δD reaching -150‰ in the final sample collected on DOY 266 (Figure IV-4). Rain water samples were collected throughout the field season for comparative isotopic composition; the average rain $\delta^{18}O$ value was -7.2‰ with a δD composition of -56‰. Ice was also collected from the KS terminus for isotopic comparison; KS terminus ice $\delta^{18}O$ was -18.2‰ and δD was -134‰.

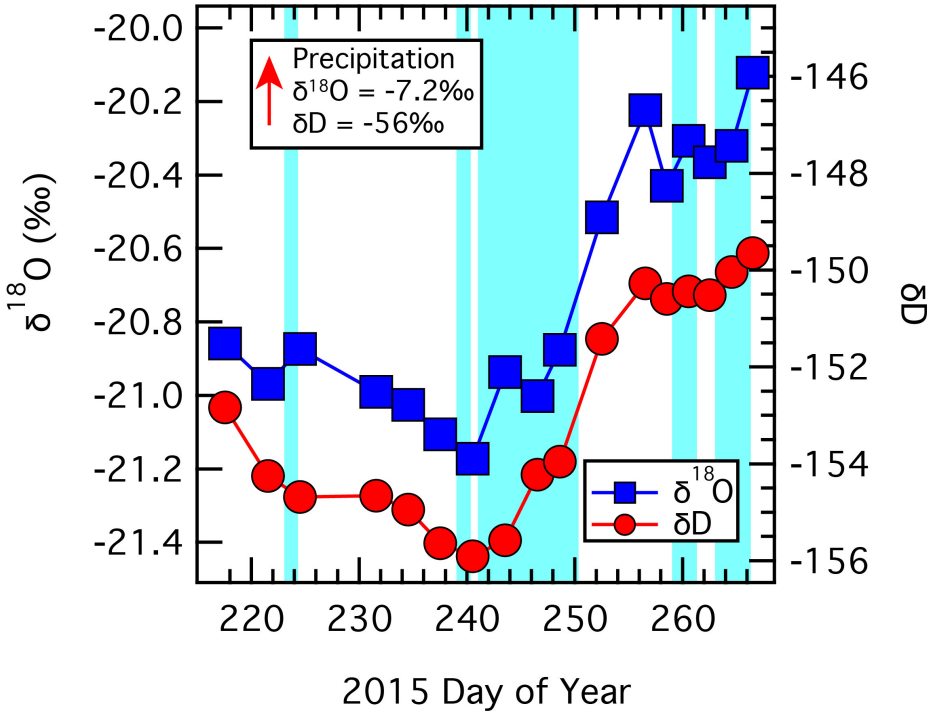

Figure IV-4: Stable water isotope composition of river outflow samples from the 2015 field study by day of year. $\delta^{18}O$ (blue squares) is plotted on the left y-axis while δD (red circles) is plotted on the right. All values are per mille (‰) relative to Vienna Standard Mean Ocean Water (VSMOW). Vertical blue bars indicate days associated with rainfall.

Water $^{87}Sr/^{86}Sr$ composition initially increased from 0.718514 to 0.718789 on DOY 246, then decreased to 0.717952 on DOY 262 (Figure IV-5). $^{87}Sr/^{86}Sr$ composition of the suspended sediment displayed much more variability and does not fall within the melt water range, varying from a high of 0.724797 on DOY 221 to a low of 0.720939 on the subsequent sample, DOY 224 (Figure IV-5). Hydrochemistry from Hullet, sampled on DOY 254, was similar to measurements at KS. pH was slightly more acidic (8.63) than at KS but EC was consistent with KS measurements at 11.80 μS cm^{-1}.

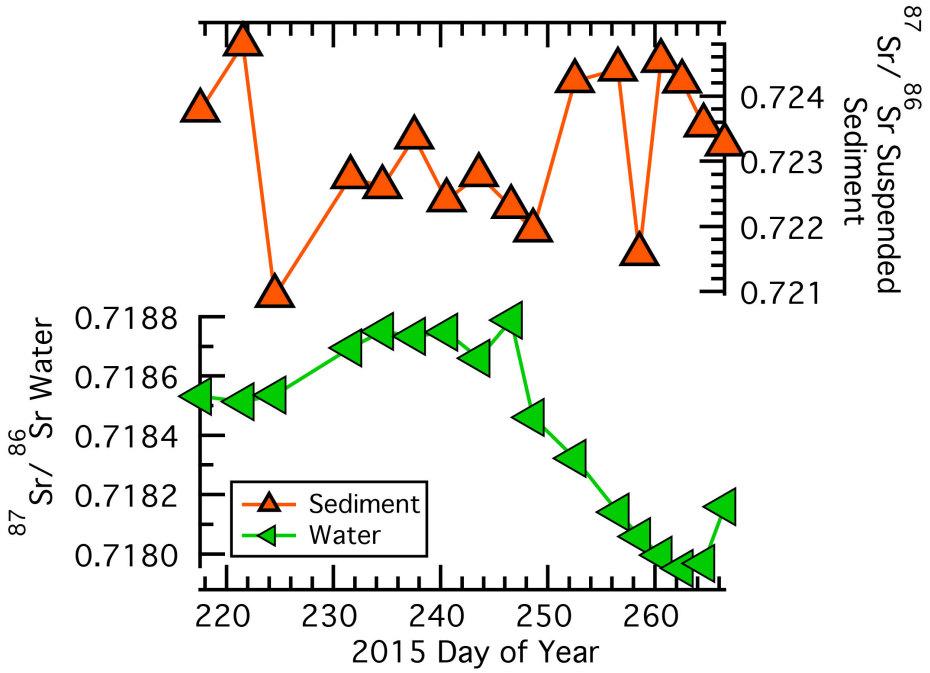

Figure IV-5: Radiogenic strontium isotopic values for collected water samples (bottom; green triangles) and suspended sediment removed from water samples via filtration (top; orange triangles) by day of year. Y-axis scales differ; sediments (y-axis range 0.721 – 0.725) are more radiogenic than waters (y-axis range 0.7180 – 0.7188).

Discussion

Part 1: 2015 Chemical Analysis of the Subglacial Hydrologic Environment

1.1 Evidence for a Well-Established, Highly Efficient Subglacial Drainage Network

Elemental concentrations in KS outflow water showed little variability throughout this study relative to the range observed in 2013 (Hatton et al., 2019), revealing a comparatively

constant solute flux from KS relative to discharge throughout this study (Figure IV-3). As summer ends and air temperatures fall below freezing, surface melt rates decrease. This process may be evidenced hydrochemically through increasing elemental concentrations owing to less dilution. With decreasing meltwater volume, subglacial hydrologic channels are understood to begin to close as the pressure of the ice overburden exceeds the pressure within the partially vacated channels (Shreve, 1972). While daily mean air temperature decreased throughout the field campaign, temperatures did not fall below 0° C (Figure IV-2), and thus there were no large freezing-driven changes in the hydrologic system.

Elemental concentration data presented here imply a stable hydrologic system in balance with environmental forcings. Major cation concentrations (Na, K, Mg, Ca) measured in KS outflow for 49 days in 2013 following the documented spring event – marked by a large change in chemistry – displayed 2-7 times greater range in concentration than our observations from August through September 2015 (Hatton et al., 2019). Solute load in glacial meltwater is a function of both water residence time, as longer time allows more chemical weathering to occur, and reactivity of the specific minerals that the water is exposed to en route to the glacier terminus (Tranter and Wadham, 2014). Freshly broken and strained mineral surfaces, prevalent in glaciated terrains, are more susceptible to chemical weathering than mineral surfaces previously exposed to, and therefore weathered by, water (Anderson et al., 1997). Reaction kinetics also affect mineral chemical weathering rates (Stumm and Wollast, 1990). If the network configuration changed in drastic ways, water may be routed over freshly ground yet previously inaccessible mineral surfaces, which would more easily contribute weathering products (solutes) to the meltwater. Similarly, broad changes in network configuration may also affect water residence time by routing previously isolated waters to the outlet or merging systems in a more circuitous manner, both of which would change the time water has to chemically weather minerals under the ice (Fountain and Walder,

1998). Measured cation concentrations for soluble chemical reaction products (Ca, Ma, K, Mg) were small (Figure IV-3), never exceeding 25% of saturation for each element in ~1°C water. In contrast, measured concentrations for the same suite from April 2013 (Hatton et al., 2019) reached ~75% saturation. These observations support a less efficient spring hydrologic network, with decreased dilution and longer water-rock interaction time, evolving to a more efficient summer configuration with increased melt and less time for chemical weathering reactions to proceed.

Although the total variability was small, EC measurements show a slight increasing trend over this 2015 two-month study period (Figure IV-2). EC decreased in early August (DOY 220-228) reflecting either increased meltwater volume (solvent) or decreased chemical weathering products (solutes). Extensive 2015 GrIS surface melt occurred from June 15 to July 28 (DOY 166-209), with a maximum on July 4 when ~50% of the ice sheet surface contained liquid water (Greenland Surface Melt Extent). While peak melt occurred prior to the field campaign, there were smaller pulses occurring in both early August (DOY 213-225) and late August/early September (DOY 239-252) (Greenland Surface Melt Extent). The initial decrease in EC correlates with the early August melt pulse, while the second decrease in EC (DOY 245 – 250) begins seven days after the start of the second melt pulse. Both instances of decreasing EC occur without any significant change in hydrochemistry, making any significant hydrological reorganization unlikely. Therefore, both periods of decreasing EC are interpreted to show the continued existence of a well-connected, efficient drainage system remaining after peak-summertime conditions and result from dilution rather than a seasonally driven reconfiguration of the network.

A large flux of water is expected to enter the KS subglacial network during the almost annual Hullet flood, impacting the efficiency of the subglacial conduits at KS. Ice-dammed lake Hullet (Figure IV-1) regularly floods through/under KS in August or September in a glacial lake outburst flood (GLOF) (Mätzler et al., 2015). In 2014, 0.45 km^3 drained over 23 days, causing > 3

m increase in water level in the outflow river (Mätzler et al., 2015). Adding such a large volume of water to the KS hydrologic system in a single short event should have massive effects on the connectivity of the subglacial hydrologic system and the size of its conduits. Post-GLOF, we expect the hydrologic system is likely comprised of larger-diameter channels relative to pre-GLOF, and is then subsequently capable of accommodating any volume of melt smaller than the GLOF volume efficiently. However, Hullet did not flood during the 2015 field campaign. Future research is needed to measure the effects of the Hullet GLOF on expressed KS hydrochemistry and the effects on seasonal change in the KS subglacial system.

Rain events were observed during the 2015 field season at KS, increasing water flux through the hydrologic system through both rain volume and increased melting of the ice surface. 1- to 3-day rain events at KS resulted only in minor transient changes in *in situ* chemistry (Figure IV-2) and no consistent effects on elemental concentrations across all measured species (Figure IV-3). Stable measurements through 1- to 3-day rain events imply the existence of a hydrologic system capable of accommodating these variable influxes of water.

The prolonged rain event from DOY 241 – 249 (August 29 – September 6) correlates to both highest relative Q and a decrease in electric conductivity (EC) (Figure IV-2). This event also corresponds with the second increased surface melt extent over the entire GrIS in late August/early September, with ~28% of the ice sheet surface containing liquid water. Some of the discharge volume is likely from rain, but meltwater contributions from further up-ice are also possible. Continuously measured EC downstream from the terminus reveal a decrease in EC beginning mid-way through the rain event (DOY 246) (Figure IV-2). Other rain events at the end of the season also generated increased relative Q, revealing effects measurable in bulk outflow but do not analogously decrease EC in meltwater (Figure IV-2). Addition of rain and rain-enhanced surface melt to the system adds solute-free water, diluting both concentrations of soluble major rock cations

(Figure IV-3) and bulk EC. While this rain event was the only event significant enough to produce a measurable effect on chemistry, it was unlikely to have forced a reorganization of the subglacial hydrologic network. If the flux of water was large enough to overwhelm the existing network, then low-solute water would have encountered weatherable minerals outside the existing channels, likely resulting in increased chemical weathering. Increased chemical weathering should be evident through products carried in meltwater, yet both elemental concentrations and bulk EC decreased – showing dilution – instead of increasing as expected with increased weathering (Figure IV-2D).

While major cation concentrations were relatively stable throughout the field season, particle reactive elements show more variability. P, Al, and Fe are insoluble; changes in their concentrations may reflect different subglacial processes than soluble elements. P, Al, and Fe all exhibit an increase in concentration on DOY 231, unassociated with rain or surface melt events and not matched by concurrent increases in soluble element concentrations (Figure IV-3). P, Al, and Fe commonly form oxides on the surface of sediments, and may exist in filter-passing sizes <0.22 μm (Hawkings et al., 2014; Raiswell and Canfield, 2012). As such, increases in concentration may be related to increases in suspended sediment concentration. DOY 231 is marked by both increased water and air temperature (Figure IV-2), potentially generating increased local melt, without a corresponding GrIS-wide surface melting event. Modeled relative Q does not increase from the prior data point at DOY 231, but a week gap between collection of these two samples may be too low resolution to observe an increase (Figure IV-2). Higher air temperatures may increase melting rates, adding more water to the subglacial system and potentially increasing the carrying capacity of subglacial water. Higher carrying capacity could evacuate more sediments from the system, including smaller particles with insoluble trace metals. An increase in sediment load, including filter-passing non-aqueous metals, would explain the abrupt increase in

concentration for these elements on DOY 231 while other elemental concentrations and *in situ* hydrological parameters remained constant.

1.2 Late Summer Change in Meltwater Source

Stable water isotopic composition of river outflow is employed to identify changes in water sources in the hydrologic network throughout the melt season as bulk composition represents a mixture of all contributing sources. Melt water composition varied over the study, initially with both $\delta^{18}O$ and δD decreasing until DOY 240, then increasing toward the end of the field season (Figure IV-4). The melt water stable isotopic composition was consistently lower than the ice collected at the KS terminus, which had a $\delta^{18}O$ composition of -18.2‰ SMOW and δD of -134‰ SMOW. Ice in the southern portion of the GrIS, ~400 km from KS has a $\delta^{18}O$ composition of ~ -28‰ (Dansgaard et al., 1982; Mayewski et al., 1986) and the isotopic composition of ice decreases towards the center of the GrIS (Vinther et al., 2006). The isotopic composition of rain collected throughout the study period averaged to -7.2‰ $\delta^{18}O$ and -56‰ δD; significantly higher than the meltwater. As meltwater $\delta^{18}O$ and δD measured during the field campaign (Figure IV-4) was lower than both rain water and KS ice collected at the terminus, outflow water at the KS terminus must incorporate melt that originates further up-ice. The KS meltwater isotopic composition reflects mixing of more negative distal water and less negative local water, and rain. As meltwater $\delta^{18}O$ and δD increase through the field season (Figure IV-4), the proportion of more distally sourced melt decreases through the late summer.

The presence of distal melt water in KS outflow requires an efficient to route it to the terminus. Outlet glaciers in the southwest portion of the GrIS lost mass through surface melting at a progressively increasing rate from 2003 – 2013 in response to increased atmospheric warming (Bevis et al., 2019), confirming increasing surface melt over large portions of the GrIS. Seasonal development of efficient subglacial hydrologic networks in GrIS outlet glaciers expands up-ice

throughout the ablation season, tracking the extent of increased surface melting (Bartholomew et al., 2010; Chandler et al., 2013). With increased melt over larger areas, efficient hydrologic network development may also extend over larger areas, providing a mechanism to evacuate melt with lower isotopic compositions from up-ice in the GrIS.

The end-summer shift in outflow water source is present in other measured hydrochemical parameters, such as radiogenic Sr isotopes ($^{87}Sr/^{86}Sr$) in KS meltwater (Figure IV-5). Sr is dissolved from minerals into water through chemical weathering reactions. $^{87}Sr/^{86}Sr$ composition varies both in minerals within a given rock unit and between bulk composition of different rock units. ^{87}Sr is a radiogenic isotope created through radioactive decay of ^{87}Rb over geologic timescales, while ^{86}Sr is stable. Both Sr isotopes can substitute for Ca in mineral lattices while Rb substitutes for K. As different minerals contain different proportions of Ca to K, and as the amount of radiogenic ^{87}Sr present is age dependent, $^{87}Sr/^{86}Sr$ is a useful tracer to identify which minerals, and which rock formations, waters have been in contact with. $^{87}Sr/^{86}Sr$ may trace changes in meltwater flow path (whether water is exposed to different minerals) but not to determine absolute flow path (exactly where the water was routed) at KS, because the $^{87}Sr/^{86}Sr$ composition of minerals in the underlying bedrock is unknown and bedrock boundaries are obscured by ice. Trends in water $^{87}Sr/^{86}Sr$ negatively correlate with trends in stable water isotope composition (R^2 = 0.87). $^{87}Sr/^{86}Sr$ was higher when water isotopes are low, then trends toward less radiogenic values as water isotope values increase (Figure IV-5). These data support a shift in water source towards more proximal melt and a change in $^{87}Sr/^{86}Sr$ bulk composition of bedrock that water encounters en route to the terminus from higher $^{87}Sr/^{86}Sr$ to lower $^{87}Sr/^{86}Sr$.

$^{87}Sr/^{86}Sr$ was also analyzed on suspended sediments filtered from collected meltwaters; values are more radiogenic than those of the water itself and no similar trends over the study period were observed (Figure IV-5). Suspended sediment $^{87}Sr/^{86}Sr$ composition broadly became more

radiogenic towards the end of the study contrary to trends observed in water. However, whereas water $^{87}Sr/^{86}Sr$ composition reflects weathering of the most easily weathered rock-forming minerals, suspended sediments are generated from all of the minerals present in the bedrock regardless of their susceptibility to chemical weathering. KS terminates in a proglacial lake with slower water velocity than the subsequent outflow river, potentially allowing larger sized sediments to settle out to the lake bed. If so, the Sr isotopic composition of the filtered sediment is likely not representative of the bulk composition of the bedrock, explaining why these data do not match trends from the water.

High resolution trends in the solute load (EC) further support the localization of melt in the subglacial hydrologic system as the season progressed. Following the solute decrease due to the protracted rain and enhanced surface melt period, solute load then increasingly rises throughout the rest of the study. While day-to-day air temperature behaved stochastically, mean daily air temperature decreased $0.14^{o}C\ day^{-1}$ ($R^2 = 0.62$), and presumably was lower further up-ice at higher elevations. Thus, lower temperatures at more distal locations would decrease melting rates of distal ice, leading to both the observed shift in water isotopes and $^{87}Sr/^{86}Sr$ composition toward more local input, which additionally decreased the dilution of the solute load.

1.3 Biological Effects on pH

The data presented thus far support a shift in proportion of meltwater source from more distal to more proximal to sampling location. Other hydrochemical parameters reveal weathering effects. Granitic bedrock under KS, containing silicate minerals, chemically weathers through hydrolysis consuming H^+ ions. pH decreases from a high of 8.99 (DOY 220) to 8.23 (DOY 265), although this first-order trend is marked by four periods of abrupt decreases and subsequent abrupt recoveries on DOYs 231, 234, 249, and 261 (Figure IV-2). Brief periods of enhanced weathering might be expected if the subglacial hydrologic system was changing routing pathways or

connectivity, exposing more weatherable fresh mineral surfaces to meltwater. It is possible that H^+ ions may be released into meltwater through ion exchange reactions, although the drops observed at KS (Figure IV-2) are abrupt.

Alternatively, the pH changes could be the result of cellular respiration: respiration in outflow water would increase in P_{CO2}, decreasing water pH. Furthermore, H^+ is also generated through both planktic respiration and algal decay:

$$C_{106}H_{263}O_{110}N_{16}P + 138O_2 \rightarrow 106CO_2 + 16NO_3^- + HPO_4^{2-} + 122H_2O + 18H^+$$

where $C_{106}H_{263}O_{110}N_{16}P$ is the average composition of planktic organic matter (Redfield et al., 1963) and decay occurs in the presence of O_2. DO concentrations were continuously oversaturated at the sonde location and fluctuated from a low of 126% to a high of 136%. These values were not as high as measured *in situ* DO saturation, but both instruments registered DO concentrations above 100% saturation, allowing for aerobic decay. Continuously measured DO showed a daily fluctuation with increases in concentration throughout the day and decreases at night, providing evidence for photosynthesis in the outflow river where green algae was observed in the field. Three of the four abrupt decreases in pH (DOYs 234, 249, and 261) are correlated with decreases in average DO at the sonde, suggesting increased decomposition. However, as an increase in DO saturation and a pH drop was observed on DOY 231 (Figure IV-2), it is allowable that the other three occurrences are coincidental and not causal.

Sonde DO percent saturation measurements exhibit daily fluctuations in-phase with daylight hours. Algae was observed in sections of the outflow river; algal photosynthesis could explain this observed daily increase in DO. pH variability and DO fluctuations measured by the sonde may thus be explained through biological effects in the outflow river.

Part II: Interannual Variability at KS: Comparing End-Summer 2015 to Early-Summer 2013

Observations in this study indicate a well-established, static subglacial hydrologic network at KS through end-September 2015, with evidence of up-ice changes in meltwater source. pH, generally, displays a slow yet steady decrease throughout the season while EC slightly increases toward the end of the field season. Similar hydrochemical data from KS outflow exists from spring and early summer 2013 (21 April – 11 August 2013; DOY 111 – 223) (Hawkings et al., 2016); when combined the two data sets reveal hydrochemical patterns for the full melt season across years (Figure IV-6).

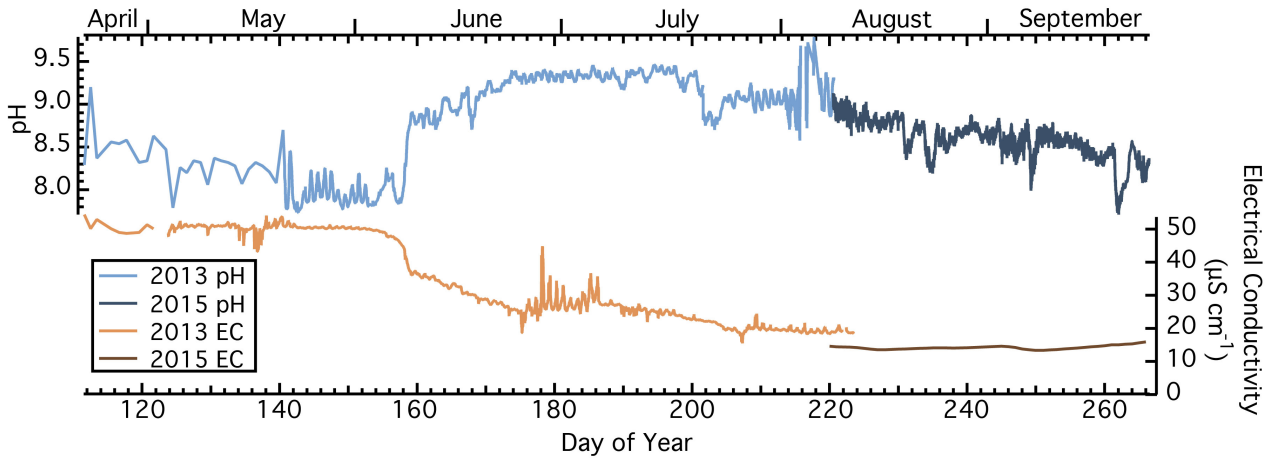

Figure IV-6: Comparison between hydrochemical data (pH [blue] and electrical conductivity [orange]) collected at Kiattuut Sermiat in 2013 (DOY 111 – 222) by Hawkings et al., (2016) and 2015 data (DOY 220 – 266) presented in this study. Years are differentiated by color; 2013 data is light blue (pH) and light orange (EC) while 2015 data is dark blue (pH) and brown (EC).

The opening of the subglacial hydrologic system begins in early June, marked by an abrupt increase in pH and decrease in EC (Figure IV-6), magnitude of which is not repeated in the record. Total shutdown of the hydrologic network is not evident in this combined data set as pH and EC values do not reach 2013 pre-opening measurements. The data sets overlap by 6 days, allowing a comparison of quantitative values in addition to qualitative seasonal trends. pH measurements match almost exactly; the 2015 data published here appear to exactly continue the 2013 trends although EC values are slightly offset (Figure IV-6). Seasonal trends in solute load

as shown by EC also vary slightly: 2013 data show more short-term deviations from the seasonal trend (although not within the last ~15 days of measurement) than the stable 2015 EC measurements.

The similarity between the years data indicates the KS subglacial hydrologic system is relatively stable through time. This subglacial network must accommodate a large, practically instantaneous volume of water (essentially) annually when Hullet drains, creating large channels capable of accommodating this high water flux. Post-flood and into winter the low surface velocity of KS (Mätzler et al., 2015)and thinning of the outlet glacier over time (Mouginot et al., 2019)have implications for the interannual lifespan of this network. Glacial ice creep is dependent on ice mass; as KS thins, there is less overburden to drive ice motion. Furthermore, flow from accumulation to ablation zone is slow at KS: ice surface velocity shows most of the ice flowing from the central GrIS is routed with QS with only a small, slow contribution to KS (Figure IV-1) (Mätzler et al., 2015) Slow flowing, thin ice deforms gradually. Thus, depending on the magnitude of the annual flood from Hullet, it is possible the deformation rate is too low to fully close drainage channels at KS each winter.

While some aspects of the subglacial system may remain open interannually, others must close. The 2013 opening of the drainage network is evident in Figure IV-6; to have an opening there must have been a closure. However, if the system is only partially closed by potentially isolating sections from the primary drainage and not complete destruction of channels, then the annual opening may be a re-opening of *the* system, instead of the opening/creation of *a* system. This is an important distinction because of the implications for subglacial sediment exposure to water, and subsequently the chemical weathering products contained in the proglacial output. Meltwaters routed through a hydrologic system with interannually open channels will continue to

be exposed to previously weathered minerals instead of encountering freshly ground unweathered minerals in other parts of the bed exposed by newly created channels. The similar pH and EC trends from 2013 and 2015 suggests the hydrologic system is likely entrenched in the KS subglacial environment; an inference further supported by the lack of seasonal variability within the 2015 glaciochemistry.

Conclusions

Better understanding of the subglacial hydrologic environment is necessary to both improve ice sheet models predicting glacial response to climate change and to improve understanding of elemental fluxes to polar oceans. This study attempted to use hydrochemical data to resolve changes in subglacial hydrology in response to decreased ice melt following summertime peak melting. Observations reveal a well-established hydrologic system relatively unchanged through mid-September 2015 with above-freezing temperatures, although the melt source appears to shift toward more proximal sources with a smaller distal contribution. Comparison with early- and mid-season 2013 data reveal similar chemical signatures in glacial outflow between multiple years. If the hydrologic system remains connected, or partially connected throughout winter, then the it may extend further up-ice more quickly in the following melt season. If so, distal water and distal weathering products may be quickly routed to the margin, with the KS hydrologic system providing an efficient conduit for this melt.

References

Aciego, S.M., Stevenson, E.I., Arendt, C.A., 2015. Climate versus geological controls on glacial meltwater micronutrient production in southern Greenland. Earth Planet. Sci. Lett. 424, 51–58. doi:10.1016/j.epsl.2015.05.017

Anderson, S.P., 2007. Biogeochemistry of Glacial Landscape Systems. Annu. Rev. Earth Planet. Sci. 35, 375–399. doi:10.1146/annurev.earth.35.031306.140033

Anderson, S.P., 2005. Glaciers show direct linkage between erosion rate and chemical weathering fluxes. Geomorphology 67, 147–157. doi:10.1016/j.geomorph.2004.07.010

Anderson, S.P., Drever, J.I., Humphrey, N.F., 1997. Chemical weathering in glacial environments. Geology 25, 399–402. doi:10.1130/0091-7613(1997)025<0399:cwige>2.3.co;2

Anderson, S.P., Longacre, S.A., Kraal, E.R., 2003. Patterns of water chemistry and discharge in the glacier-fed Kennicott River, Alaska: evidence for subglacial water storage cycles. Chem. Geol. 202, 297–312. doi:10.1016/j.chemgeo.2003.01.001

Andrews, L.C., Catania, G.A., Hoffman, M.J., Gulley, J.D., Lüthi, M.P., Ryser, C., Hawley, R.L., Neumann, T.A., 2014. Direct observations of evolving subglacial drainage beneath the Greenland Ice Sheet. Nature 514, 80–83. doi:10.1038/nature13796

Arendt, C.A., Aciego, S.M., Hetland, E.A., 2015. An open source Bayesian Monte Carlo isotope mixing model with applications in Earth surface processes. Geochem. Geophys. Geosystems 16, 1274–1292. doi:10.1002/2014gc005683

Bartholomew, I., Nienow, P., Mair, D., Hubbard, A., King, M.A., Sole, A., 2010. Seasonal evolution of subglacial drainage and acceleration in a Greenland outlet glacier. Nat. Geosci. 3, 408–411. doi:10.1038/ngeo863

Bartholomew, I., Nienow, P., Sole, A., Mair, D., Cowton, T., King, M.A., 2012. Short-term variability in Greenland Ice Sheet motion forced by time-varying meltwater drainage: Implications for the relationship between subglacial drainage system behavior and ice velocity. J. Geophys. Res. 117. doi:10.1029/2011JF002220

Bevis, M., Harig, C., Khan, S.A., Brown, A., Simons, F.J., Willis, M., Fettweis, X., van den Broeke, M.R., Madsen, F., Kendrick, E., Caccamise, D.J., van Dam, T., Knudsen, P., Nylen, T., 2019. Accelerating changes in ice mass within Greenland, and the ice sheet's sensitivity to atmospheric forcing. Proc. Nat. Acad. Sci. 116, 1934–1939. doi:10.1073/pnas.1806562116

Bhatia, M.P., Das, S.B., Kujawinski, E.B., Henderson, P., Burke, A., Charette, M.A., 2011. Seasonal evolution of water contributions to discharge from a Greenland outlet glacier: insight from a new isotope-mixing model. J. Glaciol. 57, 929–941. doi:10.3189/002214311798043861

Cappelen, J., Laursen, E., Kern-Hansen, C., Boas, L., Wang, P., Jørgensen, B., Carstensen, L., 2018. Weather Observations from Greenland 1958-2017. DMI Report 18-08.

Chandler, D.M., Wadham, J.L., Lis, G.P., Cowton, T., Sole, A., Bartholomew, I., Telling, J., Nienow, P., Bagshaw, E.B., Mair, D., Vinen, S., Hubbard, A., 2013. Evolution of the subglacial drainage system beneath the Greenland Ice Sheet revealed by tracers. Nat. Geosci. 6, 195–198. doi:10.1038/ngeo1737

Clason, C.C., Mair, D.W.F., Nienow, P.W., Bartholomew, I.D., Sole, A., Palmer, S., Schwanghart, W., 2015. Modelling the transfer of supraglacial meltwater to the bed of Leverett Glacier, Southwest Greenland. Cryosphere 9, 123–138. doi:10.5194/tc-9-123-2015

Dansgaard, W., Clausen, H.B., Gundestrup, N., Hammer, C.U., Johnsen, S.F., Kristinsdottir, P.M., Reeh, N., 1982. A new Greenland deep ice core. Science 218, 1273–1277. doi:10.1126/science.218.4579.1273

Davison, B.J., Sole, A.J., Livingstone, S.J., Cowton, T.R., Nienow, P.W., 2019. The influence of hydrology on the dynamics of land-terminating sectors of the Greenland Ice Sheet. Front. Earth Sci. 7, 580–24. doi:10.3389/feart.2019.00010

Fountain, A.G., Walder, J.S., 1998. Water flow through temperate glaciers. Rev. Geophys. 36, 299–328. doi:10.1029/97rg03579

Graly, J.A., Humphrey, N.F., Licht, K.J., 2018. Two metrics describing the causes of seasonal and spatial changes in subglacial aqueous chemistry. Front. Earth Sci. 6, 195. doi:10.3389/feart.2018.00195

Greenland Portal. http://data.geus.dk/geusmap/?mapname=greenland_portal (accessed 10 May 2019).

Greenland Surface Melt Extent, 2019. Greenland surface melt extent interactive chart. National Snow and Ice Data Center. https://nsidc.org/greenland-today/greenland-surface-melt-extent-interactive-chart/ (accessed 3 August 2019).

Hatton, J.E., Hendry, K.R., Hawkings, J.R., Wadham, J.L., Kohler, T.J., Stibal, M., Beaton, A.D., Bagshaw, E.A., Telling, J., 2019. Investigation of subglacial weathering under the Greenland Ice Sheet using silicon isotopes. Geochim. Cosmochim. Acta 247, 191–206. doi:10.1016/j.gca.2018.12.033

Hawkings, J.R., Tranter, M., Raiswell, R., Benning, L.G., Statham, P.J., Tedstone, A., Nienow, P., Lee, K., Telling, J., Wadham, J.L., 2014. Ice sheets as a significant source of highly reactive nanoparticulate iron to the oceans. Nat. Commun. 5, 1–8. doi:10.1038/ncomms4929

Hawkings, J., Wadham, J., Tranter, M., Telling, J., Bagshaw, E., Beaton, A., Simmons, S.-L., Chandler, D., Tedstone, A., Nienow, P., 2016. The Greenland Ice Sheet as a hot spot of phosphorus weathering and export in the Arctic. Global Biogeochem. Cycles 30, 191–210. doi:10.1002/2015GB005237

Henriksen, N., Higgins, A.K., Kalsbeek, F., Pulvertaft, T., 2009. Greenland from Archaean to Quaternary: descriptive text to the 1995 Geological map of Greenland, 1: 2 500 000.

Hoffman, M.J., Catania, G.A., Neumann, T.A., Andrews, L.C., Rumrill, J.A., 2011. Links between acceleration, melting, and supraglacial lake drainage of the western Greenland Ice Sheet. J. Geophys. Res. 116, 609–16. doi:10.1029/2010JF001934

Koziol, C., Arnold, N., Pope, A., Colgan, W., 2017. Quantifying supraglacial meltwater pathways in the Paakitsoq region, West Greenland. J. Glaciol. 63, 464–476. doi:10.1017/jog.2017.5

Mätzler, E., Petersen, D., Abermann, J., Strozzi, T., Weismann, A., Kääb, A., Frey, H., Caduff, R., 2015. Assessment Report for Hullet, Greenland. Asiaq, Greenland Survey, 1–23.

Mayewski, P.A., Lyons, W.B., Spencer, M.J., Twickler, M., Dansgaard, W., Koci, B., Davidson, C.I., Honrath, R.E., 1986. Sulfate and nitrate concentrations from a south Greenland ice core. Science 232, 975–977. doi:10.1126/science.232.4753.975

Moon, T., Joughin, I., Smith, B., Broeke, M.R., Berg, W., Noël, B., Usher, M., 2014. Distinct patterns of seasonal Greenland glacier velocity, Geophys. Res. Lett., 41, 7209–7216, doi:10.1002/2014GL061836

Mouginot, J., Rignot, E., Bjørk, A.A., van den Broeke, M., Millan, R., Morlighem, M., Noël, B., Scheuchl, B., Wood, M., 2019. Forty-six years of Greenland Ice Sheet mass balance from 1972 to 2018. Proc. Nat. Acad. Sci. 116, 9239–9244. doi:10.1073/pnas.1904242116

Raiswell, R., 1984. Chemical models of solute acquisition in glacial melt waters. J. Glaciol. 30, 49–57. doi:10.3189/s0022143000008480

Raiswell, R., Canfield, D.E., 2012. The iron biogeochemical cycle past and present. Geochem. Perspect. 1, 1–220. doi:10.7185/geochempersp.1.1

Redfield, A.C., Ketchum, B.H., Richards, F.A., 1963. The influence of organisms on the composition of seawater, in: Hill, M.N. (Ed.), The sea, v. 2. Interscience.

Rignot, E., Mouginot, J., 2012. Ice flow in Greenland for the International Polar Year 2008-2009. Geophys. Res. Lett. 39, n/a–n/a. doi:10.1029/2012GL051634

Schoof, C., 2010. Ice-sheet acceleration driven by melt supply variability. Nature 468, 803–806. doi:10.1038/nature09618

Shreve, R.L., 1972. Movement of water in glaciers. J. Glaciol. 11, 205–214. doi:10.1017/s002214300002219x

Stumm, W., Wollast, R., 1990. Coordination chemistry of weathering: Kinetics of the surface-controlled dissolution of oxide minerals. Rev. Geophys. 28, 53-69. doi:10.1029/rg028i001p00053

Tranter, M., Brown, G.H., Hodson, A.J., Gurnell, A.M., 1996. Hydrochemistry as an indicator of subglacial drainage system structure: A comparison of alpine and sub-polar environments. Hydrol. Process. 10, 541–556. doi:10.1002/(sici)1099-1085(199604)10:4<541::aid-hyp391>3.0.co;2-9

Tranter, M., Sharp, M.J., Lamb, H.R., Brown, G.H., Hubbard, B.P., Willis, I.C., 2002. Geochemical weathering at the bed of Haut Glacier d'Arolla, Switzerland—a new model. Hydrol. Process. 16, 959–993. doi:10.1002/hyp.309

Tranter, M., Wadham, J., 2014. Geochemical weathering in glacial and proglacial environments. Treatise Geochem, second ed. 7, 157–173. doi:10.1016/b978-0-08-095975-7.00505-2

Trusel, L.D., Das, S.B., Osman, M.B., Evans, M.J., Ben E Smith, Fettweis, X., McConnell, J.R., Noël, B.P.Y., Broeke, M.R., 2018. Nonlinear rise in Greenland runoff in response to post-industrial Arctic warming. Nature. 564, 104–108. doi:10.1038/s41586-018-0752-4

Vinther, B.M., Clausen, H.B., Johnsen, S.J., Rasmussen, S.O., Andersen, K.K., Buchardt, S.L., Dahl-Jensen, D., Seierstad, I.K., Siggaard-Andersen, M.L., Steffensen, J.P., Svensson, A., Olsen, J., Heinemeier, J., 2006. A synchronized dating of three Greenland ice cores throughout the Holocene. J. Geophys. Res. 111, 26367–10. doi:10.1029/2005JD006921

Yde, J.C., Knudsen, N.T., Hasholt, B., Mikkelsen, A.B., 2014. Meltwater chemistry and solute export from a Greenland Ice Sheet catchment, Watson River, West Greenland. J. Hydrol. 519, 2165–2179. doi:10.1016/j.jhydrol.2014.10.018

Yde, J.C., Knudsen, N.T., Nielsen, O.B., 2005. Glacier hydrochemistry, solute provenance, and chemical denudation at a surge-type glacier in Kuannersuit Kuussuat, Disko Island, West Greenland. J. Hydrol. 300, 172–187. doi:10.1016/j.jhydrol.2004.06.008

Zwally, H.J., Abdalati, W., Herring, T., Larson, K., Saba, J., Steffen, K., 2002. Surface melt-induced acceleration of Greenland ice-sheet flow. Science 297, 218–222. doi:10.1126/science.1071795

Chapter V. Conclusions

Dissertation Results

As climate warming is projected to continue to increase (IPCC, 2013), Earth's glaciers and ice sheets will continue to melt. Therefore, understanding the effects of meltwater on both glacial dynamics and the downstream environment is critically important (e.g. Flowers, 2018; Nienow et al., 2017). Due to the dynamical response of the subglacial environment to seasonal changes in meltwater, these impacts can vary temporally and spatially. This dissertation demonstrates the value of multi-month, long term field campaigns to monitor changes in chemistry in subglacial outflow waters to better understand seasonal evolution of subglacial hydrologic environments. Multi-month field campaigns, like those presented here, have advantages over shorter term campaigns, or single "spot" samples, in that they allow researchers to observe and monitor seasonal trends in glacial hydrochemistry. Results from the Athabasca Glacier show small changes in a highly dynamic alpine glacier accrue over a period of three months, cumulatively demonstrating partial subglacial hydrologic network reconfiguration, but no individual sample shows this process. Changes observed at Kiattuut Sermiat – an outlet glacier of the Greenland Ice Sheet - are more nuanced, but the two-month study presented here nevertheless reveals muted changes in up-ice water source and impacts of local biology on outlet water chemistry.

Laboratory experiments performed during this thesis demonstrate the importance of cautious sample site selection in proglacial environments such that local groundwater does not affect measurements, and potentially impact interpretations. Sampling locations for shorter duration or spot sampling may be selected due to ease of access, with other environmental concerns

overlooked, or assumed to be negligible. Results of this dissertation reveal this to be untrue at Kiattuut Sermiat; as an unexceptional Greenland Ice Sheet outlet glacier, it is possible similar processes occur at other land-terminating outlet glaciers. Future field sampling campaigns should carefully select sampling locations, with thoughts to possible groundwater incursion.

Chapter Results

Chapter 2 finds ^{222}Rn activity concentration measurements are an effective proxy for subglacial water residence time in some, but not all locations. For ^{222}Rn to be present in subglacial waters, its radioactive parent ^{226}Ra must exist in the subglacial environment. As both isotopes are intermediaries in the uranium decay chain and uranium is a common trace element in Earth's crust, this is at first a reasonable assumption. However, laboratory experiments reveal differences in ^{222}Rn production from different size fractions of glacial sediment, likely reflecting mineralogical, and therefore ^{226}Ra, differences. In areas where sediment does contain ^{226}Ra, concentrations of its daughter ^{222}Rn in outflow waters will be representative of subglacial water residence time. Additionally, this chapter illustrates the importance of selecting sampling locations for proglacial water sampling. At Kiattuut Sermiat, groundwater input – identifiable by high ^{222}Rn activity concentrations – is evident in the proglacial river at all sampling locations.

Chapter 3 presents hydrochemical changes at the Athabasca Glacier during the transition from summertime peak-melt in August to winter conditions at end-October, 2014. The subglacial hydrologic network at this alpine glacier is dynamic, responding rapidly to environmental forcings. Different proportions of solute products in meltwater reveal changes in proportions of carbonate to silicate mineral weathering in the carbonate-dominated subglacial environment, with enhanced relative silicate mineral weathering occurring with low discharge. This is interpreted to reflect longer subglacial water residence time and a shift in subglacial drainage configuration to allow

these kinetically slower reactions to proceed. Finally, concentrations of insoluble particle reactive elements (Fe, Al, P) and suspended sediments reveal likely instances where subglacial water was routed over previously isolated sections of the subglacial environment, flushing sediments and associated elements into bulk outflow.

Chapter 4 demonstrates the relatively stable hydrochemistry of Kiattuut Sermiat meltwaters throughout August and September, 2015, revealing the existence of a well-connected, highly competent glacial hydrologic network. Concentrations of soluble elements were less variable than insoluble elements, which may reflect variable rates of sediment (and associated particle reactive elements) flux in the subglacial system. Stable water isotopes reveal a gradual change in water source from more distal up-ice sources to sources proximal to the glacier terminus - a shift also supported by the radiogenic Sr composition in meltwater. High-resolution water quality data collected in 2015 is very similar to data collected in 2013 by Hawkings et al. (2014), suggesting the subglacial hydrologic network is either annually recreated in the same configuration, or perhaps persists interannually. While environmental forcing during the field campaign did not generate a discernable shift in subglacial hydrologic configuration, data are collected and presented to provide baseline geochemical measurements with which to evaluate future subglacial hydrologic change.

Future Work

In both field campaigns presented in this dissertation, concentrations of insoluble elements displayed differing trends from soluble elements, an observation attributed to filter-passing size fractions. Additionally, measured elemental concentrations from leachate laboratory experiments differed depending on filter pore size, suggesting measured concentrations were not truly dissolved. Iron, an insoluble element displaying, is a limiting nutrient in seas by both the north and south poles (e.g. Moore et al., 2013) with current research finding Fe is delivered to these locations

through melting ice (e.g. Arrigo et al., 2015; Hawkings et al., 2014; Raiswell et al., 2008). Iron concentrations from both Athabasca Glacier and Kiattuut Sermiat did not respond to changing dilution and subglacial residence time like soluble elements did. Additionally differences in Fe concentration were demonstrated to be dependent on filter pore size in laboratory experiments. I concluded that the particle-reactive behavior of Fe was impacting measured concentrations as the suspended sediment load changed in my field samples – thus sediment size fraction plays an important role in transport of Fe from bodies of ice to Fe-limited environments. An intriguing area of future research would be to analyze iron concentrations in glacial melt as filtered through a variety of pore sizes to then investigate what forms of Fe exist in each size fraction. Examining the bioavailability of different forms of Fe could improve our understanding of what extent Fe-bearing ice melt may fertilize polar seas, affecting marine productivity and CO_2 drawdown.

References

Arrigo, K.R., van Dijken, G.L., Strong, A.L., 2015. Environmental controls of marine productivity hot spots around Antarctica. J. Geophys. Res. Oceans 120, 5545–5565. doi:10.1002/2015JC010888

Flowers, G.E., 2018. Hydrology and the future of the Greenland Ice Sheet. Nat. Commun. 9, 2729. doi:10.1038/s41467-018-05002-0

Hawkings, J.R., Tranter, M., Raiswell, R., Benning, L.G., Statham, P.J., Tedstone, A., Nienow, P., Lee, K., Telling, J., Wadham, J.L., 2014. Ice sheets as a significant source of highly reactive nanoparticulate iron to the oceans. Nat. Commun. 5, 1–8. doi:10.1038/ncomms4929

IPCC, 2013: Climate Change 2013: The physical science basis. Contribution of working group I to the fifth assessment report of the Intergovernmental Panel on Climate Change [Stocker, T.F., D. Qin, G.-K. Plattner, M. Tignor, S.K. Allen, J. Boschung, A. Nauels, Y. Xia, V. Bex and P.M. Midgley (eds.)]. Cambridge Univ. P., Cambridge, United Kingdom and New York, NY, USA, 1535 pp.

Moore, C., Mills, M., Arrigo, K., Berman-Frank, I., Bopp, L., Boyd, P., Galbraith, E., Geider, R., Guieu, C., Jaccard, S., Jickells, T., Roche, L.J., Lenton, T., Mahowald, N., Marañón, E., Marinov, I., Moore, J., Nakatsuka, T., Oschlies, A., Saito, M., Thingstad, T., Tsuda, A., Ulloa, O., 2013. Processes and patterns of oceanic nutrient limitation. Nat. Geosci. 6, 701–710. doi:10.1038/ngeo1765

Nienow, P., Sole, A., Slater, D., Cowton, T., 2017. Recent advances in our understanding of the role of meltwater in the Greenland Ice Sheet system. Curr. Clim. Chang. Rep. 3, 330–344. doi:10.1007/s40641-017-0083-9

Raiswell, R., Benning, L.G., Tranter, M., Tulaczyk, S., 2008. Bioavailable iron in the Southern Ocean: the significance of the iceberg conveyor belt. Geochem. Trans. 9. doi:10.1186/1467-4866-9-7